Effect of Ligand Modification on Properties of Iron-Tetracarbene Photosensitisers

Design, Synthesis and Photovoltaic Applications

Persson, Samuel

2024

Document Version:
Publisher's PDF, also known as Version of record

Link to publication

Citation for published version (APA):
Persson, S. (2024). *Effect of Ligand Modification on Properties of Iron-Tetracarbene Photosensitisers: Design, Synthesis and Photovoltaic Applications*. [Doctoral Thesis (compilation), Centre for Analysis and Synthesis]. Lund University.

Total number of authors:
1

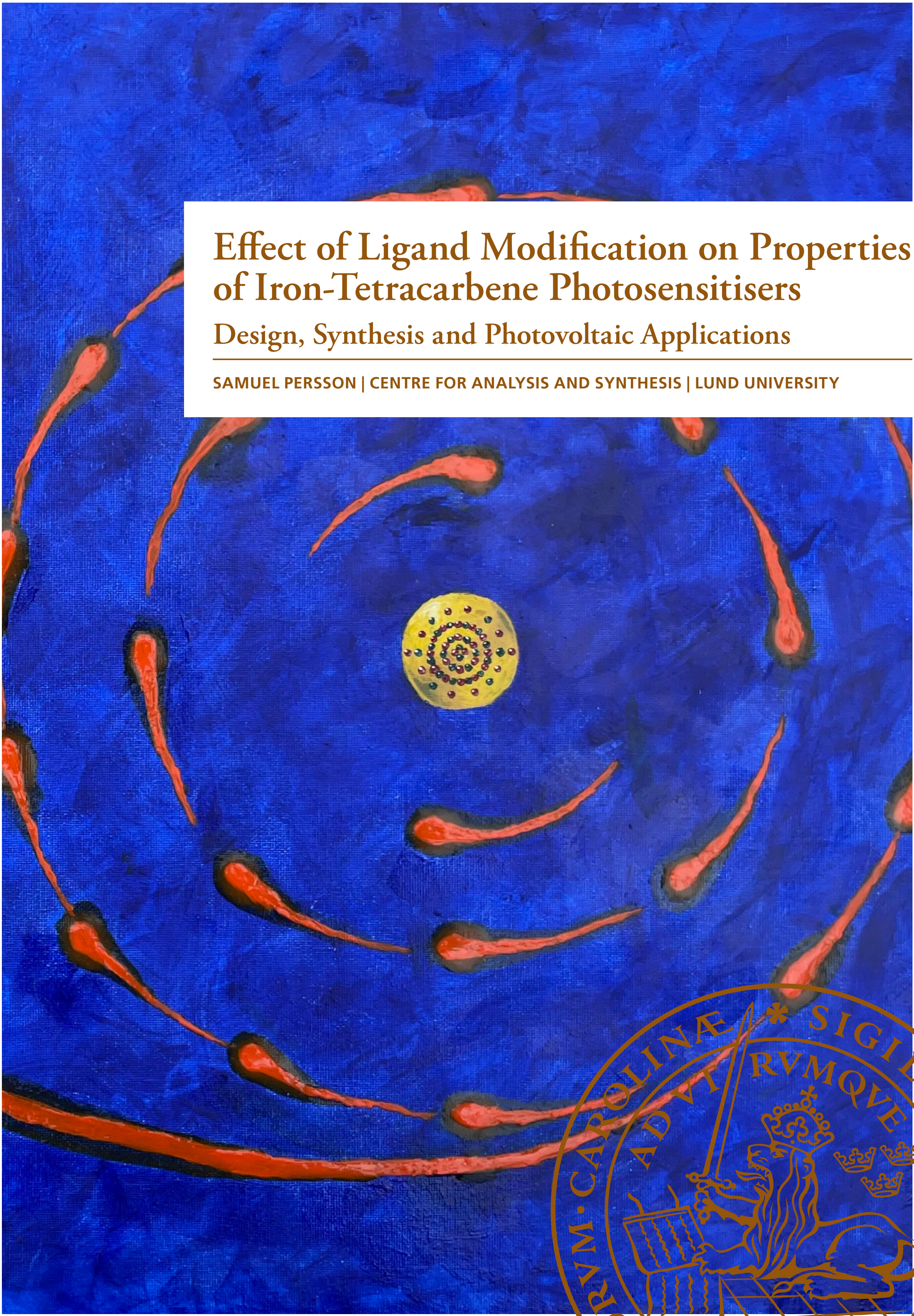

Effect of Ligand Modification on Properties of Iron-Tetracarbene Photosensitisers

Design, Synthesis and Photovoltaic Applications

SAMUEL PERSSON | CENTRE FOR ANALYSIS AND SYNTHESIS | LUND UNIVERSITY

Effect of Ligand Modification on Properties of Iron-Tetracarbene Photosensitisers

Effect of Ligand Modification on Properties of Iron-Tetracarbene Photosensitisers

Design, Synthesis and Photovoltaic Applications

Samuel Persson

DOCTORAL DISSERTATION

Doctoral dissertation for the degree of Doctor of Philosophy (PhD) at the Faculty of Science at Lund University to be publicly defended on October 31st, 2024 at 09.00 in Lecture Hall KC:A, Kemicentrum, Naturvetarvägen 22, Lund

Faculty opponent
Prof. Jerker Mårtensson, Chalmers University of Technology

Organization: LUND UNIVERSITY

Document name: Doctoral Dissertation **Date of issue:** 2024-10-07

Author: Samuel Persson

Title and subtitle: Effect of Ligand Modification on Properties of Iron-Tetracarbene Photosensitisers: Design, Synthesis and Photovoltaic Applications

Abstract:

The use of N-heterocyclic carbenes in conjunction with iron has been studied over the last decade for the purpose of achieving well-functioning iron-based photosensitisers. This is based on the strong σ-donating ability of the carbene, and the effect this has on the metal-based orbitals of iron, for achieving more stable excited states. This work has been done to harness this earth-abundant metal's potential for widespread application as a photosensitiser.

Within this thesis are presented a number of new iron N-heterocyclic carbene complexes, and investigations into their use as photosensitisers. All complexes are based on a core bis-tridentate ligand structure, where each ligand has a pyridine unit, flanked by two N-heterocyclic carbene moieties.

First is the study of heteroleptic iron complexes, and their use in photovoltaic application. The study served to give insight into the synthetic demands of the heteroleptic iron complexes, with a difference in nucleophilicity of the two involved ligands seemingly being detrimental to the yield. The new complexes showed an improved efficiency of up to 1.3%, compared to their homoleptic parent complex's efficiency of 0.7%. Further optimisation of the various other parts of the solar cell architecture resulted in even further improvement of the photovoltaic efficiencies. These investigations simultaneously revealed hysteresis effects to be present in these devices. Additionally, the study of the excited state dynamics of the photosensitisers at the solar cell surface seemingly revealed charge recombination with an excited state of the dye.

This is followed by the synthesis and investigation of a series of new iron N-heterocyclic carbene complexes bearing phenyl-ethynyl substituents. These substituents were further modified to study the effect of electron withdrawing and electron donating groups. These new substituents served to double the excited state lifetime, from 9 ps to 18 ps, compared to the unsubstituted parent complex. Furthermore, the complexes showed no major population of the metal centred states during the excitation. However, a difference in substituents on the new phenyl-ethynyl moieties had almost no effect on the excited state dynamics of the iron centre. In addition is outlined the as of yet unrealised efforts to synthesise analogs of these designs, for use in solar cell applications.

Lastly, is presented the post-complexation formation, and subsequent photophysical study, of an iron N-heterocyclic carbene complex incorporating dihydroimidazolylidene carbenes rather than simple imidazolylidenes used for other complexes. This led to a metal centred excited state lifetime of 75 ps, compared to the excited state lifetime of 9 ps for the non-hydrogenated parent complex. This strategy was not by itself adequate to improve the charge transfer state lifetime of the complex.

Key words: complexation, dye-senstised solar cell, earth-abundant, electron transfer, iron, iron complex, ligand synthesis, *N*-heterocyclic carbene, photosensitiser, photovoltaics

Language: English

ISBN: 978-91-8096-060-1 (Print)

ISBN: 978-91-8096-061-8 (Electronic) **Number of pages**: 260

Signature Date 2024-09-17

Effect of Ligand Modification on Properties of Iron-Tetracarbene Photosensitisers

Design, Synthesis and Photovoltaic Applications

Samuel Persson

LUND
UNIVERSITY

Cover by Samuel Persson (oil on canvas panel)

Faculty of Science
Department of Chemistry

ISBN 978-91-8096-060-1 (Print)
ISBN 978-91-8096-061-8 (Electronic)

Printed in Sweden by Media-Tryck, Lund University
Lund 2024

Printed matter
3041 0903

Media-Tryck is a Nordic Swan Ecolabel
certified provider of printed material.
Read more about our environmental
work at www.mediatryck.lu.se

MADE IN SWEDEN

“The power of the sun, in the palm of my hand.”

—Spider-Man 2

Table of Contents

Abstract 11

Populärvetenskaplig sammanfattning 13

List of Papers 15

Symbols and Abbreviations 17

1 Introduction 19

1.1 Harvesting of solar energy 19

1.2 Aim and outline 20

2 Photosensitisers 21

2.1 Basic principles 21

2.2 Investigation and characterisation 25

2.3 Iron carbene photosensitisers 27

2.3.1 Comparison of iron and ruthenium photosensitisers 27

2.3.2 Using NHCs to improve the excited state properties of iron complexes 29

3 Dye-sensitised solar cells 37

3.1 Basic principles of solar cells 37

3.2 Background on dye-sensitised solar cells 39

3.2.1 Working principles and components 39

3.2.2 Photosensitisers in DSCs 42

3.3 Iron-based dyes in DSCs 43

4 Synthesis of heteroleptic iron-NHC complexes and their use in DSCs (Papers I & II) 47

4.1 Background 47

4.2 Synthesis of heteroleptic complexes 48

4.2.1 Ligand synthesis 48

4.2.2 Complexation 50

4.3 Properties of heteroleptic complexes adsorbed on the semiconductor-surface 52

4.3.1 Photoexcitation dynamics and electronic structure 52

4.3.2 Basic investigation of DSCs based on iron-NHC dyes 53

4.3.3 Optimisation of solar cell systems 54
4.3.4 Iron-NHC dyes incorporating long alkyl chains 57
4.4 Conclusions 58

5 Iron-NHC photosensitisers substituted with phenyl-ethynyl moieties (Paper III) 61
5.1 Background 61
5.2 Synthesis of homoleptic phenyl-ethynyl substituted complexes 62
5.2.1 Initial attempts 62
5.2.2 Ligand synthesis 63
5.2.3 Complexation 64
5.3 Photophysical properties 65
5.4 Towards carboxylic acid derivatives of phenyl-ethynyl substituted complexes 66
5.4.1 Incentive 66
5.4.2 Synthetic strategies 68
5.5 Conclusions 72

6 Iron-NHC complexes with dihydroimidazolylidene-based ligands (Paper IV) 73
6.1 Background 73
6.2 Synthesis 73
6.3 Photophysical properties 75
6.4 Conclusions 75

7 Conclusions and outlook 77

8 Additional synthetic procedures 79
8.1 Synthesis 79
8.2 NMR spectra 84
8.3 Spectrophotometry 92

Acknowledgements 95

References 97

Abstract

The use of *N*-heterocyclic carbenes in conjunction with iron has been studied over the last decade for the purpose of achieving well-functioning iron-based photosensitisers. This is based on the strong σ-donating ability of the carbene, and the effect this has on the metal-based orbitals of iron, for achieving more stable excited states. This work has been done to harness this earth-abundant metal's potential for widespread application as a photosensitiser.

Within this thesis are presented a number of new iron *N*-heterocyclic carbene complexes, and investigations into their use as photosensitisers. All complexes are based on a core bis-tridentate ligand structure, where each ligand has a pyridine unit, flanked by two *N*-heterocyclic carbene moieties.

First is the study of heteroleptic iron complexes, and their use in photovoltaic application. The study served to give insight into the synthetic demands of the heteroleptic iron complexes, with a difference in nucleophilicity of the two involved ligands seemingly being detrimental to the yield. The new complexes showed an improved efficiency of up to 1.3%, compared to their homoleptic parent complex's efficiency of 0.7%. Further optimisation of the various other parts of the solar cell architecture resulted in even further improvement of the photovoltaic efficiencies. These investigations simultaneously revealed hysteresis effects to be present in these devices. Additionally, the study of the excited state dynamics of the photosensitisers at the solar cell surface seemingly revealed charge recombination with an excited state of the dye.

This is followed by the synthesis and investigation of a series of new iron *N*-heterocyclic carbene complexes bearing phenyl-ethynyl substituents. These substituents were further modified to study the effect of electron withdrawing and electron donating groups. These new substituents served to double the excited state lifetime, from 9 ps to 18 ps, compared to the unsubstituted parent complex. Furthermore, the complexes showed no major population of the metal centred states during the excitation. However, a difference in substituents on the new phenyl-ethynyl moieties had almost no effect on the excited state dynamics of the iron centre. In addition is outlined the as of yet unrealised efforts to synthesise analogs of these designs, for use in solar cell applications.

Lastly, is presented the post-complexation formation, and subsequent photophysical study, of an iron *N*-heterocyclic carbene complex incorporating dihydroimidazolylidene carbenes rather than simple imidazolylidenes used for other complexes. This led to a metal centred excited state lifetime of 75 ps, compared to the excited state lifetime of 9 ps for the non-hydrogenated parent complex. This strategy was not by itself adequate to improve the charge transfer state lifetime of the complex.

Populärvetenskaplig sammanfattning

Mänskligheten kräver ständigt mer energi för att möta de växande behoven från vår civilisation. Som är välkänt kommer stora delar av denna energi i dagsläget från fossila källor, såsom kol och olja. Detta innebär två problem: delvis bidrar dessa energikällor till klimatförändringar genom utsläpp av växthusgaser, vilket förväntas drabba samhället mer och mer, och delvis är dessa energikällor icke-förnybara, vilket innebär att det finns en begränsad mängd av dem. Detta gör att även om de var oproblematiska att använda, kommer de för eller senare att ta slut.

Det kanske mest lovande alternativet för energiproduktion är solenergi. Solljuset som når planeten på en timme innehåller nämligen lika mycket energi som hela mänskligheten konsumerar på ett helt år. Solen är alltså en enorm, i princip permanent, energikälla utan problemen kopplade till fossila bränslen.

Det mest kända sättet att utnyttja solljus för energi är solceller av den typen man här och var kan se på hustak. Ett mindre vida känt alternativ för att ta till vara ljusenergi är så kallade fotosensibilisatorer. En fotosensibilisator är en molekyl vilken kan absorbera ljus för att sedan använda den energin för att generera diverse kemiska reaktioner. Från synvinkeln av energiproduktion så är det mest eftertraktat att fotosensibilisatorn ska delta i en kemisk reaktion som genererar bränslen. Det troligtvis mest eftersökta och mest kända exemplet på ett sådant bränsle är vätgas.

Viktigt för att förstå fotosensibilisators funktion är att molekyler till en del består av elektroner, och att elektronerna kan ha olika mycket energi. När fotosensibilisatorn absorberar ljus överförs ljusets energi till en elektron, som då antar ett stadie med högre energi. I ett exempel av en reaktion som utnyttjar denna energi kan sedan elektronen med högre energi skickas över till ett annat ämne som ska delta i reaktionen, där elektronen får en något lägre energi. Genom att elektronen genomgår en rad stadier med lägre och lägre energi byggs bindningarna mellan atomerna i reaktionen om, för att en eftersökt produkt (d.v.s. bränslet i vårt exempel) ska bildas. Slutligen återvänder elektronen till sin utgångspunkt i fotosensibilisatorn, där den har sin lägsta energi sen den sattes i gång av ljuset. Med detta är fotosensibilisatorn tillbaka som den var innan reaktionen och kan sedan absorbera mer ljus för att delta i en ny reaktion och generera mer produkt. När elektronen rör sig till lägre energistadier, lagras en del av energin som elektronen blir av med i de bildade kemiska bindningarna. Energin utvinns sedan igen när bränslet konsumeras.

Fotosensibilisatorer kan även användas för att bygga en solcell. Funktionen har då likheter med vad som beskrivs ovan, men elektronen som skickas ut går in i en elektrisk krets, i stället för att gå till en annan molekyl. Eftersom elektroner i en elektrisk krets är det samma som en elektrisk ström så bildas just det, elektricitet. Precis som ovan återvänder elektronen efter den elektriska kretsen till fotosensibilisatorn för att den ska återfå sin ursprungsform. När elektronen här går från en högenergi-placering till en lägre energi används energin som lämnar elektronen i stället för att driva en elektrisk apparat.

I denna avhandling har jag arbetat med att tillverka nya fotosensibilisatorer, baserade på järn. Järn är eftertraktat för den här typen av applikationer, eftersom det är en metall som det finns stora mängder av. Järn skulle därför kunna användas i stor skala, för att tillgodose de stora energibehoven som finns och är ökande. Järn har dessutom egenskaper som liknar andra metaller som används till fotosensibilisator, vilket vidare gör det till en lovande kandidat för dessa användningsområden. Dock är järn mindre mottagligt för de modifikationer av elektronernas utgångsenergier som behövs för fotosensibilisator-applikationerna. P.g.a. detta har här använts speciella så kallade ligander, vilka binds till järnatomer, för att försöka inducera det förändringar hos elektronerna som behövs. Tidigare forskning har kommit en god bit på vägen för att lyckas med att introducera de nödvändiga modifikationerna till järn, men ytterligare utveckling behövs för att järnet ska bli riktigt användbart. Här har jag därför arbetat med att introducera ytterligare förändringar hos liganderna, och sedermera järnet, för att ta det hela närmare en fungerande fotosensibilisator.

List of Papers

This thesis is based on and summarises the following papers:

† These authors contributed equally to this publication

I. **Dye-Sensitized Solar Cells based on Fe *N*-heterocyclic Carbene Photosensitizers with Improved Rod-like Push-Pull Functionality**
Linnea Lindh†, Olga Gordivska†, Samuel Persson†, Hannes Michaels†, Hao Fan, Pavel Chábera, Nils W. Rosemann, Arvind Kumar Gupta, Iacopo Benesperi, Jens Uhlig, Om Prakash, Esmaeil Sheibani, Kasper S. Kjaer, Gerrit Boschloo, Arkady Yartsev, Marina Freitag, Reiner Lomoth, Petter Persson, Kenneth Wärnmark
Chem. Sci. **2021**, *12* (48), 16035–16053

I took part in the development of synthetic procedure for the target complexes. I performed the majority of chemical characterisation of new compounds. I synthesised material for the spectroscopic measurements and assisted in several of these measurements. I contributed to the writing and editing of the manuscript.

II. **Amino-substituted Heteroleptic Iron *N*-Heterocyclic Carbene Photosensitizers in Dye-Sensitized Solar Cells: Optimization and Characteristics**
Samuel Persson†, Iacopo Benesperi†, Yogesh Goriya, Dnyaneshwar Kand, Suresh Rayavarapu, Timo Keller, Marina Freitag, Kenneth Wärnmark
Manuscript

I developed new synthetic procedures for two of the included complexes and carried out characterisation of these. I produced material of all included complexes for investigation. I performed solution-based spectrophotometry. I performed photovoltaic studies, including assembly and optimisation of DSCs devices, based on earlier optimisation performed for the publication. I performed *J-V* measurements of presented devices. I analysed the data with aid from other authors. I wrote the manuscript and supporting information and edited them with input from other authors.

III. **Iron *N*-Heterocyclic Carbene Photosensitizers with Rigid Phenyl-Ethynyl Substituents as Ligand π-System Extensions**
Samuel Persson[†], Raj Kumar Koninti[†], Mariam Barakat, Abhishek Mishra, Fredrik Lindgren, Tore Ericsson, Lennart Häggström, Sven Lidin, Ana Gonzalez, Elena Jakubikova, Reiner Lomoth, Kenneth Wärnmark
Manuscript

I developed and performed the synthesis of all new compounds. I performed all chemical characterisation of all new compounds. I co-wrote and edited the manuscript and supporting information, together with other authors.

IV. **Post-Complexation Hydrogenation of Imidazolylidene Units in Iron *N*-heterocyclic Carbene Complex Giving 75 ps Metal Centered Excited State Lifetime**
Suresh Rayavarapu[†], Arvind Kumar Gupta[†], Samuel Persson[†], Minli Zhang, Eyram Asempa, Mawuli Deegbey, Aleksandra Ilic, Jesper Schwarz, Fredrik Lindgren, Tore Ericsson, Lennart Häggström, Elena Jakubikova, Reiner Lomoth, Kenneth Wärnmark
Manuscript

I revised the synthetic method used to synthesise the studied complex and synthesised material for complementary spectroscopic studies. I synthesised starting material for synthetic experiment. I co-wrote and edited the manuscript and supporting information, together with other authors.

Publications not included in the thesis:

V. **Multifaceted Deactivation Dynamics of Fe(II) *N*-Heterocyclic Carbene Photosensitizers**
Linnea Lindh, Torbjörn Pascher, Samuel Persson, Yogesh Goriya, Kenneth Wärnmark, Jens Uhlig, Pavel Chábera, Petter Persson, Arkady Yartsev
J. Phys. Chem. A **2023**, *127* (48), 10210–10222

VI. **Side-group switching between metal-to-ligand charge-transfer and metal-centered excited state properties in iron(II) *N*-heterocyclic carbene complexes**
Linnea Lindh, Nils W. Rosemann, Iria Bolaño Losada, Samuel Persson, Yogesh Goriya, Hao Fan, Olga Gordivska, Kenneth Wärnmark, Jens Uhlig, Pavel Chábera, Arkady Yartsev, Petter Persson
Coord. Chem. Rev. **2024**, *506*, 215709

Symbols and Abbreviations

bpy	2,2'-Bipyridine
CB	Conduction band
CDCA	Chenodeoxycholic acid (3α,7α-dihydroxy-5β-cholan-24-oic acid)
cpbmi	1,1'-(4-carboxypyridine-2,6-diyl)bis(3-methylimidazolylidene)
CT	Charge transfer
CV	Cyclic voltammetry
CyJohnPhos	2-(Dicyclohexylphosphino)biphenyl
DCM	Dichloromethane
dba	Dibenzylideneacetone ((1*E*,4*E*)-1,5-Diphenylpenta-1,4-dien-3-one)
DIPA	Diisopropylamine
DMF	Dimethylformamide
DPPF	1,1'-Bis(diphenylphosphino)ferrocene
DSC	Dye-sensitised solar cell, also known as Grätzel cell
EDG	Electron donating group
EDTA	Ethylenediaminetetraacetic acid
E_F	Fermi level
ES	Excited state
EWG	Electron withdrawing group
FF	Fill factor
fs	Femtosecond
FTO	Fluoride doped tin oxide coated
GS	Ground state
HOMO	Highest occupied molecular orbital
Jsc	Short circuit current density
LDA	Lithium diisopropylamide
LMCT	Ligand-to-metal charge transfer
LUMO	Lowest unoccupied molecular orbital
MC	Metal centred

MeOTf	Methyl trifluoromethanesulfonate
MLCT	Metal-to-ligand charge transfer
MPN	3-Methoxypropionitrile
MPP	Maximum power point
NHC	*N*-heterocyclic carbene
ns	Nanosecond
OC	Open circuit
pbmbi	1,1’-(pyridine-2,6-diyl)bis(3-methylbenzimidazolylidene)
pbmi	1,1’-(pyridine-2,6-diyl)bis(3-methylimidazolylidene)
PCE	Power conversion efficiency
Pd/C	Palladium on activated carbon (10% palladium)
ps	Picosecond
rt	Room temperature
SC	Short circuit
$\mathrm{S_NAr}$	Nucleophilic aromatic (addition-elimination) substitution
TA	Transient absorption
TBAI	Tetrabutylammonium iodide
THF	Tetrahydrofuran, also known as oxolane
TMS	Trimethylsilyl
tpy	2,2’;6’,2”-Terpyridine
UV	Ultraviolet
VB	Valance band
*V*oc	Open circuit voltage
XPhos	Dicyclohexyl[2′,4′,6′-tris(propan-2-yl)[1,1′-biphenyl]-2-yl]phosphane

1 Introduction

1.1 Harvesting of solar energy

One of the great challenges facing society today is the energy production needed for an ever-growing civilization.[1-2] Solar energy is a strong contender to provide a solution to meet this need for energy, as can be seen from the fact that the amount of solar radiation reaching the Earth in an hour could is equal to the world's energy demands for an entire year.[3-4] Energy today is in majority taken from fossil sources, a well-known problem both due to their limited availability, as well as the greenhouse effect and pollution their use causes.[5-6]

Solar cells are perhaps the most straightforward possibility for solar energy utilisation, where light is converted directly into electricity.[7] Alternative processes where light-energy is stored as high-energy chemicals, in the form of fuels (e.g. hydrogen), would also be highly beneficial.[8-9] Finally, light could be used to obtain more complex and high-value fine chemicals and pharmaceuticals, making production of these more efficient.[10-11]

These types of processes require materials that can absorb light and utilise the energy contained in it. In solar cells, these materials commonly consist of semiconductors that generate electricity via the photovoltaic effect.[7, 12] The direct production of chemicals with the use of light could also involve the use semiconductors or so-called photosensitisers, that participate as energy mediators in chemical reactions.[13-15] Photosensitisers can additionally also be used in certain applications for the generation of electricity.[16-17]

The solar harvesting technology available today cannot meet these energy demands, and research into improving these technologies is thus currently ongoing.[4] To improve upon this there is both a need to improve upon the efficiency of the solar harvesting capabilities of the methods used, as well as limiting the use of costly materials and work-intense processes used for their manufacture.[1]

1.2 Aim and outline

Within this work are reported various efforts to utilise iron for light harvesting. This is in the form of iron-based coordination complexes that implements *N*-heterocyclic carbene (NHC) ligands, which is a type of photosensitisers that has been investigated over the last decade. Specifically, this thesis focuses on the use of meridionally binding, tridentate ligands consisting of two imidazolylidene NHCs and one pyridine, arranged in a C^N^C binding motif to the iron centre. Investigations have been carried out to achieve a general improvement of light harvesting and photosensitiser properties of these complexes, as well as the possibilities of using these in the direct generation of electricity in photovoltaic devices. The studies oriented towards finding modifications to this core C^N^C structure, as to improve the photophysical behaviour of the complexes, as well as providing structures that can give additional insight into the dynamics at play.

Introductory chapter 2 outline the function of photosensitisers in general and the challenges and possibilities of using iron complexes (in particular iron-NHC complexes) for such applications. Chapter 3 then moves on to outline the function of solar cells with a particular focus on those devices utilising photosensitisers, particularly those based on iron-NHC complexes.

Chapter 4 discusses the development of various heteroleptic iron-NHC complexes from design principles, to synthesis, to the behaviour of these, particularly in photovoltaic devices. This is followed by a continued study into the further development of photovoltaic devices by modification of the various components of the solar cell devices, beyond the photosensitisers, further improving their efficiency. The chapter also discusses findings regarding the specific properties of devices utilising iron-NHC complexes.

Chapter 5 is focused on the development of a series of iron-NHC complexes with extended ligand structures based on phenyl-ethynyl moieties, and the properties of these complexes as photosensitisers. The chapter also relates the so far unrealised attempts to implement these complexes in photovoltaic devices.

Chapter 6 focuses on the modification of the imidazolylidene structures by hydrogenation, and the effect of this on the photosensitiser properties of iron-NHC complexes.

2 Photosensitisers

2.1 Basic principles

A photosensitiser is a molecular entity which has the ability to absorb light and as a result induce a chemical or physical change in another molecular entity.[18] Photosensitisers based on many different principles and materials have been introduced and developed over time. Photosensitisers based on transition metals are widespread, with ruthenium and iridium being among the most commonly used metals,[19-22] but there are also purely organic photosensitisers that also have been extensively investigated.[22-24]

The function of photosensitisers revolves around a change in the electronic structure upon absorption of light. Simplistically, this consists of the promotion of an electron from one orbital to another orbital of higher energy. The overall distribution of electrons is termed an electronic state. The electronic state induced by the absorption of a photon, where there are unfilled orbitals at lower energies than the highest occupied orbital, is termed an excited state (ES). The energy difference between the electron in its original orbital, and the electron's energy in the new one it comes to occupy, will be matched by the photon absorbed to induce the electronic transition (Figure 2.1).[25-26] After the excitation, the energy absorbed should preferably somehow be utilised. This can involve the transfer of the energy to another species, to induce an excitation in this other species instead. The most common use of the photoexcitation is however electron transfer, where the excited photosensitiser acts as an oxidant or a reductant, respectively by an electron being transferred from the other species to the newly formed electron vacancy in the photosensitiser, or the excited electron being transferred to another species.[27-28]

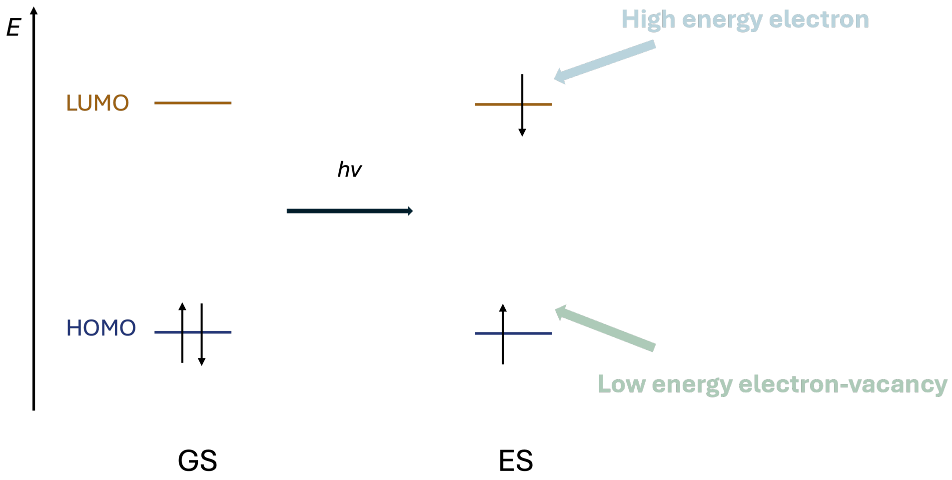

Figure 2.1: Schematic drawing of the orbitals in an arbitrary photosensitiser, and the electron promotion occuring upon absorbtion of a photon.

The nature of light-induced electronic transitions is such that overlap between the wave functions of each state involved in the transition is required, for the transition to be possible. This gives rise to so-called selection rules, predicting if a certain electronic transition may or may not occur. Electronic transitions that would go against a selection rule are said to be forbidden. Due to interactions between the various nuclei and electrons of the molecule, principally forbidden transitions commonly result in the concerned transition absorbing a small fraction of incoming photons of the correct energy (as opposed to no incoming photons), and will thus have a low extinction coefficient (meaning low molar absorption light).[29]

One selection rule states that the for a transition to be possible, no change in overall spin-state of the molecule may occur during the transition. Spin forbidden transitions can however still be observed to some extent, due to electrons transitioning between orbitals, thereby counteracting the change in angular momentum (this is termed spin-orbit coupling).[26, 29] The need to conserve the spin-state means that the spin of the excited electron is unchanged upon excitation. If all electrons are paired before excitation, the transition takes place from one singlet state to another. In transition metal complexes, since higher spin multiplicities are more stable, the excited electron commonly quickly undergoes a spin flip, giving a triplet state. Such a transition to another state of a different spin is termed an intersystem crossing.[27] Another selection rule concerning symmetry elements, when applied to centrosymmetric molecules, is the Laporte rule. This rule states that the change in occupied orbitals occurring during the electronic transition must involve a change in parity of the involved orbitals (gerade to ungerade, or vice versa). This for example forbids transitions between two d-orbitals or an s-orbital and a d-orbital.

However, also this rule is not absolute, due vibrations in the molecule leading to modes of appropriate symmetry for transition, being entered by the complex.[29-30]

Once the photosensitiser has been excited, it can from there enter another state of a lower energy. For this change in electronic state to have a high probability of occurring, the change must take place at a point where the difference in bond lengths (nuclear coordinate) and energy between the states are small. Such a point may be reached by the molecule traveling along a potential energy surface defined by nuclear coordinate and energy. Simply put, the molecular bonds oscillate, resulting in an overall different potential energy of the system. If the molecule enters a nuclear coordinate that overlaps with another electronic state, where the two states also have the similar energy, a transition between the states can occur. This is known as radiationless decay. The new state will commonly be entered at a higher vibrational level, from where the excess energy can be displaced to the overall system as heat. (Figure 2.2a).[26, 29, 31]

If these types of radiationless decay are not favoured to occur due to poor overlap of the states, radiative deactivation is another possible path for the photosensitiser to return to ground state (GS). This occurs by the excited molecule emitting a photon corresponding to the energy gap between the ES and the GS. Radiative deactivation also leaves the molecule in question at the same nuclear coordinate. (Figure 2.2b).[26, 29, 31]

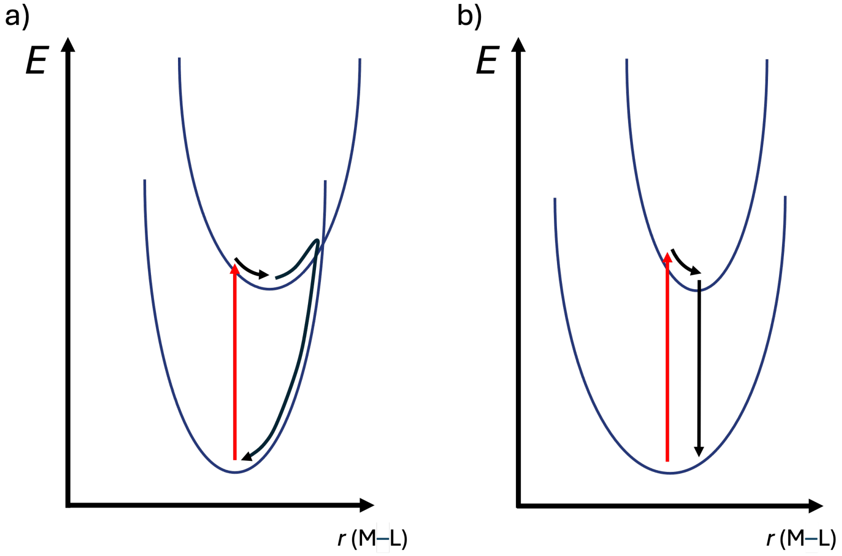

Figure 2.2: Schematic representation of the potential energy surfaces involved in photoexcitation (denoted by red arrow) and subsequent deactivation (denoted by black arrows) between two different electronic states. a) shows radiationless decay while b) shows radiative decay. Note the lack of overlap between the curves in b.

In photosensitisers based on transition-metal complexes, much of the photophysical behaviour revolves around the interaction between the frontier orbitals of the metal and the ligands. Consider an octahedral transition-metal complex with ligands having orbitals with π-character (e.g. tris(bipyridine)ruthenium(II) ($[Ru(bpy)_3]^{2+}$)). This complex will have the normal orbital splitting of the metal d-orbitals into the t_{2g}, and e_g set of orbitals (mainly resulting from bonding interactions between ligand orbitals of σ-bonding character, and the metal's d-orbitals), as well as the ligand based π-orbitals that have only minor interaction with the metal-based orbitals (Figure 2.3). This results in transition-metal complexes mainly being excited into so called charge transfer (CT) states. Photoexcitation from the t_{2g} set of orbitals to π*-orbitals formally gives rise to the metal-to-ligand charge transfer (MLCT) excited state, while transitions from π-orbitals to the t_{2g} set of orbitals give the ligand-to-metal charge transfer (LMCT) excited state (Figure 2.3). Whether MLCT or LMCT occurs is dependent on the occupancy level of the involved orbitals, as well as the energy level of the various orbitals.[25, 32-33] MLCT excitations can further be characterised as an oxidation of the metal and reduction of the ligand (and vice versa for LMCT excitations), meaning that the redox potentials of the involved parts of the complex are of importance in understanding these excitations.[28, 34-35]

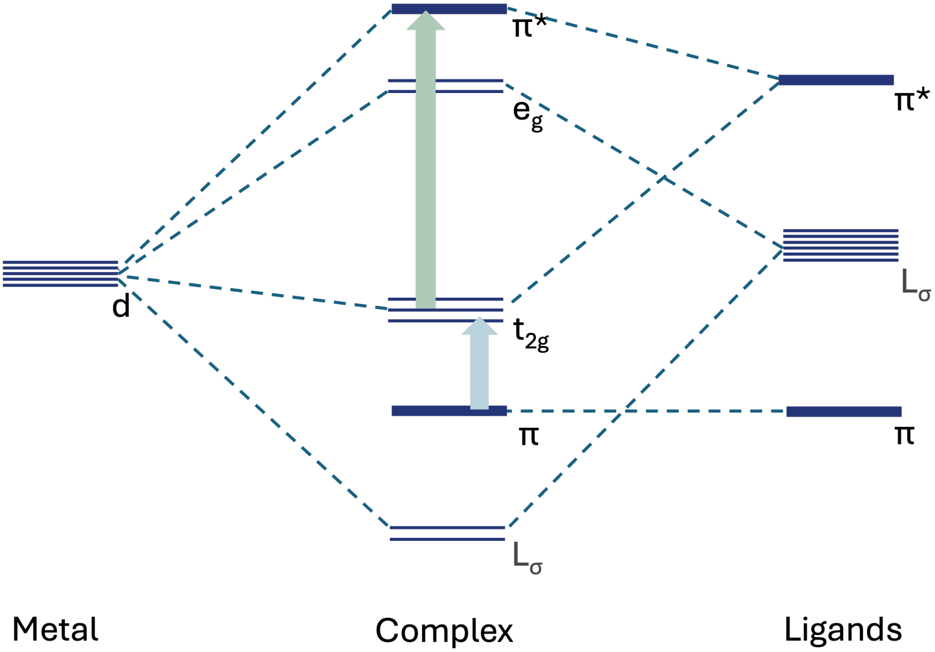

Figure 2.3: Schematic drawing of the frotier orbitals of transition metal and incoming ligands, as well as orbitals of the resulting complex. Bolded lines denote an indeterminate number of π-orbitals. $L_σ$ denote linear combinations of ligand-orbitals with σ-character with regards to the metal. Green and blue arrows denote a possible MLCT and LMCT transitions, respectively.

A number of properties are important for a photosensitiser to have the proper function. Firstly, the photosensitiser needs to absorb as much light as possible in order to efficiently convert photons into chemically useful reactions. This relates to a high extinction coefficient, as for the maximal number of incoming photons to result in ESs. This is necessary for the photosensitisers to participate in the maximal number reactions with other species, as is integral to their function. To utilise photosensitisers for absorption of sun or ambient light, the absorption should preferably be panchromatic (able to absorb light from the whole visible spectrum) as well. As the excited photosensitiser should be able to transfer its absorbed energy to another species, there is also a need for the ES to last for a long enough time, before relaxation to the GS (commonly termed the ES lifetime), for the electron transfer event to take place. In solution-based chemistry, this type of reaction is diffusion controlled, and takes place on a nanosecond timescale. Thus, the ES should preferably be present for at least a number of nanoseconds.[28, 35] This hurdle can however be circumvented by pre-coordination between photosensitiser and substrate.[36]

For the transfer of electrons to and from the photosensitiser to be efficient and drive a reaction, there is a given need for the electron transfer to have a thermodynamic driving force of an appropriate magnitude. There is thus a need to tune the photosensitiser to the task it needs to accomplish, so that its electronic states are of an appropriate energy for proper interaction with the other species in reaction. Furthermore, the photosensitiser should be stable and not be subject to decomposition, even in an ES where anti-bonding orbitals are populated.[10, 28]

Most commonly in transition-metal based photosensitisers, the ES that is utilised is a CT state, as discussed above.[14, 28] This is for several, interconnected reasons: firstly, the CT excitations are allowed by the selection rules described above, meaning that the extinction coefficient will be larger and more incoming light may be used to drive a desired process (as opposed to transitions that occur between metal-based orbitals, which are Laporte forbidden).[28, 30] The CT state should then preferably also be the state used to drive the reaction, as transition to another state by necessity means a loss of energy, consequently not utilised in the reaction. Additionally, the CT induces an intramolecular charge separation, conducive to the redox-type reactivity normally desired for the photosensitiser to participate in.[28, 34] Functional photosensitisers with a long-lived metal centred (MC) excitations have however also been demonstrated.[37-38]

2.2 Investigation and characterisation

Among the simplest photophysical investigations available for photosensitisers is steady state spectrophotometry. This gives basic insight into the energy of the ESs that are active during the photochemical processes of the photosensitiser under study.[29, 31]

The ES lifetime of a given photosensitiser can be measured in different ways. If the ES is emissive, the intensity of the emission can be measured over time after an initial excitation. This can in essence give the lifetime of the emissive state. Various techniques can achieve this, with varying resolution.[29, 39-40]

If the ES is non-emissive, other methods are needed to probe the ES. Transient absorption (TA) spectroscopy is essentially a spectrophotometric measurement of an already photoexcited species. By doing this with a variety of delay times between initial excitation and a second measurement, it is possible to observe the development of the ES over time. This can be done either by probing the ES with white light or with a single wavelength for each measurement, depending on the precise method used. This also allows for a more intricate investigation of the ES, as it can detect the conversion between different ESs, before the photosensitiser returns to GS.[29, 31, 39]

Furthermore, various insights can be gained from the electrochemical characteristics of the photosensitiser (or the species which it is to interact with). These are commonly obtained by cyclic voltammetry (CV). In CV, the compound of interest is dissolved in an electrolyte and (with the use of a working electrode and a counter electrode), a potential is applied over the solution of compound and tracked against a chosen reference electrode. By then changing the potential and tracking the flow of electrons to and from the solution (i.e. the current), it is possible to ascertain the potential at which the compound is oxidised or reduced, depending on if the potential is increasing or decreasing. The scanning direction is then reversed and modulated until the potential returns to the starting point. This is repeated a number of times, allowing for determination if the investigated compound reacts further after the redox event or if the oxidised/reduced species remain intact.[41] This can begin with give insight into the ability of the photosensitiser to donate and accept electrons from various species, by comparing oxidation and reduction potentials of the reacting species. This is, as discussed above, integral to the function of a photosensitiser.[42]

Finding the potential of metal oxidation and ligand reduction furthermore gives an estimate of the energy of an MLCT transition, as this transition is akin to a simultaneous oxidation of the metal and reduction of the ligand, as mentioned above. Similar reasoning can also be used to investigate LMCT transitions.[28, 34]

Electrochemical oxidation/reduction of molecular species can also be coupled to spectroscopic techniques, in what is called spectroelectrochemistry. This allows for the investigation of *in-situ* electrochemically generated species that may otherwise be too short-lived to be studied.[43-44] This allows for determination of the spectroscopic signature of oxidised and reduced species formed in redox reactions, for the purpose of monitoring these reactions.[28] Spectroelectrochemistry has further been used in the assignment of absorption features in ES absorption of a CT excited state, again by equating a MLCT states to an oxidation of the metal and reduction of the ligand and that the ES should have absorption properties of both. While this approach has limitations, the method can in concept allow for the distinction of different absorption features in the same ES.[45-46]

2.3 Iron carbene photosensitisers

2.3.1 Comparison of iron and ruthenium photosensitisers

Iron coordination complexes that function well as photosensitisers have been pursued for some time.[21, 35] As iron is isoelectronic with ruthenium, a metal commonly used in photosensitiser complexes, it stands to reason that iron could likewise have properties conducive to use as a photosensitiser.[35, 47] Furthermore, as iron is the second most abundant metal in the Earth's crust (after aluminium) by mass (and fourth most abundant in general),[35, 48] it has the makings of being widely and cost-effectively applied.

Iron does however have certain characteristics that put it apart from ruthenium, which make its use in photosensitisers significantly more challenging. The smaller size of iron leads to a lower polarizability of the metal-based orbitals. This means that for equal ligand sets the orbital splitting of the metal d-orbitals is smaller in iron than it is in ruthenium.[21] At the same time, the MLCT transition is, as touched on above, more closely related to the oxidation potential of the metal and reduction potential of the ligand, meaning that the energy of the MLCT transition is somewhat decoupled from the energy levels the orbitals. These facts together mean that while the MC states of iron are lower in energy compared to those in ruthenium, the MLCT energy level is similar for both metals. Figure 2.4a shows a Tanabe-Sugano diagram of d^6-complexes. The effective ligand field strength experienced by iron and ruthenium with a tris(bpy) ligand set is marked in this diagram. This thus shows the energy levels of the resulting MC states for each type of complex (MC states are in the diagram denoted by the states A, T and E, the superscript denoting spin-multiplicity). This is compared to the MLCT state, which is at a common energy level for reasons explained above. MC states for each ruthenium and iron thus end up above or below the MLCT state, respectively.[34] Thus, in the case of iron, an unoccupied, lower-lying e_g set of orbitals are available for forming a low-lying MC state. (Figure 2.4b).

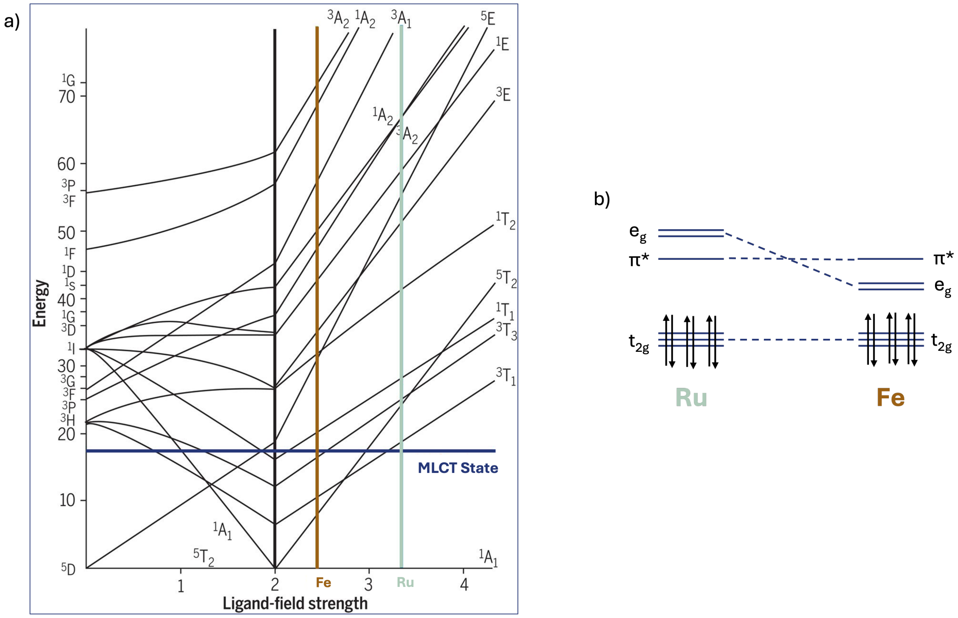

Figure 2.4: The difference in energy states between tris(bipryridine) complexes ($[M(bpy)_3]^{2+}$) of ruthnium and iron. a) Tanabe-Sugano diagram, showing the energy of the various MC excited electronic states compared to the GS, for a d^6-complex, depending on ligand field strength. The ligand field strengths of $[Fe(bpy)_3]^{2+}$ and $[Ru(bpy)_3]^{2+}$are marked in the diagram. The energy level of MLCT state applicable to both complexes is also shown. b) Simplified picture of the frontier orbitals of complexes of each metal. a adapted from Ref. 34. Reprinted with permission from AAAS.

The electronics of iron complexes thus results in a MC excited state being available through which a deexcitation can take place from the π*-orbital, i.e. from the MLCT state (Figure 2.5).[49-50] The smaller splitting of orbitals in first-row transition metals has also been linked, as a way of explaining the metals' lower polarizability, to the fact that the 3d-orbitals, which are the orbitals participating in bonding for these metals, lack radial nodes. This means that the 3d orbital extend less beyond the occupied 3s- and 3p-orbitals, which weakens orbital interactions and hampers bonding.[34]

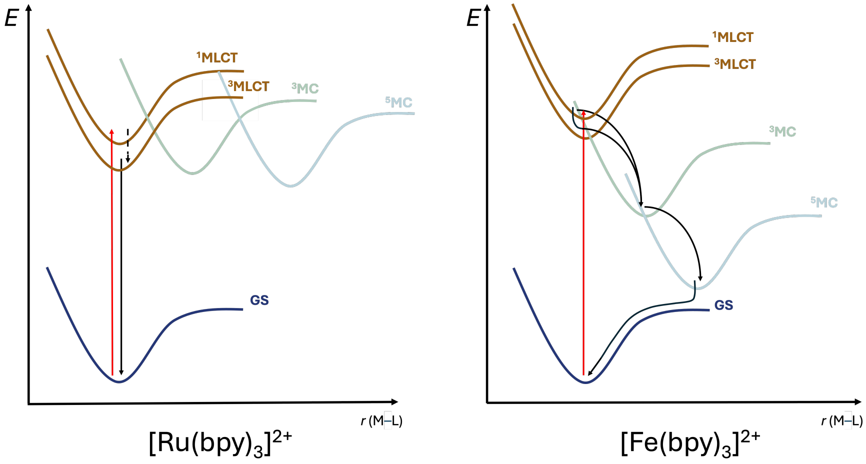

Figure 2.5: Schematic picture of potential energy surfaces, qualitatively showing the energy states of $[Ru(bpy)_3]^{2+}$ and $[Fe(bpy)_3]^{2+}$, as well as the dynamics of the photoexcitation. Red arrow denotes photoexcitation while black arrows denote deactivation (radiative deactivation in the case of $[Ru(bpy)_3]^{2+}$). Adapted from Ref. 47 — copyright 2016 American Chemical society.

2.3.2 Using NHCs to improve the excited state properties of iron complexes

To achieve the ES dynamics found in ruthenium, the relative energies of the e_g set of orbitals and the π^* set of orbitals in iron, should be reversed as described in the previous section. For this purpose, stronger σ-donating ligands were of interest for achieving larger ligand field splitting, by a stronger interaction with the e_g-orbitals to increase their energy to be closer to, or preferably above, the π^*-orbitals. Examples of such strong σ-donors are NHCs. NHCs are cyclical, non-charged organic moieties containing one carbene atom and at least one nitrogen atom. The most common form of NHCs are five-membered rings with two nitrogen atoms, one on either side of the carbene atom (essentially based on an imidazole structure with a carbene atom in the 2-position, then called imidazolylidene; Figure 2.6). This gives NHCs their particular properties. The nitrogen atoms mesomerically stabilise the empty orbital at the carbene (Figure 2.6a), while inductively stabilising the free electron pair of the carbene (Figure 2.6b). This yields a structure that is relatively stable (commonly very stable when coordinated to a metal) for being a carbene, and strongly σ-donating to metals (Figure 2.6c).[51-53]

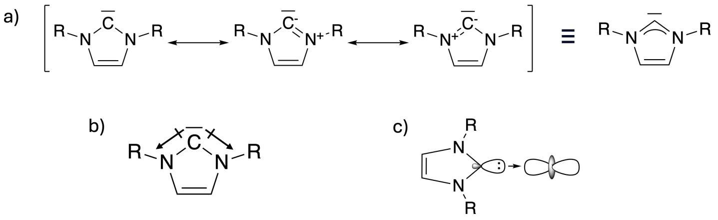

Figure 2.6: Principles governing NHCs (imidazolylidene taken for example). a) Mesomeric stabilisation of empty p-orbital at carbene. b) Inductive stabilisation of free electron pair at carbene. c) σ-donation of free electron pair at carbene into an empty metal d-orbital.

NHCs have thus been used with iron, in an attempt to increase the energy of the e_g-orbitals (due to the binding interaction between ligand and metal; Figure 2.3), and consequently any MC excited states, to make these less available as a relaxation pathway. As the strategy does not place the MC state above the MLCT state, the stabilisation seen is by creating a higher barrier for transition between states, placing the cross over point between states at a higher energy (Figure 2.7).[47, 54] A pyridyl based unit of the ligand was also introduced in early realisations of this strategy, as to have an aromatic system that could provide an appropriately low-lying π*-orbital that could accept electrons and provide the possibility of an MLCT transition. The pyridine was assumed necessary as NHCs have relatively poor π-accepting properties. Pyridine furthermore provided structural stability to the complex, while also serving as a starting point for further functionalisation to tune sensitiser properties (Figure 2.8).[47]

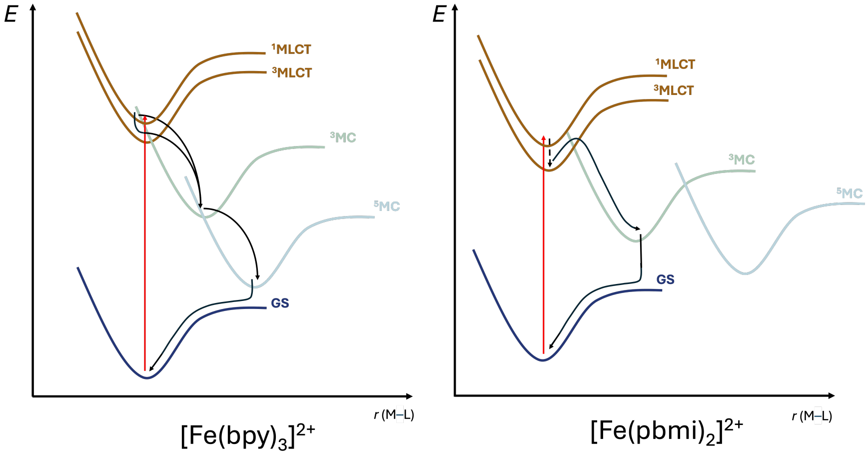

Figure 2.7: Schematic picture of potential energy surfaces qualitatively showing the energy states of Fe(II) complexes with bpy ligands and NHC-containing pbmi ligands. Also shows the dynamics of the photoexcitation. Red arrow denotes photoexcitation while black arrows denote deexcitation Adapted from Ref. 21 and Ref. 47 — copyright 2016 American Chemical society and 2019 Wiley -VCH Verlag GmbH & Co.

First attempt in realising the iron-NHC strategy was in the form of the complex $[Fe(pbmi)_2](PF_6)_2$ (**1** in Figure 2.8) (pbmi = 1,1′-(pyridine-2,6-diyl)bis(3-methylimidazolylidene)). From TA spectroscopy it was found that a somewhat long-lived ES, that was determined to be MLCT in character, was achieved through this strategy. This ES had a lifetime of 9 ps, as compared to 145 fs for the MLCT lifetime in the bis(terpyridine)iron(II)-complex ($[Fe(tpy)_2]^{2+}$).[54] The poor π-accepting character of the NHCs still proved a hinderance, despite the retention of a pyridine unit, as the π*-orbitals of the pbmi ligand were also at a higher energy, compared to a pure polypyridyl system.[47] Nevertheless, this provided the first step and proof of principle towards obtaining an iron photosensitiser by the use of strongly binding NHC ligands.

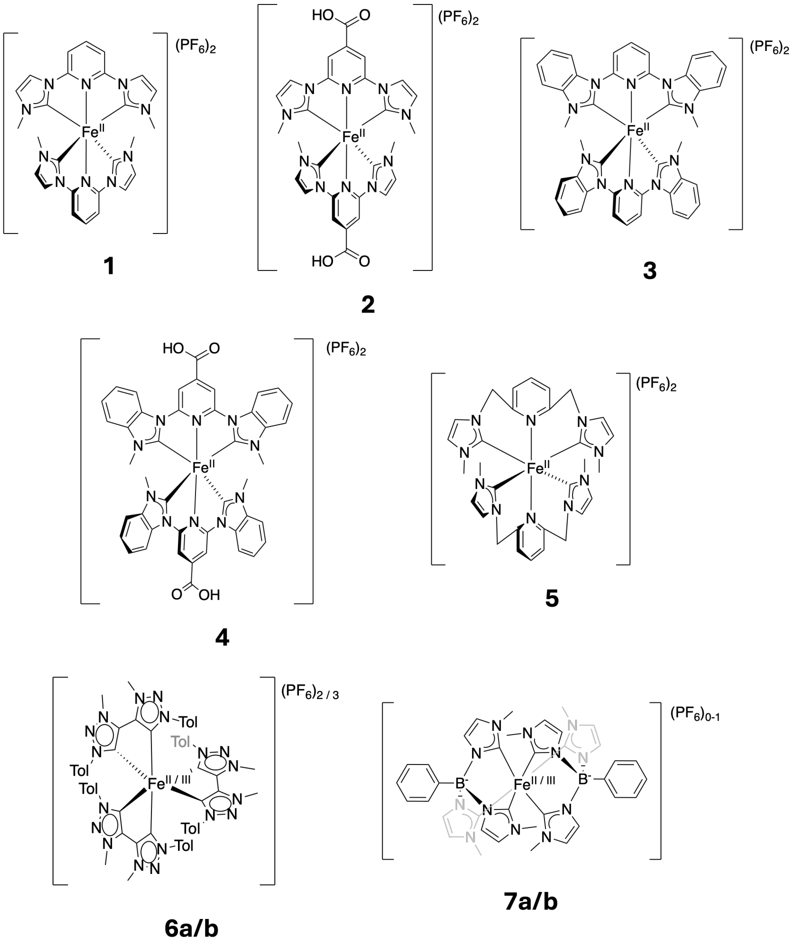

Figure 2.8: Structure of various iron-NHC photosensitisers exemplifying various concept and properties of this type of compounds. a and b respectivly refers to the Fe(II) and Fe(III) forms of the so marked complexes.[54-63]

Alternative strategies to achieve improved photosensitiser properties of iron have been explored in the literature and may be used separately or in conjunction with the strong σ-donating ligands described above. This can involve the lowering of the π*-orbitals in energy, to place it lower in energy than the e_g set of orbitals (rather than moving the e_g-orbitals above the π*-orbitals). This can be achieved by placing electron withdrawing groups (EWGs) on the ligand, or by extending the π-system of the electron-accepting ligand (Figure 2.9). These strategies can also be combined with the strong σ-donor ligand to simultaneously shift the orbitals in an advantageous fashion.[35, 47, 64] In combination with NHC ligands, this effect can for example be seen in the case of $Fe(cpbmi)_2$ (**2** in Figure 2.8) (cpbmi = 1,1′-(4-carboxypyridine-2,6-diyl)bis(3-methylimidazolylidene)), where the introduction of the electron withdrawing carboxylic acid extends the ES lifetime to 18 ps, as compared to 9 ps for the unsubstituted parent complex (**1** in Figure 2.8).[55-56] The introduction of the carboxylic acid also shifts the metal centred t_{2g} set of orbitals/HOMO to a lower energy, but this is much less pronounced than the effect on the π*-orbital.[55] This then gives the observed effect on the lifetime on the ES.

The π*-orbital levels can, as mentioned, also be lowered by an extension of the π-system of the ligand accepting an electron during the MLCT excitation (Figure 2.9). An example of this can be seen in the case of $Fe(pbmbi)_2$ (**3** in Figure 2.8) (pbmbi = 1,1′-(pyridine-2,6-diyl)bis(3-methylbenzimidazolylidene)), reported by Gros et al., where each imidazole subunit is replaced with benzimidazole. This achieved an MLCT lifetime of 16 ps, and also showed that the NHC units have some participation in accepting electron density during MLCT excitations in these complexes. The use of an EWG and an extended π-system can also be combined, as in the complex **4** (Figure 2.8), achieving an MLCT lifetime of 26 ps.[57-58]

Improving the octahedricity of the ligand cage also has the potential to improve the properties of an iron-based photosensitiser. This is by improving the orbital overlap between the ligand and the metal-based d-orbitals, which increases the strength of the bond between the iron and the ligands. In essence, improved octahedricity can thus have the same effect as improving the inherent σ-donation of the ligand (Figure 2.9).[21, 47, 64] A strategy like this have been investigated by Gros et al., using the complex **5** (Figure 2.8). The investigation however also relied on a structure were the π-system of the whole ligand was disrupted by methylene bridges, seemingly giving the ligand structure more flexibility, which opens the system up to vibrational modes that led to a lowering of the barrier of transition between states and give faster deactivation via MC states.[59] Another study came to a similar conclusions using an iron-tris(bidentate) structure (also with methylene spacers).[65] While the use of improved octahedricity has the promise to be able to give improved photosensitiser properties,[21] it has yet to be successfully realised in the sphere of iron-NHC complexes.

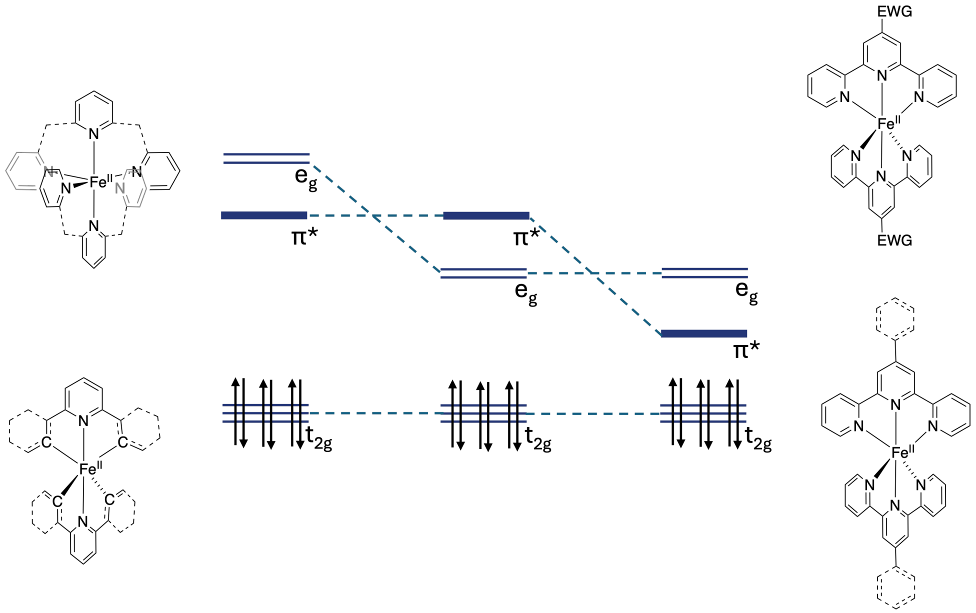

Figure 2.9: Generalised strategies for affecting orbitals of an iron complex, for improved photosensitiser properties. Iron bis(tpy) taken as example starting point for modifications. Left: increse in ligand field splitting of metal centred orbitals, by improved orbital overlap or strongly σ-donating ligands. Right: stabilisation of the ligand centred π*-orbitals, by introduction of EWGs on the ligand or extension of the ligand π-system.

Further adding to the usefulness of iron-NHC complexes is their method of synthesis. Commonly, it is a simple matter of adding the desired pre-carbene ligand, and deprotonating it to form the free carbene (most often using KO*t*-Bu as a base), before adding an iron(II) halide salt to coordinate with the carbenes in solution. The syntheses have however been limited by relatively poor yields of these reactions. Purification of the complexes has additionally in many cases required relatively arduous processes.[54-55, 58] As the field has matured there have been additional reports of complexation reactions that have been more successful in terms of yields, in several cases by utilizing other bases.[66-67] Further methods for the synthesis of metal-NHC complexes are widely explored in literature and could prove useful for the synthesis of iron-NHC complexes as well.[51, 53]

Some doubt has recently been put into the nature of the ESs in these basic iron-NHC systems discussed above. Ultra-fast TA spectroscopy revealed evidence that the MLCT state formed in certain reported iron-NHC complexes decays to an MC state within a sub-ps timescale, with this resulting MC state in fact being the one with a multi-ps lifetime. This has for example been suggested to be the case in complex **1** (Figure 2.8). Introduction of EWGs to lower the π*-orbital however shows an MLCT state stable enough were no evidence to contradict a multi-ps MLCT lifetime can be found. The MLCT excited state, would thus seem very finely balanced and small modifications can seemingly make its ultrafast deactivation a possibility.[68-69] The validity of this assignment has however been disputed by other studies,[70] and further investigations are necessary to come to a conclusive determination.

Since their first introduction, several different iron-NHC complexes have been investigated and reported, in order to achieve a variety of goals. Among the most noteworthy continuations is the move from a tetracarbene structure to a hexacarbene structure. This naturally imposes an even stronger ligand field, and the increased effect led to great improvement in MLCT lifetime. The lack of a competent π-accepting system in direct contact with the metal seems to not have hampered the efficacy of the photosensitiser to an inordinate degree. It can however be noted that relatively large aromatic units are available that might serve as π-acceptors (**6a** in Figure 2.8).[60] There are however also examples where the Fe(II) hexacarbene complexes have much more unstable MLCT states, possibly due to a lack of appropriate π-acceptor (**7a** in Figure 2.8).[61]

In addition to these Fe(II) complexes, various hexacarbene Fe(III) complexes are known as photosensitisers. The higher electron density introduced by the several σ-donating NHC-ligands makes the Fe(III) state the most stable oxidation state of the iron in such hexacarbene complexes. The main excitation in these photosensitisers is consequently LMCT in nature, rather than MLCT as in the complexes discussed above. This has shown great success in generating long-lived photo-generated CT states for an iron complex, giving lifetimes as long as 2 ns. These LMCT states are also emissive (**6b** and **7b** in Figure 2.8).[62-63]

Other paths towards achieving long-lived CT states in iron photosensitisers have also been presented in the literature. Among the most successful to date is the use of cyclometalated Fe(II) bis-tridentate complexes capable of achieving MLCT lifetimes of 1 ns and displaying luminescence (**8** in Figure 2.10). This is seemingly from achieving the promise of placing the ^{3}MLCT state as the lowest lying ES by applying the methods discussed above.[71] Another successful report involves a strategy apart from the ones mentioned so far, where a rigid ligand structure has successfully placed the potential energy surfaces of the various energy states in such a way that no efficient deactivation pathway from the MLCT state is available, despite lower-lying states being present. This is by denying an available crossover point between states (**9** in Figure 2.10). This achieved an MLCT lifetime of 1.25 ns, but no luminescence.[72]

There are further reports of iron complexes that were originally reported to have long-lived the MLCT states. One is a Fe(II) complex using strongly binding amido ligands coupled to ligands with extended π-systems, a strategy analogues to those described above (**10** in Figure 2.10). This was initially reported as having an MLCT excited state lifetime of 2.5 ns. Further investigation however proved this ES to be

MC in nature.[46, 73] While still an achievement, it additionally serves to show the intricacies of understanding and characterising these types of systems.

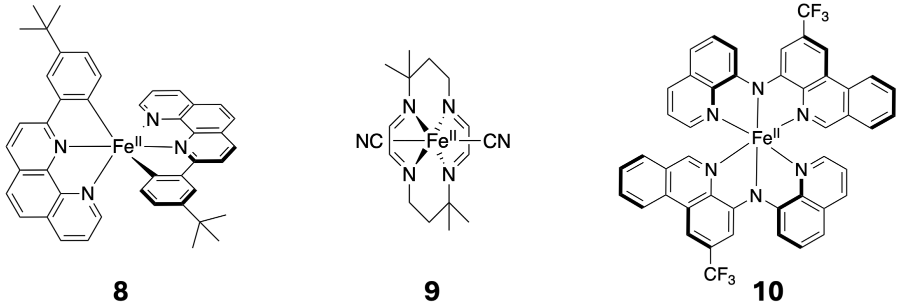

Figure 2.10: Structure of various Fe(II)-based photosensitisers that have achieved ns excited state lifetime. ES is of MLCT character for complex **8** and **9**, and ligand field in nature for **10**.[71-73]

3 Dye-sensitised solar cells

3.1 Basic principles of solar cells

Solar cells are devices used to convert the energy from photons into electricity. This is principally accomplished by the generation of a charge separation within a surface, with the resulting electrical potential being exploited to generate an electrical current.[7] Within the crystalline silicon solar cells, which are the type of devices that are wide-spread and commercially available,[12] this charge separation is induced in the interface of two silicon-based semi-conductors of different types.[7]

Integral to the full understanding of the working principles of solar cells is the concept of valance band (VBs) and conduction bands (CBs) within solid state materials. These bands are energy levels in a solid which can be occupied by electrons. The difference between the two is that, at the equilibrium state of the material, the VB is occupied by electrons while the CB is not.[29-30] Coming from the point of view of molecular chemistry, it can be helpful to see the VB and the CB as being respectively analogous to the HOMO and LUMO found in a molecule.[29, 74] The difference in energy between the VB and the CB is termed the band gap.[29-30] A semiconductor has its Fermi level (E_F), which is the (hypothetical) energy level of a material that has 50% chance of being occupied at thermodynamic equilibrium, located between the highest energy level of the VB and the lowest level of the CB. The composition of a semiconductor can shift the energy levels of these bands up or down. If the VB is close in energy to the E_F, the semi-conductor is of p-type, while if the CB is close in energy to the E_F, the semi-conductor is of n-type.[7, 29]

This is the basis for the function of a crystalline silicon solar cell, in which a n-type and a p-type semiconductor are fused together. Photoexcitation of an electron from the VB to the CB in the p-type semiconductor, gives the possibility for the migration of the excited electron in the lower lying CB in the n-type side of the solar cell. This generates the above-mentioned charge separation and can give rise to an electrical current (Figure 3.1).[7, 12]

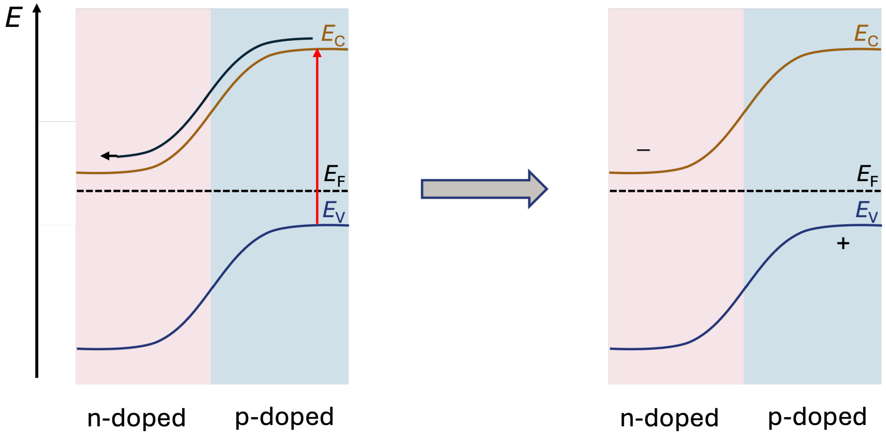

Figure 3.1: Schematic diagram energies of the valance band (E_V) and conduction band (E_C) in a crystalline silicon solar cell. The arrows in the left diagram show the movement of an electron upon photoexcitation, with the red arrow denoting the initial photoexcitation. The right diagram shows the charge separation developed by the photoexcitation.

The most important measure of a solar cell is the power conversion efficiency (PCE). This measures the maximal percentage of the energy in the incoming light which can be converted into electricity. This is found by constructing a so-called J-V curve, which is done by incrementally modulating the potential between the two sides of the solar cell under illumination and measuring the resulting current. For each voltage-value, a corresponding current is thus given, resulting in a curve (see Figure 3.2 for an arbitrary example of this). When the potential is set high enough no current can flow, giving the open circuit voltage (V_{OC}). Reversely, when the potential is set to zero the current becomes as high as possible, giving the short circuit current (J_{SC}). Each point at the J-V curve correspond to the power output for a given potential (and corresponding current), as the product of voltage and current gives the power. This also allows for finding the *maximum power point* (MPP) were the product of voltage and current is at its highest (which directly means the power is the greatest). This is of importance as the ultimate purpose of a solar cell is to power an electrical device, requiring an appropriate power output. Comparing the power output in this point to the power of the incoming light gives the PCE (Equation 3.1).[7, 74]

Furthermore, comparing the product of voltage and current in the MPP to the product of the J_{SC} and V_{OC} gives the so-called fill factor (FF), the factor by which the product of J_{SC} and V_{OC} needs to be multiplied to give the power in the MPP (Equation 3.1). FF can also be considered a measure of the “squareness” of the J-V curve, indicating the ability of the solar cell to have a simultaneous output of current and potential.[7, 74] See Figure 3.2 for these above-mentioned concepts visualised in a J-V curve.

$$PCE = \frac{P_{MPP}}{P_{light}} \times 100\% = \frac{V_{OC}J_{SC}FF}{P_{light}} \times 100\% \qquad (3.1)$$

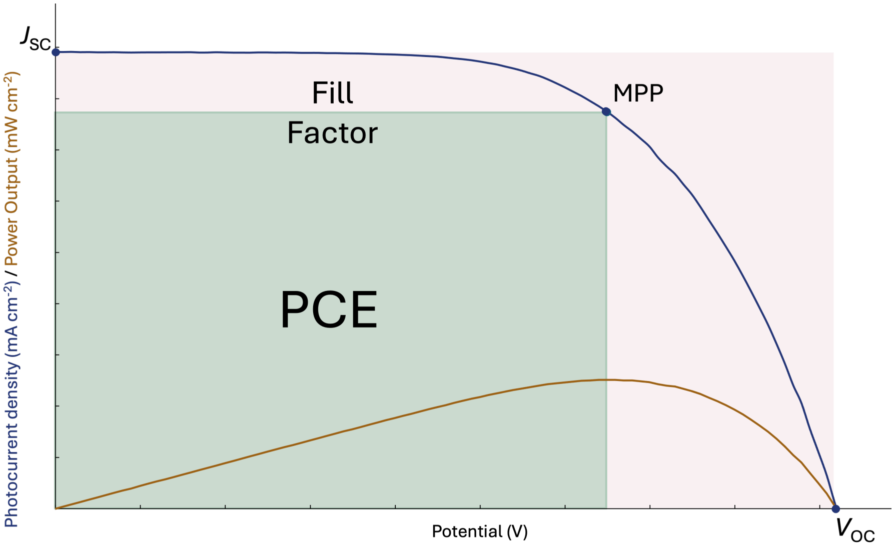

Figure 3.2: Arbitrarily drawn *J-V* curve (blue) with various important concepts noted. Additionally shows the curve for power output plotted against voltage (brown), showing the power output's dependence as the product of voltage and current. PCE is defined as the area of the green rectangle. Fill Factor is placed in between the two coloured rectangles, to signify that it is a quotient of the two areas.

3.2 Background on dye-sensitised solar cells

3.2.1 Working principles and components

A dye-sensitised solar cell (DSC) is a type of photovoltaic device that rose to prominence with the report by Grätzel et al. in 1991[75] (for which reason a DSC is also known as a Grätzel cell).

The component responsible for photoexcitation in a DSC is a photosensitiser. Within the field of DSCs, this photosensitiser is commonly termed the dye, which gives DSCs their name. This photosensitiser is adsorbed onto a semiconductor surface. Within a DSC the charge separation needed to generate an electrical current is effected from the interplay of the semiconductor and the molecular photosensitiser. This comes about by the excited electron in the dye after photoexcitation, being injected into the CB of the semiconductor (*1* and *2* in Figure 3.3).[76] As the photosensitiser is in direct contact with the semiconductor, here acting as a quencher for the ES, the electron injection from the excited photosensitiser may occur on sub-ps timescales for some dyes, almost concurrently with the photoexcitation.[39, 77] The electron is from there channelled to an electrode (commonly in the form of conductive glass) upon which the semiconductor is deposited. This is linked to an electrical circuit where the injected electrons generate an electrical current (*3* in Figure 3.3). The dye and semiconductor substrate are surrounded by a redox active electrolyte, which is also in contact with the counter electrode connected to the electrical circuit. This electrolyte contains some species that function as a redox mediator, capable of accepting electrons through reduction and then donating them by its own oxidation. At the counter electrode the electrons work to reduce the redox mediator (*4* in Figure 3.3). The re-reduction of the photosensitiser is then achieved by migration of reduced redox mediator which transfers electrons to the photosensitisers oxidised by the photoinduced electron injection (*5* Figure 3.3). All these various electron transfer events form a closed electrical circuit.[74, 76]

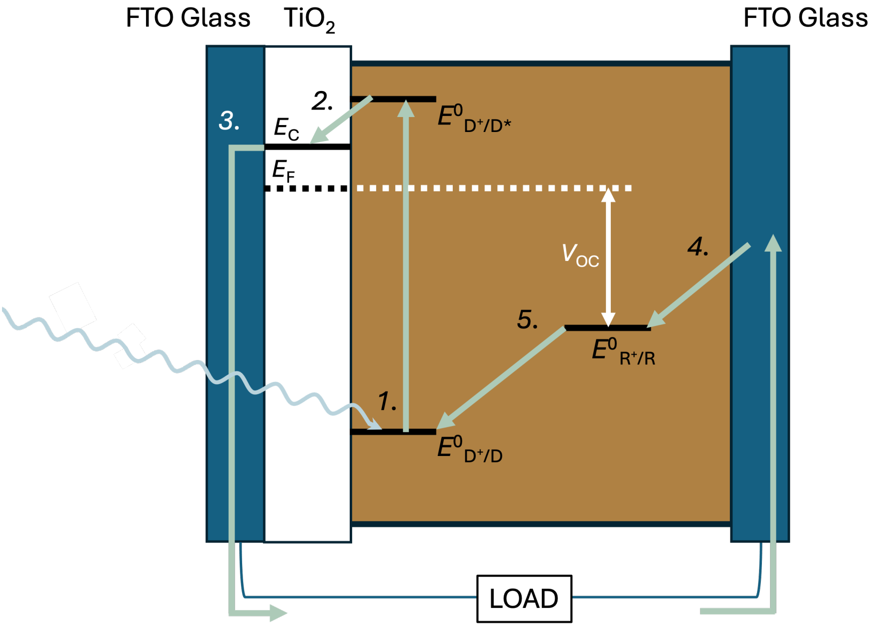

Figure 3.3: Schematic of a DSC, showing its integral parts as well as arrows denoting productive movement of electrons through the system, with the different energy levels they ocupy. Blue wavey arrow denoting incoming light, exciting the dye. FTO Glass denotes fluoride doped tin oxide coated glass, commonly used for transparent electrodes in DSCs *1*. Photoexcitation of the photosensitiser (dye, D). *2*. Injection of the excited electron. *3*. Channeling of the injected electron to the electrical circuit. *4*. Reduction of the redox mediator (R) by electrons from the circuit. *5*. Re-reduction of the photosenistiser by the redox mediator.

In the most common and successful type of DSC, the semiconductor upon which the dye is deposited is of n-type. The semiconductor most commonly used is TiO_2, the use of which stretches back to the paper by Grätzel et al., which originally brought interest to the field.[75] The wide-spread and lasting use of mesoporous TiO_2 for making DSCs stems from its non-toxicity and stability, while simultaneously having a CB that has proven conducive to solar cell function.[17] TiO_2 can additionally be made with a good level of transparency, important for the semiconductor, as for a good portion of incoming light can reach the photosensitiser.[74, 78] This is related to the large band gap within TiO_2, meaning light that excites the photosensitiser is not absorbed by the semiconductor.[74] There are also examples of DSC devices using p-type semiconductors, were the flow of electrons between the various components is reversed. These types of devices have as of yet not achieved the same success as those using n-type semiconductors.[74, 79] The discussion within this thesis will solely focus on devices based on n-type semiconductors.

The redox active electrolyte was in early publications often composed of I_3^-/I^-. This redox mediator proved to have redox potentials well aligned with many dyes as well as having good diffusivity in a range of solvents.[74] More recently there has been a development of other redox mediators, that has led to more efficient devices. One of the more commonly used is $[Co(II/III)(bpy)_3]^{2+/3+}$, which has been used to achieve many of the most efficient DSC-devices so far published.[80-81] Among the advantages of $[Co(II/III)(bpy)_3]^{2+/3+}$ over I_3^-/I^- is the lower redox potential of $[Co(II/III)(bpy)_3]^{2+/3+}$ which gives a device capable of higher potentials, as the V_{OC} of a DSC device is determined by the difference in potential between the E_F of the semiconductor and the redox potential of the redox mediator (Figure 3.3).[74] Despite its shortcomings, the widespread use of the I_3^-/I^- redox mediator has also given devices that have PCEs that are no more than a few percent short of those utilising $[Co(II/III)(bpy)_3]^{2+/3+}$.[82-83] While liquid interface devices have been developed to counter issues of solvent leakage and evaporation, solid state electrolytes have also been introduced in a pursuit of attaining more stable devices.[74, 76, 78]

This gives a great many components which can all be modified and tuned to give the optimal result. In theory, all components can be optimised independently of one another, giving great possibility for research within the field. It can however not be fully excluded that various exotic modifications to a component will result in unforeseen interactions with other parts of the device.

In addition to the above-mentioned electron transfer events, there are a number of possible electron transfers that results in a loss of power and overall lowering of efficiency. The simplest of these is the deactivation of the ES in the photosensitiser before an electron is injected (*1* in Figure 3.4). The same effect can also in essence come about if a newly injected electron recombines with the newly formed electron hole on the photosensitiser (*2* in Figure 3.4). The redox mediator can also bring about detrimental paths for the electrons. Firstly, the oxidiser can quench the ES of the photosensitiser rather than let the electron be injected into the CB (*3* in Figure 3.4), and secondly, the redox mediator can be reduced directly by electrons from the CB of the semiconductor (*4* Figure 3.4).[17, 74]

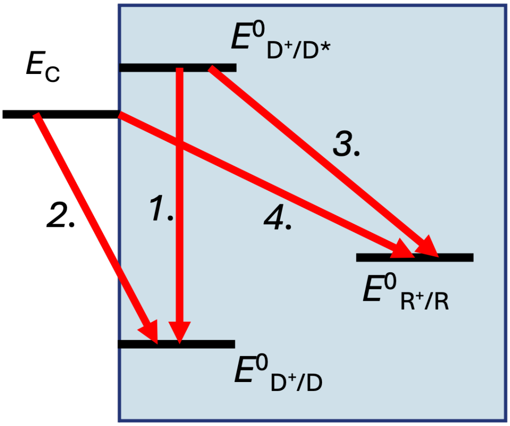

Figure 3.4: Unproductive electron transfer events in DSCs. *1*. Deexcitation of the excited photosensitiser (dye, D). *2*. Recombination of the injected electron with the GS of the photosensitiser. *3*. Quenching of the ES of the photosensitiser by the redox mediator (R). *4*. Reduction of the redox mediator by the injected electron.

Since their initial conception DSC have seen a steady increase in achieved PCE, with reported efficiencies of 13-14% under one sun illumination. The very highest results have been achieved by combining several dyes together in one device, but almost equally impressive results are also reported using single dyes.[80-81, 84-85]

This can be compared to the best performing single junction solar cells overall, with the most efficient silicon- and GaAs-based solar devices reaching PCEs above 27%. Multi-junction devices have furthermore reached even higher efficiencies with several examples breaking 30%.[86-87]

While DSCs are currently very much outperformed by solid state solar cells, there is an interesting possibility for their use in low-power indoor applications. DSCs devices achieving PCEs above 30% when illuminated with ambient, indoor light. are known in the literature.[85] This outperforms other known solar cell technologies for these types of applications. This could open these devices up to their usage in various wireless applications in indoor appliances.[88]

3.2.2 Photosensitisers in DSCs

To achieve an efficient DSC, the incorporated photosensitiser needs to have a number of characteristics. The most obvious is of course the compound's ability to absorb light in the solar spectrum, or whatever wavelength of photon is desired. A good coverage of the entire spectrum is necessary for best possible efficiency. Furthermore, the photosensitiser must be able to adsorb onto the semiconductor layer. This adsorption must be stable and such that electron injection from the photosensitiser into the semiconductor surface is efficient. This is commonly achieved by the incorporation of one or several acid groups on the photosensitiser, such as $–COOH$, $–PO_4H_3$, $–SO_4H_2$. This is commonly termed the anchoring group.[17]

There is furthermore a need for the dyes to be stable under extended periods in the environment of the solar cell, where it is exposed to both light and heat. The need for longevity of photosensitisers is perhaps even more prominent in DSCs compared to other photosensitiser applications, as solar cells should ideally stay functional over a period of years with minimal outside interference.[76]

For electrons to flow efficiently through the system, there also needs to be a good driving force for electrons to move from and to the photosensitiser. The ES of the photosensitiser needs to be so much higher in energy than the CB of the semiconductor that electron injection has an appropriate driving force. Likewise, the GS of the oxidised photosensitiser needs to be lower in energy than the redox mediator for dye regeneration to take place, according to similar principles.[17]

The photosensitisers used in DSCs have been designed, based on many different ideas, much like photosensitisers in general. The earliest examples were largely based on ruthenium polypyridyl systems, with these types of dyes providing a benchmark, which other dyes are tested against.[74, 89] Dyes of other metals have also been investigated, with those dyes based on earth-abundant metals receiving special attention recently for the need of having widely available materials for these types of applications.[90]

Organic photosensitisers have received comparatively more attention for use in DSCs than for other photochemical applications. The dyes used for the most successful applications have largely been organic dyes. A design principle that has found widespread use and success for DSCs are so called donor-acceptor dyes. Within these dyes, photoexcitation induces a CT excitation, where electron density is redistributed from one part of the photosensitiser to another. Commonly, an amine-based electron donating group (EDG) is placed on the end of the dye, while the opposite, anchoring side has an EWG. This EWG, or acceptor, thus play a part in the interaction of the dye with the semiconductor surface. Between the two sides are various conjugated π-systems for transferring electrons through the dye.[74, 78]

3.3 Iron-based dyes in DSCs

Following the ruthenium polypyridyl-based photosensitiser as the first dye used in the modern DSC by Grätzel et al.,[75] attempts were made to use the iso-electronic iron in a similar fashion, somewhat mirroring the investigations into iron photosensitisers, as discussed above. Earliest attempts to use an iron polypyridyl system were carried out by Ferrere and Gregg, showing function but very low PCE, due to a current density around 0.25 mA/cm^2. It could however be surmised that electron injection took place from the very short lived MLCT excited state.[77] Several attempts toward utilising iron with polypyridyl and ferrocene structures in DSCs are known, but failed to achieve even 1% in efficiency.[90-91]

Somewhat more successful iron-based dyes have been achieved by the use of iron-NHC photosensitisers. The first iron-NHC complex investigated for use in DSC application was the homoleptic complex $[Fe(cpbmi)_2]^{2+}$ (**2** in Figure 3.5), where carboxylic acids are introduced on each side of the simple complex $[Fe(pbmi)_2]^{2+}$ (**1** in Figure 2.8), also described in Chapter 2. A simple DSC based on this complex failed to generate much in terms of PCE, but proved the possibility of using this type of complex in a DSC device.[56] An in-depth investigation however showed a 37 ps ^{3}MLCT lifetime of the complex while attached on a metal oxide surface and electron injection from this state taking place on a timescale of approximately 3 ps. This then suggested that as much as 92% of all photoexcited electrons are injected into the semiconductor. In the absence of other processes, the large majority of these electrons recombine to the GS of the photosensitiser on a time scale of 30-150 ps.[55] This led to further interest into the possibility of harnessing the substantial electron injection into electrical power.

The high yield of injection into TiO_2, as mentioned above, suggests that the main process limiting the efficiency of iron-NHC photosensitisers in DSC applications is an issue of electron recombination (*2* in Figure 3.4), or possibly a quenching of excited or injected electrons by the redox mediator (*3* and *4* in Figure 3.4). There are however later findings by Gros et al., that have been interpreted as low injection of electrons being the main limitation for the function of these DSC devices. Spectroscopic evolution of the complex **2** (Figure 3.5) adsorbed onto TiO_2 suggested a blue-shift of the GS bleach during TA measurements. This may be attributed to the development of a new ES from the initial excitation, that hampers injection. The measurement additionally reveals a quicker recovery of the GS in the presence of iodide, that is naturally linked to the reduction of the photosensitiser. These findings are taken to mean that charge recombination is of little issue and that relaxation to a lower lying triplet state is the limitation in efficiency.[92-93]

The findings of injection limiting the function of iron-NHC dyes are of course at odds with the reports of 92% of excited electrons being injected into the semiconductor. It is currently unclear which conclusion is the correct one.

The main reported improvement of iron-NHC–DSCs has been found by the use of specialised electrolytes, implemented by Gros et al. These electrolytes incorporate MgI_2, guanidium thiocyanate and tetrabutylammonium iodide (TBAI). Magnesium ions are believed to improve injection yields by placing a positive charge by the anchoring group. Guanidinium is supposed hinder charge recombination between the I_3^-/I^- redox mediator and injected electrons, while TBAI is introduced to increase the iodide concentration without affecting V_{OC} by the addition of additional metal ions.[92, 94]

In combination with this electrolyte, further improvements in efficiency have been found by the design of the dye. The removal of a carboxylic acid from **2** (Figure 3.5), giving the heteroleptic complex **11** (Figure 3.5), leads to improved efficiencies, presumably by improving directionality of charge separation upon excitation.[58, 95] The effect of the heteroleptic dyes have been further explored in the literature by the introduction of various substituents at the 4-position of the non-carboxylic acid substituted pyridine. The most successful example of this is introduction of 2,4-dimethoxyphenyl (**12** in Figure 3.5), reported as yielding solar cells with PCEs as high as 1.8%, when combined with the above-mentioned electrolyte.[96]

Further modifications to the anchoring ligand have also been reported, consisting of modifications of the structures mentioned above. These modifications to the anchoring ligand include simpler structures where the anchoring carboxylic acid is separated by an aromatic spacer moiety (**13** in Figure 3.5). These simple changes however failed to outperform **11**, supposedly due to the spacer hampering injection.[93, 95] More complicated structures are also known, incorporating anchoring groups based on cyanoacrylic acids, a widely used anchoring moiety for organic dyes in DSCs. A homoleptic iron-NHC complex with thiophene-cyanoacrylic acid (**14** in Figure 3.5) resulted in a PCE of 1.7%. Furthermore, co-sensitisation of the complexes **2** and **14** yielded impressive results of as high as 2% PCE. The improved results using the complex **14** (Figure 3.5) seem to at least partially be due to the dyes strong absorption in the visible spectrum.[94]

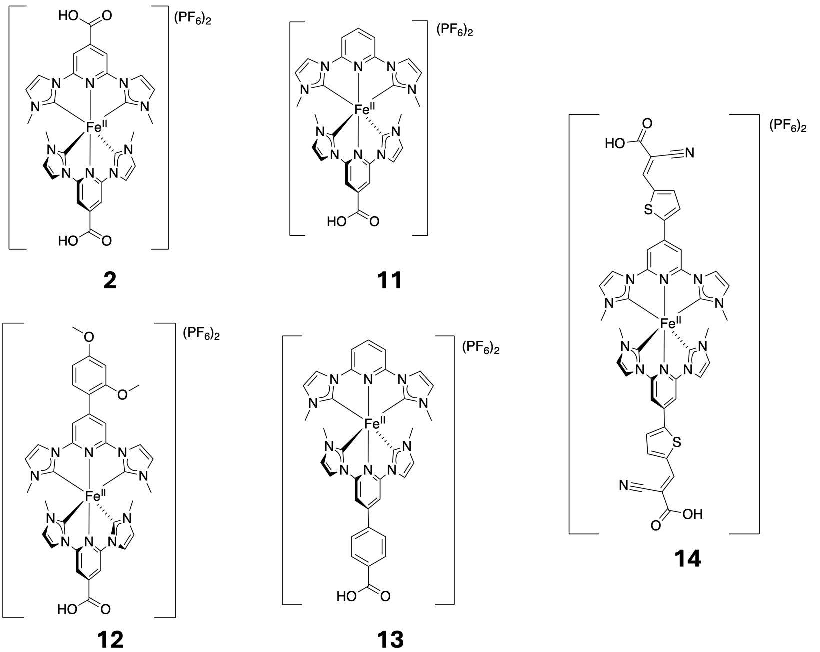

Figure 3.5: Structures of various iron-NHC complexes utilised in DSC applications.[55-56, 58, 94-96]

4 Synthesis of heteroleptic iron-NHC complexes and their use in DSCs (Papers I & II)

4.1 Background

As is discussed above, previous findings had suggested that iron-NHC photosensitisers used in DSCs could efficiently inject electrons into a TiO_2 surface, to which they were adsorbed. Simultaneously, efficiencies achieved with DSC devices utilising these compounds remained poor. It was thus reasoned that charge recombination effects may significantly hamper the use of iron-NHC complexes in DSCs. In an attempt to counteract charge recombination and simultaneously improve electron injection dynamics, dyes with EDGs on the opposite side of the complex from the anchoring group, were designed (**15-16** in Figure 4.1). The main reasoning behind this design was to generate a complex with a HOMO spatially shifted away from the anchoring group, while simultaneously having a LUMO spatially shifted towards the anchoring group (Figure 4.2). Investigation of complex **11** (Figure 4.1) was also carried out due to its simplicity and reported high efficiency.

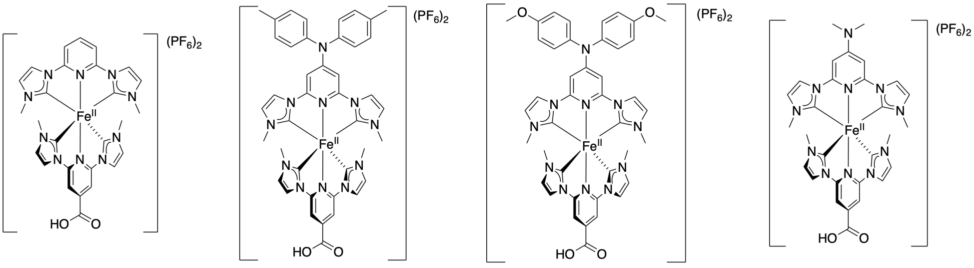

11 **15** **16** **17**

Figure 4.1: Structures of the heteroleptic iron-NHC complexes investigated within this chapter, for use in DSC devices.

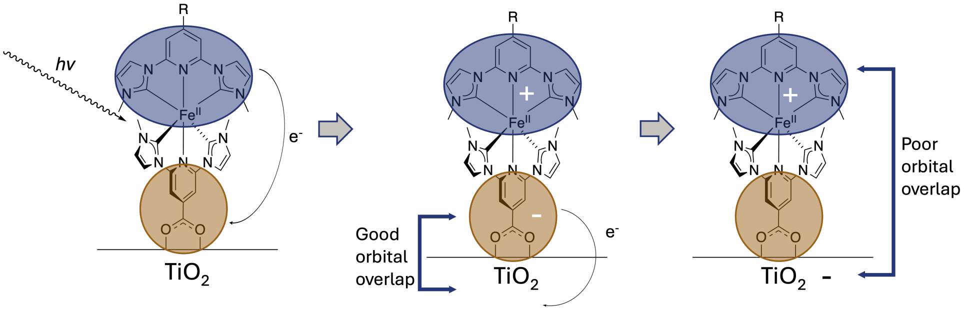

Figure 4.2: Model of the design principle of the iron-NHC complexes **15-17** for use in DSCs. HOMO denoted by blue and LUMO denoted by brown.

The general motif of an EDG linked to an EWG has been widely used for DSC dyes, but mainly for organic dyes where the donor-acceptor structure serves to create the possibility of an intra-molecular CT state which gives the dye light absorbing properties.[74]

4.2 Synthesis of heteroleptic complexes

4.2.1 Ligand synthesis

The carboxylic acid substituted ligand **P2** was known from previous literature and is simple to obtain through an S_NAr reaction (Scheme 4.1).[55-56] Acidification of the mixture after reaction was found to improve the yield of reaction as the protonated form of the ligand salt was simpler to recover.

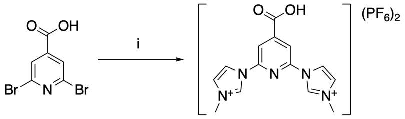

P1

P2 (71%)

Scheme 4.1: Reaction for the formation of the carboxylic acid substituted pre-carbene ligand **P2**. i) Methyl imidazole, DMF, 150 °C.

The new ligands with nitrogen-based EDGs were more complicated to synthesise (Scheme 4.2). Synthesis began from 4-amino-2,6-dibromopyridine (**P3**), to which imidazole was introduced via copper-mediated C-N coupling, giving **P4**. The two aryl groups were then attached by two Buchwald-Hartwig aminations, preformed in a single step, yielding **P5-P6**. Finally, to form the pre-carbene structure, imidazolium moieties were formed by methylating each imidazole group with MeOTf, giving **P7**-**P8**. The Buchwald-Hartwig amination was the most challenging step of this synthesis, as the amine is relatively electron-poor while the aryl-bromide is more electron rich. This in opposition to the preferred electron demands of the reaction. For the reaction to be functional, specialised dialkylbiaryl phophine ligands were necessary for the palladium catalyst to be active enough to perform the reaction without catalyst deactivation. Even after these optimisations, the transformation required long reaction times (5 days) and gave relatively poor yields (27-28%). It should be noted that since the reaction requires two overall catalytic cycles to give the product, the yield of each coupling reaction is closer to 52%.

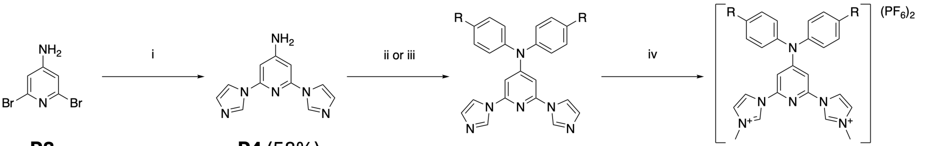

P3

P4 (58%)

R = N(*p*-Tolyl)$_2$: **P5** (28%)
R = N(*p*-Anisyl)$_2$: **P6** (27%)

R = N(*p*-Tolyl)$_2$: **P7** (52%)
R = N(*p*-Anisyl)$_2$: **P8** (35%)

Scheme 4.2: Reactions for the formation of pre-carbene ligands **P7** and **P8**. i) Imidazole (3 eq.), CuI, L-proline, K_2CO_3 (5 eq.) DMSO, 140 °C; ii) 4-Bromotoluene (3 eq.), $Pd_2(dba)_3$ (cat.), XPhos (cat.), NaO*t*-Bu (3 eq.), toluene, 110 °C (used for **P5**); iii) 4-Bromoanisole (3 eq.), $Pd_2(dba)_3$ (cat.), CyJohnPhos (cat.), NaO*t*-Bu (3 eq.), toluene, 110 °C (used for **P6**); iv) MeOTf, $C_2H_4Cl_2$, 95 °C.

Alternatively, the amine in the intermediate **P4** could be transformed into a bromide, via a Sandmeyer reaction, giving the brominated intermediate **P9**. This bromo-intermediate could then be coupled to a diarylamine, again via a Buchwald-Hartwig amination. For this alternative Buchwald-Hartwig amination, the electronics are more in line with the ideals for the coupling reaction. The Sandmeyer reaction was initially a problematic step, giving only lower yields of around 35%, and this alternative Buchwald-Hartwig amination was also only moderately yielding.[97] The direct double Buchwald-Hartwig reaction was thus deemed preferable. It was later hypothesised that the copper from the Sandmeyer reaction coordinates to the product and limits the yield of reaction during work up. By sequestering the copper with ammonia, the yield could be improved up to 82% (Scheme 4.3). Later findings have used ethylenediaminetetraacetic acid (EDTA) to improve the reaction even further.[98] With these improvements to the Sandmeyer reaction, the option of going via the brominated intermediate (**P9**) becomes a more attractive strategy from both the point of view of yield and reaction time. An alternative, though untested, strategy is the use of the 2,6-diimidazol-4-iodopyridine (**P17**; see Section 5.2.2), as a starting material for a Buchwald-Hartwig amination with a diarylamine.

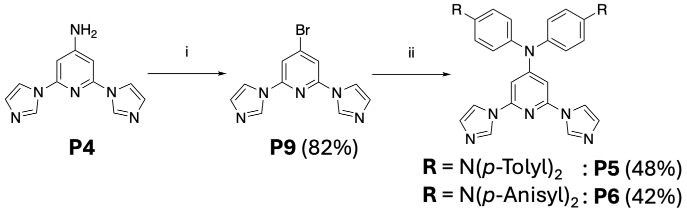

Scheme 4.3: Alternative reactions for forming intermediates **P5** and **P6,** via Sandmeyer bromination. Second step acording to Ref. 97 i) CuBr (2 eq.), NaNO$_2$ (10 eq.), HBr (48%, aq.), rt. ii) Di(tol-4-yl)amine / Bis(4-methoxyphenyl)amine (1.25 eq.). Pd$_2$(dba)$_3$ (cat.), DPPF (cat.), NaO*t*-Bu (1.25 eq.), DMF, 120 °C.

The 1,1'-(4-(dimethylamino)pyridine-2,6-diyl)bis(3-methylimidazolium) pre-carbene ligand (**P13**) was known in literature when this work with it started. The synthesis of it followed a similar principle, with the difference being that the amine group was first methylated, after which the methylimidazolium groups were built up in a stepwise fashion, with imidazole introduced via an S$_N$Ar reaction using sodium imidazolate (Scheme 4.4).[66]

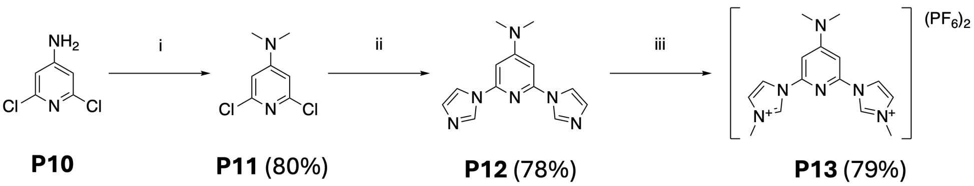

Scheme 4.4: Literature reactions[66] for the formation of dimethylamino pre-carbene ligand **P13**. i) 1. NaH (3 eq.), THF/DMF, 0 °C. 2. MeI (3 eq.) 80 °C; ii) Sodium imidazolate (2.8 eq.), DMF, rt; iii) MeI (4 eq.), MeCN, reflux.

4.2.2 Complexation

Synthesis of the complexes was made difficult by the lack of a method for sequentially attaching one of the ligands for the complexes, at the time. The one method available was thus letting the two desired ligands attach simultaneously, first explored for iron-NHCs by Gros et al.[58] To achieve this, the ligands were mixed together, dissolved, and consecutively treated with KO*t*-Bu and FeBr$_2$, to generate free carbenes and coordinate them to iron (Scheme 4.5). The pre-carbene ligand **P13** seemed to be more sensitive than the other ligands, as a lower temperature was needed for it to react successfully. This type of procedure gave the two possible homoleptic complexes, as well as the desired heteroleptic one. The various complexes then needed to be separated by flash chromatography. This process was relatively simple, as the varying number of carboxylic acid substituents made their affinity for the stationary phase profoundly different. Alumina gel was found to be the preferred stationary phase, with a strongly polar eluent mixture of acetonitrile and water. Silica gel could also serve as the stationary phase, but KNO_3-salt was then needed to be added to the eluent to achieve elution of the complexes. Alumina was thus preferable as it does not complicate the system with the introduction of additional anions. Alumina was also used for the purification of the complex **11** (Figure 4.1), in opposition to the literature,[58] as this was found to function better for the same reasons. This method also relied on the fact that the complexes are more or less completely substitution inert, a property offered by the very strong iron-NHC bond, and further increased by the tridentate nature of the used ligands.

It could be seen that the two types of ligands (carboxylic acid and amine) have different propensity to attach to iron, as a larger amount of homoleptic complexes without carboxylate substituents were present in all reaction mixtures when synthesising the heteroleptic complexes. This is possibly linked to the higher nucleophilicity of the pyridine nitrogen for the non-carboxylate substituted ligands, as these lack the electron withdrawing effect of the carboxylate. The amines also delocalise electrons into the pyridine ring, further increasing its nucleophilicity. The hypothesis is enforced by the electron donating ability of the substituent being reversely proportional to the yield of the resulting heteroleptic complex.

The most striking example of this was in the case of the synthesis of the dimethylamino complex **17** (the dimethylamine being the most electron donating substituent due to not interacting with phenylene substituents, themselves electron acceptors). Attempted synthesis by use of the two ligands and $FeBr_2$ in a 1:1:1 ratio yielded the homoleptic complex incorporating only ligand **P13**, by a very large majority and no dicarboxylic acid complex was detectable. This is in line with the pyridine in this ligand being expected to be the most nucleophilic of the investigated ligands.

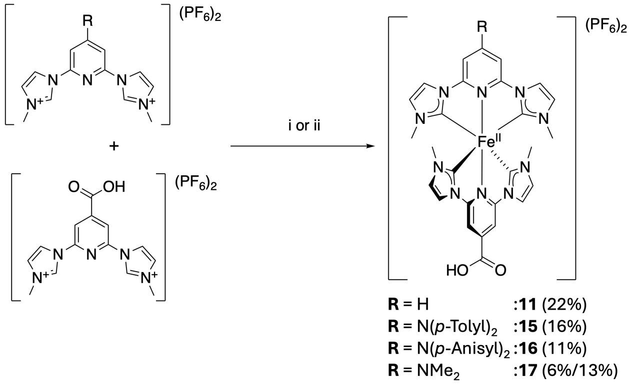

Scheme 4.5: Reaction for the formation of the heteroleptic iron-NHC complexes with carboxylic anchor ligand as well as various non-electron withdrawing substiuents. i) 1. KO*t*-Bu (THF, 3 eq.), 0 °C, DMF, 2. FeBr2 (1 eq.), DMF, rt (used for **11**,**15**-**16**). ii) 1. KO*t*-Bu (THF, 3 eq.), -78 °C, THF, 2. FeBr2 (1 eq. / 2 eq.; giving 6% / 13% yield respectivly), THF, rt (used for **17**).

Due to the finding that the complex **17** was almost the only product from the attempted complexation, and thus only a small amount of present the carboxylic acid ligand **P2** was found to react, it was reasoned that only a fraction of the added iron was reacting. This problem was attempted to be circumvented by adding an extra equivalent of iron. This gave the desired complex in a yield comparable to what was observed in the syntheses of the complexes **15-16**. Adding 3 eq. of $FeBr_2$ led to lower yields (see Table 4.1 for the effect of amount of $FeBr_2$ on the yield). Literature reports, published after the synthesis was established for this complex, state that this complex can be formed in comparable yields under conditions used for other complexes,[96] but this was not found to be possible to replicate by us. The use of additional equivalents of $FeBr_2$ in the synthesis of the other heteroleptic complexes (**11** and **15-16**) has not been closely studied but may prove beneficial also there, as a mismatch between the different ligands is present in all these cases, to varying degrees.

Table 4.1: Overview of the yields achieved during the complexation of complex **17**, using different equivalents of $FeBr_2$.

EQ. OF $FeBr_2$	YIELD
1	6%
2	13%
3	3%

Despite the use of acid during the work-up of the dimethylamino complex **17**, no sign of protonating the dimethyl amine moiety could be observed. This suggested that the free electron pair on the amine is largely delocalised over the pyridine ring and that electron donation from this moiety to the overall complex is indeed present. This is in line with the properties of the well-known 4-dimethylaminopyridine, which is mainly nucleophilic on the pyridine nitrogen.[99]

4.3 Properties of heteroleptic complexes adsorbed on the semiconductor-surface

4.3.1 Photoexcitation dynamics and electronic structure

The most striking finding was that under TA spectroscopy of the photosensitisers adsorbed on TiO_2, the spectral features first developed into one resembling the oxidised form of the dye and over time turned into the signature resembling that of the ES of the dye. This surprising finding was explained by the ^{1}MLCT state of the dye being the state from which electrons were injected into the CB of TiO_2 (itself not particularly unique[39]) after which charge recombination took place into the ligand-based π^*-orbital, effectively generating the ^{3}MLCT state. It has since the publication of the paper been suggested that an alternative explanation may involve an initial ES involving orbitals of both the photosensitiser and TiO_2, resembling the oxidised dye when measured by TA spectroscopy, which decays into the ^{3}MLCT.[100] These observations could also serve as a possible explanation to combine the incongruous findings, regarding efficiency of iron-NHC dyes being limited by poor injection or charge recombination, discussed and compared in Section 3.3.[55, 92]

Calculations showed that the lowest unoccupied ligand orbital was indeed localised to the anchoring side of the complexes, on the carboxylate substituted ligand. Calculations however also showed the HOMO of the complex as located on the metal, with little or no shift towards the amino-substituted ligand. This orbital distribution suggested that the strategy should indeed be beneficial for improving electron injection (as the orbital populated by photoexcitation is close to the TiO_2 surface), to whatever extent this was a limitation in DSC devices. The ability of the strategy to hinder electron recombination was however more doubtful, according to these calculations (as the HOMO of the complex is located at a similar distance from the TiO_2 surface, as in the parent complex).

4.3.2 Basic investigation of DSCs based on iron-NHC dyes

The complexes **15-16** were used in photovoltaic application, as dyes in DSCs, and compared to the homoleptic complex **2**. The dyes were in these initial studies applied only in a relatively simple system, with little optimisation of other DSC components being carried out. Specifically, the photosensitisers (in a 0.2 mM solution) were deposited on a TiO_2 semiconductor substrate followed by co-adsorption with chenodeoxycholic acid (CDCA; in a 0.5 mM solution) to ensure complete coverage of the semiconductor surface (which is a common practice within DSC research) and hinder charge recombination between the semiconductor and redox mediator (*4* in Figure 3.4). This TiO_2 substrate with adsorbed photosensitiser was then combined with a platinum-based counter electrode and an electrolyte containing a I^-/I_3^- redox mediator. The main attempt at optimisation of the system was the use of cobalt-based redox mediator ($[Co(II/III)(bpy)_3]^{2+/3+}$). This failed to produce an efficient system, most likely due to the recombination between the CB of TiO_2 and the cobalt-based redox mediator (*4* in Figure 3.4).

Nevertheless, the new dyes showed a marked improvement compared to the homoleptic complex **2**. This can perhaps be mainly explained by the greater directionality of CT state, induced by using heteroleptic complexes. Despite the larger complexes leading to noticeably lower dye loading, the J_{SC} and V_{OC} improved, as well as the PCE. The improvement was by far larger for the complex **15**, compared to the complex **16** (Table 4.2). The stronger donating ability of the *para*-methoxyphenyl could be expected to give a stronger effect of the EDG in the complex **16** dye. The lack of this effect could possibly be explained by the free electron pairs of the ether oxygens giving unwanted interactions with the electrolyte, such as coordinating metal ions.

Table 4.2: Best solar cell characteristics of cells from iron-NHC complexes, using CDCA coadsorbant, thermoplastic sealant and I^-/I_3^- in MPN electrolyte. Avrage of four devices in parenthesis.

DYE	V_{OC} (mV)	J_{SC} (mA cm^{-2})	FF	PCE (%)
2	466 (460±20)	2.09 (1.9±0.2)	0.752 (0.74±0.1)	0.73 (0.63±0.07)
15	512 (500±10)	3.52 (3.3±0.2)	0.724 (0.714±0.08)	1.31 (1.2±0.1)
16	416 (400±20)	3.23 (2.7±0.4)	0.694 (0.69±0.1)	0.93 (0.8±0.2)

As mentioned in the introduction, the same design principles as used here has been used elsewhere in the literature. This research was carried out concurrently with our own investigations. By the use of a more optimised system, efficiencies as high as 1.8% were reached.[96]

4.3.3 Optimisation of solar cell systems

To further investigate the behaviour of heteroleptic iron-NHC photosensitisers in DSC applications, research into the possibilities to improve the method for solar cell composition was undertaken, as well as expanding the scope to include complexes **11** and **17**, in addition to the already investigated complexes **15** and **16**.

One of the main improvements made to device efficiency, was the use of UV-curing glue to assemble the two electrodes of the devices together, instead of a thermoplastic frame, as was done previously. As the electrodes here are in essence placed as to be in direct contact with one another, the current is improved by shortening the distance needed for the redox mediator to diffuse. Common understanding suggest that the cell should not be functional when the platinum electrode and the TiO_2 semiconductor are in direct contact, as it should lead to a short circuit of the system. This was evidently not the case, however. The most likely explanation for this is that the scattering layer, which is more or less isolating, applied to the TiO_2 substrate was sufficient to hinder the flow of electrons between the TiO_2 semiconductor and the counter electrode.

Improvements in efficiency could also be achieved by lowering the concentration of the sensitisation bath for amine-substituted the photosensitisers **15-17**, from 0.2 M to 0.05 M. This may have led to less aggregation of the photosensitisers on the surface as they are introduced before the addition of CDCA to the surface, as too little space is allowed for the CDCA to efficiently isolate the photosensitisers from one another. However, in the case of the photosensitiser **11**, sensitisation bath of

0.2 M was found to be preferable. Additionally, some improvements were achieved by the use of TiO_2 of mixed particle sizes (Table 4.3).

Table 4.3: Characteristics of best performing solar cells (with regards to PCE) four iron-NHC complexes, using CDCA coadsorbant, UV-curing sealant, TiO_2-substrate of mixed particle size and I^-/I_3^- in MPN electrolyte. Measurments for scanning SC to OC. Avrage of six devices within parenthesis.

DYE	V_{OC} (mV)	J_{SC} (mA cm^{-2})	FF	PCE (%)
11	438 (439±1)	4.93 (4.2±0.3)	0.584 (0.591±0.002)	1.260 (1.10±0.05)
15	447 454±1)	4.41 (4.08±0.06)	0.597 (0.599±0.003)	1.176 (1.108±0.009)
16	459 (458±3)	3.71 (3.4±0.2)	0.596 (0.613±0.005)	1.015 (0.94±0.03)
17	459 (471±2)	4.46 (4.21±0.08)	0.614 (0.613±0.0004)	1.257 (1.211±0.006)

The PCEs found by these modifications were a significant improvement compared to what was previously seen for these complexes, but still outperformed by the findings by Gros et al. using the iron-NHC–based dye substituted with a dimethoxyphenyl group (**12** in Figure 3.5).[96] However, these record devices were assembled with some different parameters than was used here, the better performing devices utilising a more complex electrolyte, as discussed in Section 3.3. These devices also lacked any co-adsorbent (as opposed to our study, using CDCA). It was therefore attempted to combine the solar cell architecture used here with the electrolyte mixture employed by Gros et al. in their impressive findings.[95-96] The mixture of salts was attempted to be employed in both acetonitrile and 3-methoxypropionitrile (MPN), but the less polar MPN failed to dissolve all the additives and a saturated solution of various additives in MPN was investigated as an electrolyte instead. Under the investigated conditions, the additives proved detrimental or lacking any significant effect for all complexes, except **11**, where it was beneficial. It was thus determined that the choice of electrolyte should be dependent on the precise structure of the photosensitiser used.

It was additionally found that a substantial hysteresis effect was present when performing *J*-*V* investigations of devices using the four complexes. Within solar cells, hysteresis refers to a phenomenon where the characteristics obtained from the measurements are different depending on the scan direction of the measurement, i.e. if the scan performed from open circuit (OC) to short circuit (SC) voltage, or SC to OC voltage. In this case, a significant increase in V_{OC} was recorded when scanning from OC to SC, compared to the SC to OC scan direction. In addition, a distortion of the *J*-*V* curves around the MPP showed currents that were higher in some points than the recorded J_{SC} (Figure 4.3).

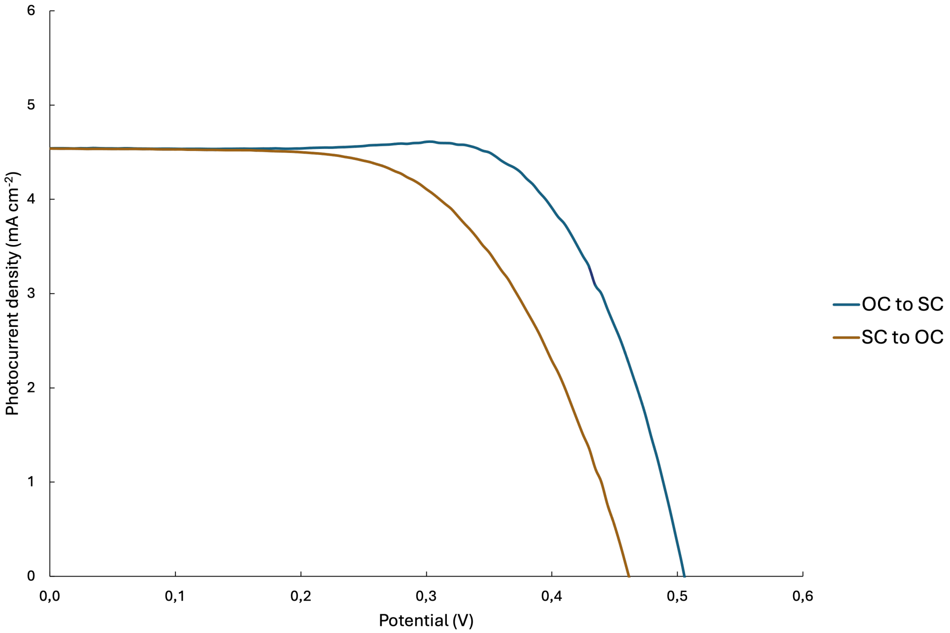

Figure 4.3: Comparison of *J-V* scans, depending on scan direction, for **17** (the complex taken as an example, similar bahviour is also found for dye **11**, **15** and **16**). Note the distortion of the curve around MPP, showing higher current than the measured J_{SC}.

These types of hysteresis effects are well known in the field of perovskite solar cells,[101] but is much less commonly observed and less studied in DSCs. These effects are nevertheless also known in the field of DSCs, and have been attributed to capacitance effects, where injected charges are kept in place within the semiconductor for an extended time.[102-103] DSC-devices presented here, as well as others in the literature utilising Fe-NHC dyes, have made use of uncommonly thick TiO_2-layers.[94-96] Thicker TiO_2-substrates have been shown to lead to these types of capacitance effects.[102] This could thus be the explanation for the hysteresis effects found here. This capacitance can also explain the distortion of the curve, as it in a sense “pre-loads” charges in the surface (acting as a capacitor) while the potential is kept high. These charges can then be released all at once as the potential between the electrodes is lowered to a point where current can flow.[103]

The presence of the hysteresis makes comparison between these and the findings described in the previous section problematic, as these were carried out under conditions scanning from OC to SC. For the purpose of comparing results, characteristics for devices when scanning from OC to SC can be found in Table 4.4.

Table 4.4: Characteristics of best performing solar cells (with regards to PCE) from iron-NHC complexes using, CDCA coadsorbant, UV-curing sealant, TiO_2-substrate of mixed particle size and I^-/I_3^- in MPN electrolyte. Measurments for scanning OC to SC. Avrage of six devices within parenthesis.

DYE	V_{OC} (mV)	J_{SC} (mA cm^{-2})	FF	PCE (%)	HYSTERESIS INDEX
11	476 (480±1)	4.908 (4.2±0.3)	0.729 (0.744±0.004)	1.703 (1.51±0.05)	0.150 (0.158±0.002)
15	513 (486±2)	3.963 (4.08±0.06)	0.718 (0.704±0.001)	1.459 (1.40±0.02)	0.107 (0.11±0.02)
16	502 (497±4)	3.717 (3.4±0.2)	0.723 (0.717±0.008)	1.348 (1.19±0.06)	0.141 (0.12±0.02)
17	522 (511±2)	4.191 (4.21±0.08)	0.698 (0.697±0.001)	1.526 (1.493±0.005)	0.106 (0.104±0.001)

4.3.4 Iron-NHC dyes incorporating long alkyl chains

The introduction of long alkyl chains to photosensitisers can help improve DSC-efficiency. This is accomplished by hindering the redox mediators from coming into contact with the semiconductor surface by introducing a large steric bulk that hinders diffusion into the dye-monolayer. This then prevents non-productive quenching of photo-injected electrons directly by the redox mediator (*4* in Figure 3.4) Concepts akin to this have been explored with iron-NHC photosensitisers by Constable et al., where butyl groups were introduced on the 3-positions of the imidazolylidenes, with some success.[104] To investigate this concept in the context of Fe-NHC photosensitisers, structures based on the complexes **15-16**, incorporating alkyl substituents, were created (Figure 4.4).[105]

Preliminary studies of these dyes suggested worse performance compared to the photosensitisers lacking these alkyl substituents. This lower efficiency is related to both a lower voltage and a lower current. One detail that set these dyes apart from the other dyes was that consecutive baths of dye and CDCA were not found to be preferable, and a more normal bath of a mix of dye and CDCA was used instead.

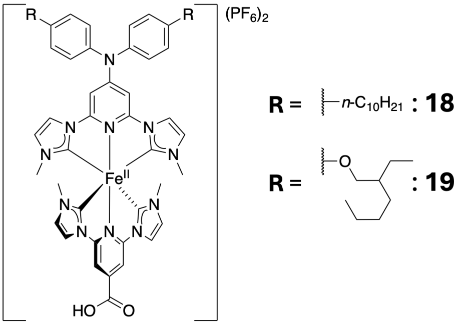

Figure 4.4: Structure of investigated iron-NHC photosensitisers for DSCs, modified with long alkyl chains.

4.4 Conclusions

Four heteroleptic Fe-NHC complexes were investigated for their use in DSCs. The complexes were synthesised according to principles of mixing the desired ligands together and separating the three possible complexes that result from this reaction.

During the synthesis, a trend of the difference in nucleophilicity between the involved ligands influencing the yield of the various complexes was observed. This somewhat limited the yield of the reaction but not to an inordinate degree. Later in the project it was also found that these issues could be mitigated by addition of multiple equivalents of the iron(II)-source. While at the time this work was carried out this was mostly considered a hurdle to be overcome, these findings could perhaps be of use in the pursuit of heteroleptic iron-NHC complexes in the future.

All complexes were applied in DSC systems and found to be more successful compared to the homoleptic dicarboxylic acid complex $[Fe(cpbmi)_2](PF_6)_2$ (**2** in Figure 3.5). The use of heteroleptic complex design gave clear improvement to the properties of the dyes, leading to both improvements in voltage and current. This may hint at both more efficient electron injection and limiting the electron recombination, the sought effect of the photosensitiser design. The possibility of the photosensitisers giving a better performance due to better light absorption properties should however not be overlooked.[94, 96] The use of heteroleptic iron-NHC complexes with extended alkyl chains was briefly investigated but failed to outperform the simpler dyes.

Various improvements to the DSC systems could be made by modifying the overall solar cell system. While this failed to reach the heights found in literature for other iron-NHC–DSCs, it provides new tools that may be applied in further developing the field in the future. Additives present in the electrolyte of the leading Fe-NHC–based cells were however found to be detrimental for several of the dyes used and suggests that these additives should not be used as a matter of routine and be applied with care. Simultaneously, this also marks the trouble of working with dyes with more complicated substituents, as it was the amino-substituted complexes that had detrimental interactions with the additives, outlining the possibility of unwanted interactions between components in a DSC device.

It should also here be mentioned that in the grand scheme of things, the differences in efficiency between all Fe-NHC devices here and in the literature are quite small. While statistically significant, most devices fall around the fairly small span of 1-2% PCE.

Furthermore, it was found that devices using heteroleptic iron-NHC complexes displayed very significant hysteresis effects, where scan direction significantly affected the observed potentials achieved. The hysteresis effects were linked to the uncommonly thick semiconductor layer used in these devices.

It should also be pointed out that fs-TA spectroscopy could provide great insight into the interactions between semiconductor and dye, where several ESs could be found to participate in the development of the ES on the surface. Advanced TA spectroscopy will likely continue to be a potent tool, and perhaps wholly integral, to gain the necessary insights that will make it possible for Fe-NHC dyes to be significantly improved. Even then these systems are highly complicated, and interpretation of their dynamics will be a great challenge.

5 Iron-NHC photosensitisers substituted with phenyl-ethynyl moieties (Paper III)

5.1 Background

Iron-NHC complexes substituted with phenyl-ethynyl groups were pursued to separate the charges developed during photoexcitation. Separation of charges could be of importance in artificial photosynthesis applications and serve to improve the ES lifetime. Complexes with similar structures have previously been explored in the literature.[106-107] Ethynyl subunits have for example been used to link iron-NHC complexes to substructures that are themselves chromophores. This was found to give doubling in extinction coefficient, as well as redshift of the main absorption features, both attributed to the expanded π-system. Incorporation of additional ethynyl-units further increased this effect. These studies however failed to report on the extension of ES lifetimes for these complexes.[108] The introduction of a porphyrin at the end of an ethynyl bridge gives an absorption spectrum dominated by the porphyrin, but also shows new absorption features. The introduction of the porphyrin simultaneously seems to give a system with an MLCT excited state that develops after initial relaxation. This MLCT state has a lifetime more than an order of magnitude longer than the parent complex ($[Fe(pbmi)_2](PF_6)_2$ (**1**) in Figure 2.8).[109]

The use of rigid and linear spacers for achieving separation between the photosensitising unit of the central metal coordination sphere, and the other parts of the complex participating electronically is of importance for optimal implementation of this strategy. This is due to it allowing for the most substantial spatial separation of developed charges in the excited molecule, opening up for extension of the lifetime of a CT state by hindering charge recombination.[110]

The concept is here expanded to include additional types of substituents to more closely investigate the extended π-system in conjugation with the particular ligand structure used here (Figure 5.1).

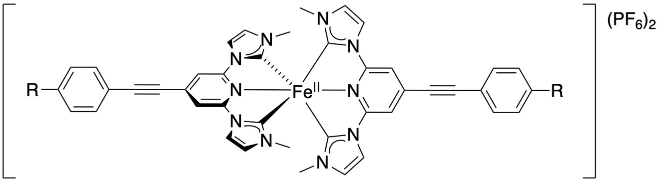

R = Br : **20**
R = NMe$_2$: **21**
R = H : **22**

Figure 5.1: Structure of the three phenyl-ethynyl substituted iron-NHC complexes studied in this chapter.

5.2 Synthesis of homoleptic phenyl-ethynyl substituted complexes

5.2.1 Initial attempts

A number of strategies were considered and investigated for the purpose of obtaining the desired complexes. The earliest synthetic attempts revolved around creating a core complex from which the desired ethynyl-based substitutions could be introduced by Sonogashira couplings. One such attempt was the creation of a homoleptic complex, based on $[Fe(pmbi)_2]^{2+}$ (**1** in Figure 2.8), substituted with bromides in each 4-position of the two pyridines (**23** in Scheme 5.1). This failed, as while it was possible to produce the pre-carbene ligand **P14**, it failed to form a complex with iron (Scheme 5.1a). It was reasoned the ligand may be unstable under the basic conditions and undergo aryne or S_NAr (with the base replacing the bromide) type reactivity. A similar strategy was also considered, consisting of creating a complex substituted by two ethynyl moieties that could be used as the handle for further substitution. The pursuit of a complex substituted by ethynyl moieties in each 4-position of the pyridines (Scheme 5.1b) was abandoned before being fully explored due to the problems, observed in other projects, associated with carrying out palladium catalysed couplings on charged ligands and complexes.

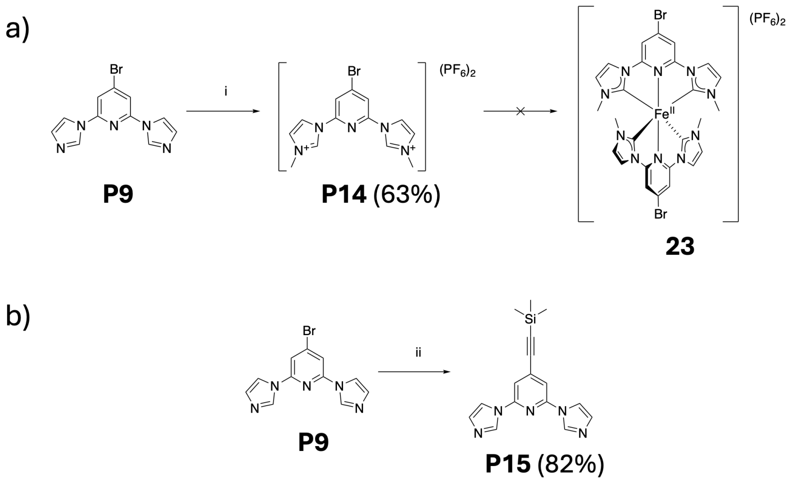

Scheme 5.1: Investigated syntheses towards a bis(phenyl-ethynyl) iron-NHC complex. a) Attempted synthesis of a dibromo-complex **24**. b) Synthesis of a TMS-ethynyl intermediate (**P15**). i) MeOTf, DMF, 95°C. ii) TMS-acetylene, Pd(PPh$_3$)$_2$Cl$_2$ (cat.), CuI (cat.), Toluene, DIPA, 80°C (MW irradiation).

5.2.2 Ligand synthesis

The synthesis eventually settled on was a relatively simple one, where the entire pre-carbene ligand is synthesised and then used to form the complex, as was done in the vast majority of other known iron-NHC complexes, as discussed above. The different ligands were synthesised from a common di(imidazolyl)pyridine derivative by first introducing the appropriate phenyl-ethynyl unit by Sonogashira coupling, at which point the pre-carbene ligand could be obtained by methylation of the imidazole groups. In order for the brominated substituent to be efficient to introduce, it was thought desirable to start from 2,6-di(imidazole-1-yl)-4-iodopyridine (**P17** in Scheme 5.2), as to have good kinetic control of the reaction site during the Sonogashira coupling (avoiding issues of oxidative addition to the Br-C bond). Similar strategies for the Sonogashira coupling involving brominated substituents were found in literature.[106] This compound **P17** was obtained by reacting 2,6-difluoro-4-iodopyridine with sodium imidazolate (reaction of **P16** to **P17** in Scheme 5.2). A precise control of equivalents yielded the desired compound cleanly and in a good yield. This compound could then be converted to the various phenyl-ethynyl derivatives at room temperature, under Sonogashira conditions (reaction of **P17** to **P18**-**P20**, in Scheme 5.2).

The methylation conditions were different for each ligand. Methylation of brominated intermediate **P18** was carried out using MeOTf. The dimethylamine substituted intermediate **P19** could however not be methylated using MeOTf. This was thought to be due to the nucleophilic character of the amine also making it susceptible to methylation by the strong methylating agent. The use of MeI partially solves this issue, plausibly because of the higher reversibility of this reaction. Despite this, significant impurities formed also while using MeI, requiring flash chromatography to purify the product. The unsubstituted intermediate **P20** was methylated using MeI, over 1 h at 130 °C. This was a method found in literature[96] and was only discovered after the synthesis of the other ligands had been finalised. It is possible that this method could also be applied to the other two ligands, but this has not been investigated. MeI was not investigated for the methylation of **P18** as MeOTf was already found to yield the desired pre-carbene ligand **P21** in excellent yields at low temperatures (Scheme 5.2).

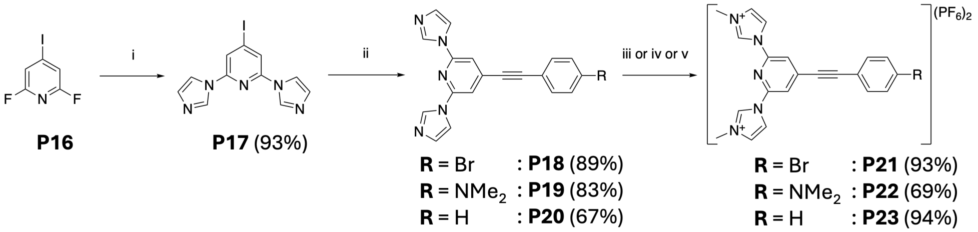

Scheme 5.2: Reactions for the formation of pre-carbene ligands with phenyl-ethynyl moieties, with various substitutions (**P21**-**P23**). i) Sodium imidazolate (2 ep.), DMF, 50 °C. ii) Phenyl acetylene/1-Bromo-4-ethynylbenzene/1-(*N*, *N*-Dimethylamino)-4-ethynylbenzene, $Pd(PPh_3)_2Cl_2$, CuI, DIPA, DMF, rt. iii) MeOTf, DCM, rt (used for **P21**). iv) MeI, MeCN, 85 °C (used for **P22**). v) MeI, DMF, 130 °C (used for **P23**).

5.2.3 Complexation

The formation of these phenyl-ethynyl substituted complexes was throughout more problematic, than that of other complexes based on $[Fe(pmbi)_2]^{2+}$ (**1** in Figure 2.8), of C^N^C type. The complexes containing the ethynyl π-linkers were nevertheless obtained in a manner similar to what has been used previously, with some modification. Most success was found by applying different complexation-conditions for the different ligands. This mainly revolved around the choice of base for the formation of the carbenes. Surprising was that the use of KO*t*-Bu as base, in the case of formation of the brominated complex **20**, gave only trace amounts of the target complex. The use of LDA as the base mostly alleviated these issues, forming the complex in a yield of up to 32% (Scheme 5.3), respectable in comparison with other iron-NHC complexes. This could possibly be explained by the alkoxide adding to the triple bond, with the added electron density being somewhat stabilised by the electron withdrawing bromide. Reversely, use of LDA together with the dimethylamine substituted pre-carbene ligand **P22** was detrimental, and better yields (up to 24%) is achieved by use of KO*t*-Bu, for the formation of the dimethylamino complex **21** (Scheme 5.3). The unsubstituted pre-carbene ligand **P23**, being the intermediate of the three, seem susceptible to detrimental effects of both types of bases and a procedure that consistently gives the complex in a good yield was not found (reproducibly not reaching a yield over 14%; Scheme 5.3). LDA being functional in the formation of one complex but not in the other two is difficult to explain. The most readily available hypothesis is the varied electron density influencing unwanted coordination between LDA (plausibly with the lithium) and the pre-carbene ligand, but any concrete conclusion is not made at this point.

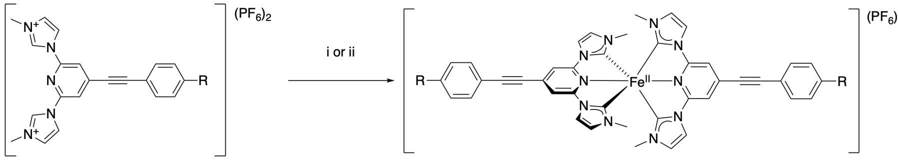

R = Br : **P21**
R = NMe$_2$: **P22**
R = H : **P23**

R = Br : **20** (32%)
R = NMe$_2$: **21** (24%)
R = H : **22** (14%)

Scheme 5.3: Reaction for the formation of various iron-NHC complexes with phenyl-ethynyl moieties with various substitutions. i) 1. LDA (2 eq.), THF, -40 °C; 2. FeBr$_2$ (0.5 eq.), THF, rt (used for **20**). ii) 1. KO*t*-Bu (2.5 eq.), THF, -78 °C; 2. FeBr$_2$ (0.5 eq.), THF, rt (used for **21** and **22**).

Purification of complexes after formation was necessary due to formation of a darkly-coloured, uncharacterizable, impurity. Uncoordinated ligand was also found in the reaction mixtures. The use of size-exclusion chromatography on “bio beads” was found to be the preferred purification method for all three complexes. Chromatography on silica was attempted but ultimately deemed unusable for the removal of the dark impurity as it created severe tailing over the column, making separation impossible. The size-exclusion chromatography does however not provide full separation of complex and impurities, and the chromatography had to be repeated twice to gain pure compound in good amount. The method gives mixed fractions also after repeating the process, which limited the yield somewhat. These mixed fractions can however be collected and subjected to further chromatography to gain more pure material, if desired.

5.3 Photophysical properties

The introduction of the phenyl-ethynyl substituents gave some change to the photophysics of the complexes, compared to the parent complex [Fe(pmbi)$_2$](PF$_6$)$_2$ (**1** in Figure 2.8). The new substitution of the ligand brings about a red-shift of the MLCT transition, as the π*-orbital is lowered in energy. The lower π-system furthermore led to a twofold increase in the ES lifetime, to 18 ps, in line with a π*-orbital energy that is closer to e$_g$-orbital energy. The new substitution additionally served to remove any noticeable sign of an MC state being populated during the deexcitation, as revealed by TA spectroscopy. This could be due to direct deexcitation of the initial MLCT state to GS, or that the deexcitation from any MC state being so much faster than its population, that no significant amount of MC state population could be observed.

Interesting was that the substitution on the phenyl at the end of the ethynyl-bridge brings almost no effect on the photophysical processes involving the iron. All three complexes show the same photophysical behaviour. The one exception was the complex **21**, which showed a strong absorption around 400 nm, in addition to the MLCT band present in all three complexes. This absorption was also observed in the corresponding free ligand **P22**. The transition was thus most probably corresponding to an intra-ligand excitation, effected by the electron donating property of the dimethylamine.

5.4 Towards carboxylic acid derivatives of phenyl-ethynyl substituted complexes

5.4.1 Incentive

One of the reasons for pursuing complexes with phenyl-ethynyl substituents was the possibility of achieving a dye for a DSC, with increased spatial separation between the metal-based HOMOs of the dye, and the CB in TiO_2 (Figure 5.2). This is intended to prevent charge recombination by limiting the overlap between the CB and the orbital principally participating in the recombination event. The use of the phenyl-ethynyl to link the light absorbing dye to an anchoring carboxylic acid (Figure 5.3a) and semi-conductor layer has found wide use and success in the DSC literature, especially in metal-free dyes. Incorporation of a benzo-2,1,3-thiadiazole moiety to improve electron injection is also a commonly used strategy (Figure 5.3b).[74, 81, 111] The desire was to investigate these types of structures in the context of iron-NHC photosensitisers, to see if the issue of charge recombination can be mitigated and if the other successes found with these types of anchoring groups can also be applied in the context of these iron-based dyes.

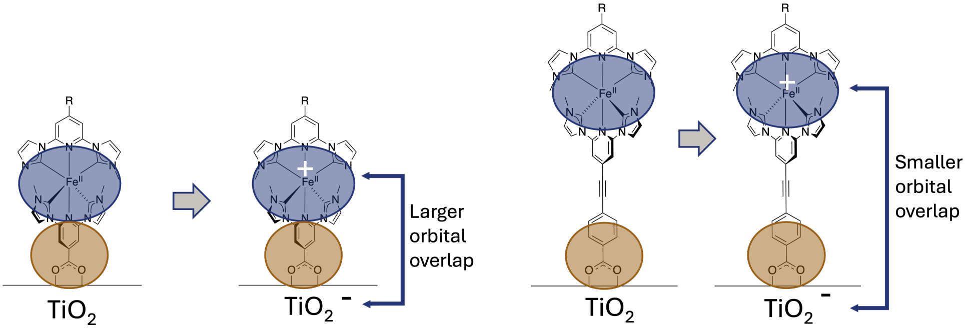

Figure 5.2: Comparison of the hypothetical orbital distribution of the iron-NHC complexes adsorbed to semiconductor surface, with or without an ethynyl-based π-linker. HOMO denoted by blue and LUMO denoted by brown.

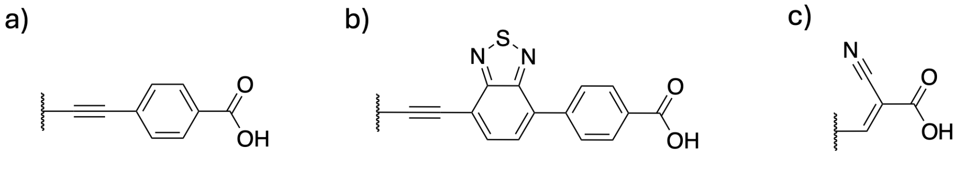

Figure 5.3: Various anchoring units used in DSC-dyes. a) 4-(ethynyl)benzoic acid, b) 4-(7-(ethynyl)-2,1,3-benzothiadiazol-4-yl)benzoic acid, c) cyanoacrylic acid

It should be mentioned that somewhat similar strategies are present in literature, with aromatic units being used to separate the core iron complex from the TiO_2 surface. These failed to generate the same efficiency as a complex where the carboxylic acid is bound directly to the central pyridine, as discussed in Section 3.3. The study claims the issue with these structures is injection, due to the main orbital distribution of the LUMO being located on the aromatic spacer group, rather than the actual anchor, and thus further away from the semi-conductor.[95] The hypothesis of LUMO localisation and injection is however wholly based on calculations, which may be misleading as this is not an issue found in other dyes with more complicated anchoring structures (such as the one pursued here). Additionally, the more advanced cyanoacrylic acid anchoring unit (Figure 5.3c), also widely used in DSC-dyes, showed noticeable improvements in the efficiency of the dye.[94] It was thus believed that these structures warranted investigation, due to their proven efficacy in other dyes and possibility of them helping to avoid charge recombination, a problem postulated to be present for these structures, as per the studies discussed in Chapter 3 and 4.

5.4.2 Synthetic strategies

5.4.2.1 Direct synthesis of carboxylic acid ligand

Several strategies to achieve an ethynyl π-linker with carboxylic acid substituents, have been explored. The first and simplest attempt was the direct synthesis of the ligand and then coordinating it to iron as is done with other ligands (Scheme 5.2 and 5.3). The synthesis of the ligand containing a free carboxylic acid proved difficult. 4-Ethynylbenzoic acid could be reacted with 2,6-dichloro-4-iodopyridine (**P24**) under Sonogashira conditions, to form the desired intermediate (**P25**). Methyl-imidazole groups were however never successfully introduced to this compound (Scheme 5.4a). Reversely, the desired product could not be recovered from an attempted Sonogashira-cross coupling reaction between 4-ethynylbezoic acid and the iodo-intermediate **P17** (Scheme 5.4b).

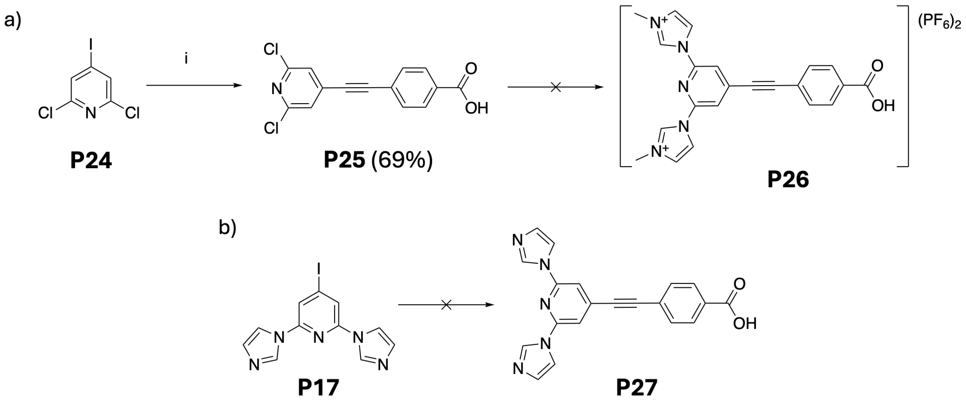

Scheme 5.4: Investigated syntheses towards a carboxylic acid substituted phenyl-ethynyl pre-carbene ligand (**P26**). a) Attempted synthesis starting with Sonogshira coupling. b) Attempted synthesis starting with introduction of imidazole units. i) 4-Ethynylbenzoic acid, $Pd(PPh_3)_2Cl_2$, CuI, DIPA, DMF, rt.

A ligand with a carboxylate unit was seen to be more feasible to be synthesised in the form of a methyl or *tert*-butyl ester (**P28** (not pictured) and **P29**), following the same principles as was used for synthesis of above phenyl-ethynyl containing ligands (Scheme 5.2). The methylation step for these compounds was not made to function as reliably as in previously mentioned reactions (to form the pre-carbene ligands **P21**-**P23**), but evidence of the desired product (**P30**) was found by ^{1}H NMR. Preliminary studies furthermore suggested that the *tert*-butyl ester could be hydrolysed under acidic conditions, giving **P31** (Scheme 5.5). However, further studies showed this ester-containing ligand failed to form the complex under the conditions used to form the complexes **20**-**22** (Scheme 5.3). Both KO*t*-Bu and LDA were tried as a base, but neither gave any evidence of an iron-NHC complex forming. The free carboxylic acid ligand (**P31**), formed by hydrolysis of the ester, likewise failed to form a complex. It has previously been seen that esters are problematic in iron-NHC complex formation, reasoned to be due to the esters susceptibility to undergo attack from the alkoxide base.[112] These structures have the further complication of having Michael-acceptor–like structure, possibly susceptible to nucleophilic attack.

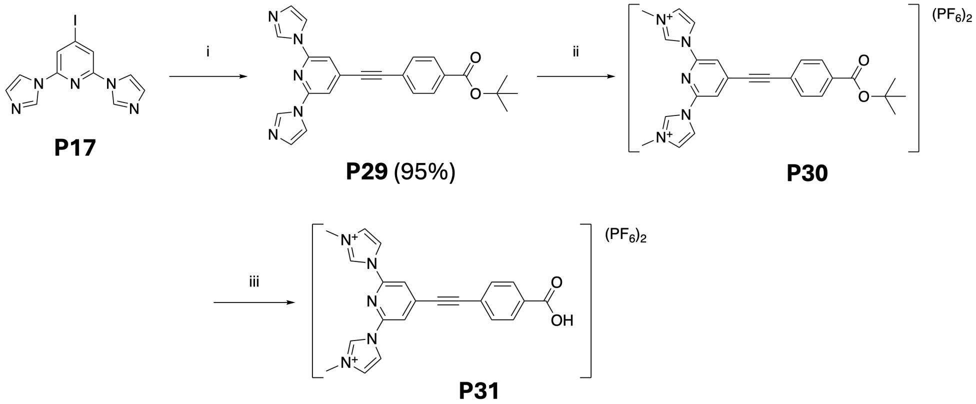

P17

P29 (95%)

P30

P31

Scheme 5.5: Reactions to form a carboxylic acid substituted phenyl-ethynyl pre-carbene ligand **P31**. i) *t*-Butyl 4-ethynylbenzoate, $Pd(PPh_3)_2Cl_2$, CuI, DIPA, DMF, rt. ii) MeI, DMF, 130 °C. iii) Trifluoroacetic acid, DCM.

The introduction of the carboxylic acid concealed as a furanyl group was also considered. It has been shown in other iron-NHC complexes that furanyl moieties can be converted to carboxylic acids by treatment with aqueous $KMnO_4$, while leaving the overall structure of the complex intact.[56, 113] A pilot study was performed were 1-ethynyl-4-furanylbenzene was treated with aqueous $KMnO_4$. As this reaction did not show the desired compound, the strategy was abandoned. It is likely that the ethynyl was also oxidised under the harsh conditions.[114-115]

The use of oxazole as a masked carboxylic acid was also considered, but not pursued due to deprotection conditions being incompatible with the overall synthetic strategy.[116]

5.4.2.2 Carboxylic acid via reaction with carbon dioxide

As more direct attempts failed to give the desired complex, the already synthesised bromo-substituted complex **20** (Figure 5.1) was used in an attempt to replace the bromide with carboxylates. The complex **20** was thus treated with *n*-BuLi for a lithium-halogen exchange reaction which then would yield a nucleophilic carbon, that could react with carbon dioxide. Investigation of the reaction by quenching the so formed lithiated species with deuterium oxide revealed that while the lithium halogen exchange takes place, the proton at the 5-position of the imidazolylidene is acidic enough to be deprotonated by the *n*-BuLi. This could be observed by ^1H

NMR, where the compound matched that of a hexadeutero version of the complex **22** (Figure 5.4). Signals corresponding this hexadeutero analog were also observed by mass spectrometry. This suggests the hexa-lithiated version of the complex as an intermediate during this reaction.

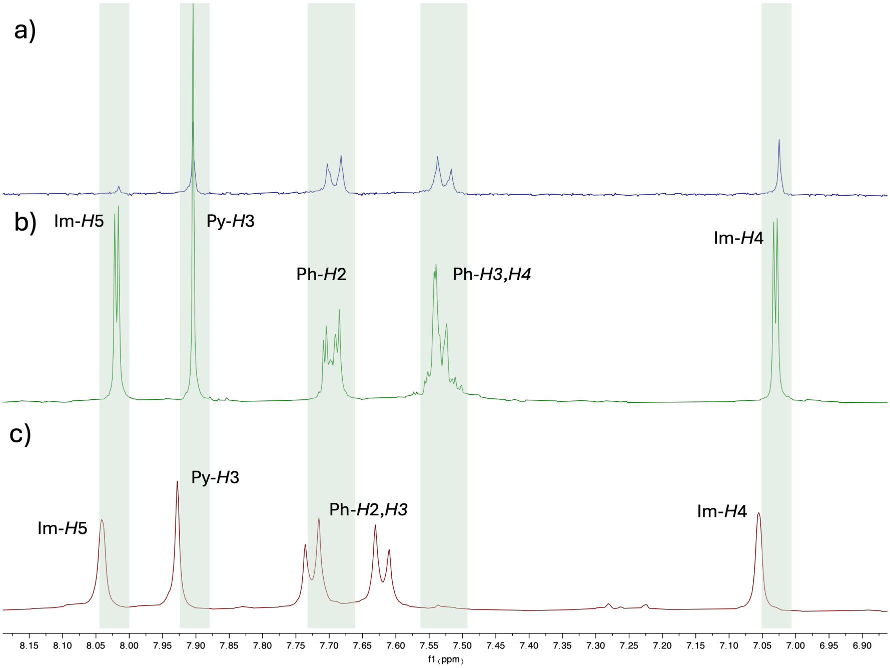

Figure 5.4: Comparison of the aromatic region of ^{1}H NMR of various phenyl-ethynyl substituted complexes. a) Resultant spectrum from treatment of the complex **20** with *n*-BuLi, followed by D_2O. b) Spectrum of the complex **22**. c) Spectrum of the complex **20**. Assigment of peaks as determined by COSY and NOESY experiments. Note change in shape of multiplett at 7.5 ppm between a and b, due to assumed deuteration of the Ph-4 position in the case of a.

Treating the so formed lithiated species with carbon dioxide led to decomposition of the material (Scheme 5.6). Attempts to control the amount of *n*-BuLi to 2 eq. led to a mixture of lithium-halogen exchange events and deprotonations (again, as seen by quenching with D_2O and probing with ^{1}H NMR).

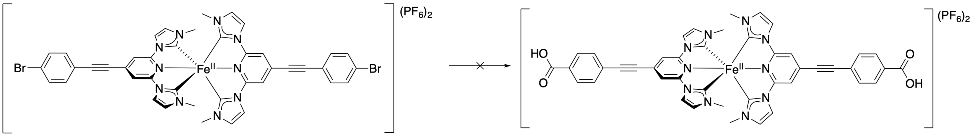

20 **24**

Scheme 5.6: Attempted carboxylation in the pursuit of a phenyl-ethynyl complex bearing carboxylic acid moieties.

To avoid the problem of deprotonation, the possibility of transforming the brominated positions of the bromo-substituted complex **20** into Grignard reagents by reaction with magnesium was also investigated. Conditions as forcing as refluxing the material in THF, with iodine present, led to no observable reaction with the complex **20** . Issues with this transformation may be linked to the low solubility of both reactants (the complex and magnesium) in THF (Scheme 5.6).

Finally, in order to circumvent the issue of deprotonation of the imidazole, a strategy of blocking the apparently acidic imidazole-5*H* position was devised. For ease of synthesis, an imidazole moiety methylated at the 4 and 5 positions was introduced, in a synthetic path otherwise identical to the synthesis of the complex **20** (Scheme 5.2 and 5.3). Following the same synthetic principles yielded the analog of the complex **20** with two additional methyl groups for each imidazolylidene group (**25**). Yields for these reactions were generally lower than those achieved during the synthesis of the complex **20** (Scheme 5.7). Especially the purification of the complex was arduous, as impurities of the free ligand were very difficult to remove, severely limiting the yield. Furthermore, additional signals were found in the NMR spectra of the intermediates **P33** and **P34**. This may be attributed to impurities, but as repeated chromatography led to no change in the intensity of these additional signals. It may thus be that the additional methyl groups impose a rotation barrier such that two rotamers are detectable by NMR. The absorption spectrum of the complex **25** is redshifted by 15 nm, compared to the complex **20**, more or less consistent with its closest comparison in literature.[66]

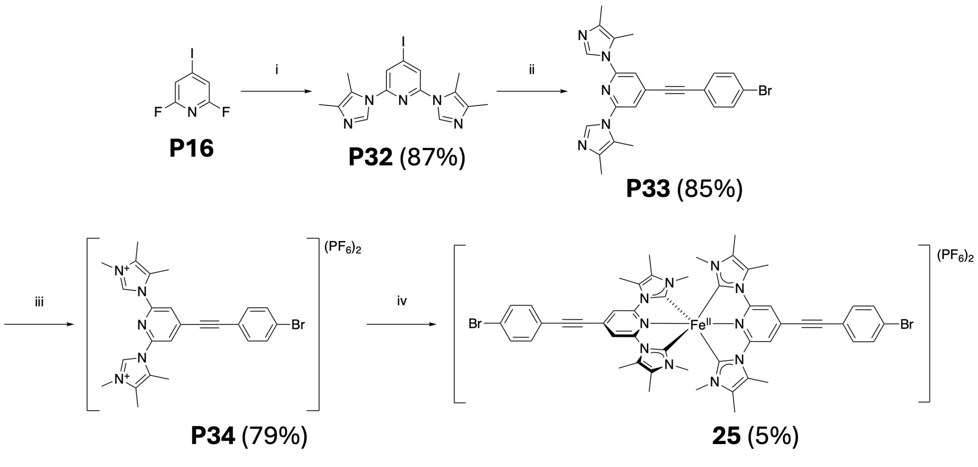

Scheme 5.7: Reactions to form an analog of the complex **20**, with methyl groups introduced at 4- and 5-position of each imidazolylidene unit (**25**). i) Sodium imidazolate (2 ep.), DMF, 50 °C. ii) 1-Bromo-4-ethynylbenzene, $Pd(PPh_3)_2Cl_2$, CuI, DIPA, DMF, rt. iii) MeOTf, DCM, rt. iv) 1. LDA (2 eq.), THF, -40 °C; 2. $FeBr_2$ (0.5 eq.), THF, rt.

Exposure of the material to *n*-BuLi followed by carbon dioxide, again did not lead to the desired outcome. The several failed attempts at obtaining the desired complex may point to some fundamental issue with the carboxylic acid in combination with the ethynyl spacer on the iron-NHC, that is as of yet not understood.

5.5 Conclusions

The introduction of phenyl-ethynyl units to the core ligand structure could be efficiently done using Sonogashira cross-coupling. This was especially true following the obtaining of 2,6-di(imidazole-1-yl)-4-iodopyridine (**P17**), giving an intermediate with an iodide substituent as a handle for efficient derivatisation. The complexation of these new ligands to iron was more complicated, compared to the majority of previously published iron-NHC complexes. The choice of base proved to have a large influence on the outcome of the complexation reactions, for reasons that are not wholly understood. Complications were especially severe on the point of introducing a phenyl-ethynyl group substituted by a carboxylate unit, where no successful reaction was ever accomplished.

The introduction of the phenyl-ethynyl substituent provided some extension of the ES lifetime, doubling it from the corresponding ES lifetime of the unsubstituted parent complex ($[Fe(pbmi)_2](PF_6)_2$ (**1**) in Figure 2.8), probably due to the influence on the ligand orbitals, induced by the large conjugate phenyl-ethynyl moiety. However, substitution pattern on the other end of the phenyl-ethynyl moiety had almost no effect on the ES dynamics of the complex. This could call into question the possibility of long-distance CT within these iron complexes, as the peripheral parts of the complex seem to have no influence on the iron centre.

The use of these types of complexes in solar cell applications proved highly difficult due to the failure to incorporated carboxylic acid groups to the necessary complex. Furthermore, the lack of influence of the peripheral substituent on the ES of the complex may hint at a lack of electronic communication between the sections of the complex, and thus prove a hinderance to electron injection in a DSC application. This would then be somewhat in line with previous literature discussed above.[95]

A different π-linker that may prove less challenging to synthesise, should perhaps be devised for use in DSC applications, rather than continuing the pursuit of this deeply challenging structure. This may make it possible to more closely investigate the effect of spatial separation of the compound from the semiconductor surface.

6 Iron-NHC complexes with dihydroimidazolylidene-based ligands (Paper IV)

6.1 Background

It has long been known that NHCs based on dihydroimidazole are stronger σ-donors than those based on imidazole (Figure 6.1).[53] While not the most drastic of changes, it held the promise of increasing the ligand field and thus inducing the desired, larger splitting of the metal centred orbitals.

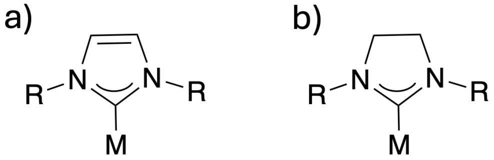

Figure 6.1: Comparison of two types of NHC ligands: a) imidazolylidene and b) dihydroimidazolylidene.

6.2 Synthesis

It was found that the iron-NHC C^N^C structures are susceptible to hydrogenation under heterogeneous catalysis, using 10% palladium on activated carbon (Pd/C). This allowed for quick and efficient synthesis of the dihydroimidazolylidene version (**26**) of compound $[Fe(pbmi)_2](PF_6)_2$ (**1**; Scheme 6.1). This is a departure from previous synthetic modifications of iron-NHC structures, which have generally taken place before the final formation of the complex.

The reaction rate of hydrogenation steadily decreases (as tracked by ^{1}H NMR), after initiation. The lowering of the reaction rate is such that if full hydrogenation is not reached within 17 h, the reaction rate will have dropped so significantly that full conversion of all four reactive double bonds in the starting material, becomes untenable. Tentatively this issue is related to deactivation of the catalyst, as addition of further Pd/C after reaction has stopped led to renewed reactivity. This seeming deactivation is also observed when as much as three equivalents (by weight) of Pd/C are initially added, but the reaction stopping due to an inadequate volume of hydrogen gas being present. The deactivation of the catalyst seems to be more or less only a function of time in the presence of the utilised iron-NHC complex.

When running the reaction in a very small scale, three equivalents (by weight) of Pd/C were necessary for the reaction to go to completion. The hydrogenation was then complete within 17 h. The use of smaller amounts of catalyst led to a mixture of complexes, with different degrees of hydrogenation.

Scaling up the reaction to 50 mg of complex to be hydrogenated slowed down the reaction further. The hydrogenation then did not finish after being left over night and complete reaction could not be achieved, as discussed above. The larger scale reaction could be made functional by the addition of two additional equivalents of Pd/C (again by weight) after the reaction had stopped. The reaction then finishes within another 20 h, resulting in a total reaction time of 43 h.

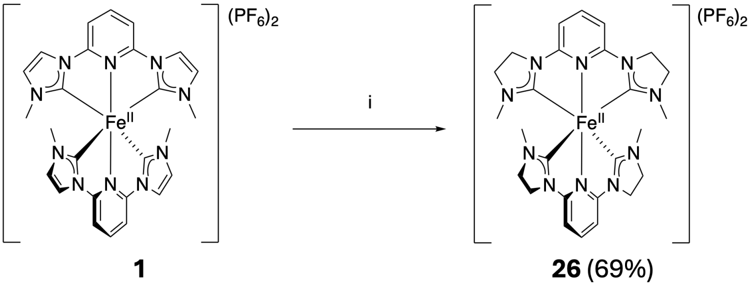

Scheme 6.1: Reaction to form the complex **26** by hydrogenation of the imidazolylidene units of iron-NHC complex [Fe(pbmi)$_2$](PF$_6$)$_2$ (**1**). i) Pd/C, H$_2$ (g), acetone, rt.

Additionally, attempts to hydrogenate the uncoordinated, pre-carbene ligand of **1** (H$_2$[pbmi](PF$_6$)$_2$), failed to give any reaction under the same conditions as those applied to the complex, outlined above. This shows a substantial change in electronics of the NHC units upon coordination to the metal. The observed lack of reactivity in the pre-carbene ligand is expected for an aromatic system, such as imidazolium. The coordination of the NHC thus seem to break the aromaticity of the imidazole-ring to such a degree that it can react similarly to a normal alkene. It is known in literature that the π-electrons of the NHC are not fully delocalised over the backbone.[53, 117]

Furthermore, the method of using Pd/C for the hydrogenation of imidazolylidenes has additionally been tested on the previously known complexes [Fe(cpbmi)$_2$](PF$_6$)$_2$ (**2** in Figure 2.8),[55-56] as well as a Co(III) version of [Fe(pbmi)$_2$](PF$_6$)$_2$ (Figure 2.8), [Co(III)(pbmi)$_2$](PF$_6$)$_3$.[118] Preliminary findings suggest that the reaction is also possible for these complexes, but fully functional procedures have not been established for these conversions as of yet.

6.3 Photophysical properties

The small structural change to the ligand induced by the hydrogenation seems to have a profound effect on the photophysical properties of the complex. The dihydroimidazolylidene units seem to induce a somewhat stronger σ-donation to the iron centre of the complex. This destabilised the MC electronic states of the complex. Simultaneously, the smaller ligand π-system that comes about by hydrogenation also destabilise the ligand centred orbitals. This led to a blue-shift of the absorption band attributed to the MLCT transition in the complex. Additionally, the changes in the states of the complex effected an ES with a lifetime of 75 ps. This state was determined to be to be MC in nature, developing from a deactivation of the MLCT state that takes place on sub-ps time scale.

6.4 Conclusions

The photophysical properties of $[Fe(pbmi)_2](PF_6)_2$ were substantially affected by the relatively small change of exchanging imidazolylidene ligands for dihydroimidazolylidene ligands. This was accomplished by the relatively simple synthetic transformation of hydrogenation under heterogenous catalysis.

The extended lifetime of the complex is still somewhat short for the photosensitiser to be clearly applicable in the context of photochemistry. While a substantial extension, the 75 ps MC excited state lifetime observed are only a fraction of the ns time scales commonly quoted as being necessary for photocatalysis.[28, 35] The ES was furthermore of an MC nature, as opposed to the MLCT commonly strived for with these photosensitisers. Despite this shortcoming, the findings may provide a step towards a new strategy for realizing Fe-NHC photosensitisers.

The apparent possibility of applying this methodology to other related structures could additionally make this strategy of further interest. The possibility of combining this strategy with others known ligand systems, known to provide stabilisation to the MLCT state (i.e. $[Fe(cpbmi)_2](PF_6)_2$ (**2** in Figure 2.8)), could plausibly counteract the issues of a destabilisation of π*-orbitals induced by the hydrogenation of the imidazolylidenes. This may allow for the effect garnered by the increased σ-donation from the dihydroimidazolylidene to be of use. The ease with which this strategy can seemingly be utilised may furthermore give the possibility of applying it to other complexes not yet investigated, to further explore its impact on the photophysics of iron-NHC photosensitisers.

7 Conclusions and outlook

Throughout this work are described the efforts to produce coordination complexes of iron, in order to understand and improve the photophysical properties of this metal, which has long been of interest for photosensitiser-applications. Specifically, the studies here aimed to try to leverage the well-studied, core iron-bis(tridentate) structure, with four NHC units (the basic structure of $[Fe(pbmi)_2](PF_6)_2$ (**1** in Figure 2.8)), in order to obtain complexes with new properties.

In these systems, the strongly σ-donating NHC groups provide the basis for the improvement of photosensitiser properties of iron. Simultaneously, the 4-positions of the core pyridines provide a clear point for modification, giving good electronic communication with the metal centre, as well as the possibility for linearly aligned substituents. This approach allowed for the utilisation of well-tested methods for the synthesis of iron-NHC complexes, where the pre-carbene ligand is deprotonated to form the free carbene, which then coordinates to iron. Modifications to the ligand structures have generally been accomplished before the formation of the complexes, by known chemical transformations. Palladium-mediated bond-forming reactions have found wide utility for these derivatisations of the ligands, due to the large extent to which these systems are aromatic. An alternative strategy focused on modifying the NHC groups by hydrogenation, for the purpose of increasing σ-donation from the carbenes. This required the establishment of new procedures for post-complexation modification of the complexes, which led to an easily utilised tool for the tuning of photosensitiser properties. The strategy was however limited by it increasing the energy of the ligand centred π*-orbitals, detrimental to extending the lifetime of the MLCT state.

The various complexes were investigated in a variety of contexts. The effect of the modifications of the complexes, on their light absorption properties as well as ES dynamics, were studied. These were of interest for a deeper understanding of these types of photosensitisers, in the pursuit of iron-NHC complexes with new and improved properties.

Additionally, carboxylic acid complexes capable of being adsorbed onto TiO_2, were also investigated in DSC applications. This allowed for the study of the effects of ligand-substitution on solar cell properties, as well as these substituents' interactions with various parts of the solar cell. This was done by the realisation and application of heteroleptic complexes with different amino-based substituents, along with the mentioned carboxylic acids. The resulting complexes furthermore showed a clear improvement in efficiency, compared to the homoleptic, dicarboxylic acid complex $[Fe(cpbmi)_2](PF_6)_2$ (**2** in Figure 2.8). More complicated structures did however not necessarily show better performance compared to simpler heteroleptic complexes. Despite this success found in the use of iron-NHC complexes as dyes for solar cell application, these complexes still have a long way to go before being viable. Many avenues remain which could be explored for improved photophysical dynamics of the iron-NHC photosensitiser on a semiconductor surface, and in a DSC context. However, a substantial change to how these dyes function must be achieved in order to come close to the best performing DSCs, much less the best solar cells in general.

The relatively small modifications applied to the core structure could bring about relatively large changes in the photophysical properties in the complexes. This is perhaps best exemplified by exchanging imidazolylidene units for dihydroimidazolylidene units, bringing about a 75 ps MC excited state lifetime. It can furthermore be clearly seen that modifications of the core structure are far more impactful than peripheral modifications, as modification at the end of a long π-system gave almost no effect on the photophysical processes the iron-centre undergoes, as seen phenyl-ethynyl substituted complexes.

Based on the work presented here, and the trends in literature, the use of ligands with strong σ-donation and π-systems that can accept photoexcited electrons, still seem to have a good potential for bringing about a well-functioning iron-photosensitiser. Whether or not such a photosensitiser will come in the form of a complex with *N*-heterocyclic carbenes the future will tell, but its discovery will most likely require a deep and detailed understanding of the chemical and physical characteristics specific to iron.

8 Additional synthetic procedures

This chapter contains the experimental procedures that have been investigated and established during the work with this thesis, which are related to, but fall outside the scope of the included papers.

8.1 Synthesis

General. All commercial reagents and solvents were used as received unless otherwise specified. 4,5-Dimethylimidazole[119] and *t*-Butyl 4-ethynylbenzoate[120-121] were synthesised according to literature procedure. CuBr was purchased from Acros. HBr (concd. aq.), $NaNO_2$, $Pd(PPh_3)_2Cl_2$, CuI, diisopropylamine (DIPA), trimethylsilylacetylene, KPF_6, methyl 4-ethynylbenzoate, NaH (60 % in mineral oil), and *n*-BuLi (2.5 M solution in hexanes) were purchased from Merck. NaH was additionally washed three times before use; this was done by stirring the reagent with dry hexane (obtained from MBraun MB-SPS 800 solvent purification system) before decanting of the solvent. Ammonia (25 % in water) and methyl triflate (MeOTf) was purchased from ThermoScientific. Ammonium hexafluorophosphate (NH_4PF_6) was purchased from Apollo Scientific. 2,6-difluoro-4-iodopyridine was purchased from AmBeed (via Chemtronica). 1-Bromo-4-ethynylbenzene was purchased from TCI. Hydrochloric acid (concd. aq.) was purchased from VWR. Anhydrous iron(II) bromide ($FeBr_2$) was purchased from Alfa Aesar and stored and weighed under nitrogen in a glovebox. Dry toluene and dichloromethane (DCM) were obtained from MBraun MB-SPS 800 solvent purification system. Tetrahydrofuran (THF) without stabilizer was dried over Na/benzophenone and subsequently distilled under N_2, and further dried over activated molecular sieves (3Å), before use. Dimethylformamide (DMF) was dried over activated molecular sieves (3 Å) for approx. 1 h before use. Reactions run at room temperature (rt) were in the range of 18-23 °C. Metal heating mantels were used to achieve required reaction temperatures. Air- and moisture-sensitive reactions were carried out in oven-dried glassware capped with rubber septa, under a positive pressure of nitrogen. Flash column chromatography (⌀ x h) was carried out on silica gel (60 Å, 230-400 mesh, purchased from Merck) using reagent-grade eluents. Size exclusion chromatography (⌀ x h) was carried out on BioBeads S-X1 (200-400 mesh, purchased from Bio Rad). Before loading on size exclusion column, all samples were dissolved in minimal amount of eluent and filtered through syringe filter (Fisherbrand, PTFE, 0.45 µm porosity, 13 mm diameter). Analytical thin-layer chromatography (TLC) was carried out on TLC Silica gel 60 F254 and visualized with a UV-lamp (254 nm/365 nm). ^{1}H NMR and ^{13}C NMR spectra were recorded at rt on a Bruker Avance II spectrometer (at 400.1 MHz and 100.6 MHz, respectively) or on a Bruker Avance III HD spectrometer (at 500 MHz and 126 MHz, respectively). The spectra were recorded in $CDCl_3$, CD_3CN or CD_3OD and the residual solvent signals (7.26/77.16; 1.94/118.26; 3.31/49.00 ppm, respectively) were used as reference. Chemical shifts (δ) are expressed in parts per million (ppm) and coupling constants (*J*) are reported in Hertz (Hz). The following abbreviations are used to indicate apparent multiplicities: s, singlet; d, doublet; dd, doublet of doublets; t, triplet; m, multiplet. Melting points were measured using a Stuart melting point apparatus SMP3 and were corrected against 3,5-dinitrobenzoic acid (mp 205 °C[48]), High resolution mass spectrometry was carried out using a Waters - XEVO-G2 QTOF spectrometer employing electrospray ionization and run in positive mode. Elemental analyses were performed by A. Kolbe, Mikroanalytisches Laboratorium, Germany.

4-Bromo-2,6-di(imidazol-1-yl)pyridine (P9). A solution of 4-amino-2,6-(imidazol-1-yl)pyridine (**P4**) (501 mg, 2.21 mg) and CuBr (641 mg, 4.47 mmol) in HBr (48 %, aq, 24 mL) was cooled to -20 °C and $NaNO_2$ (1532 mg, 22.21 mmol, aq., 7 mL) was added to it dropwise over 25 min. After complete addition the resulting reaction mixture was allowed to warm to rt and was stirred for 21 h. Brown gas was released from the reaction and the reaction mixture turned black. The reaction was cooled to 0 °C and basified by dropwise adding ammonia (12%, aq., 55 mL). The reaction turned blue, and precipitate formed as pH increases. The reaction was extracted with EtOAc/*n*-BuOH (9:1; 4 x 100 mL). The combined organic phases were washed with brine (2 x 100 mL), dried over Na_2SO_4, and evaporated *in vacuo*. The resulting solid was dissolved in DCM/MeOH (9:1) and the resulting solution filter through a plug of silica (5 x 2 cm). The silica plug was extracted with several portions of DCM/MeOH (9:1) and the filtrate was evaporated *in vacuo*, giving the product as a white solid (530 mg, 82 %). R_f = 0.26 (DCM/MeOH 20:1) Mp: 208 °C dec; ^{1}H NMR (400 MHz, CD_3OD) δ = 8.71 (t, *J* = 1.1 Hz, 2H, Im-*H*2), 8.03 (t, *J* = 1.5, 2H, Im-*H*5), 8.01 (s, 2H, py-*H*3), 7.19 (dd, *J* = 1.7, 1.0 Hz, 2H, Im-*H*4) ppm; ^{13}C NMR (101 MHz, CD_3OD) δ 150.01, 138.64, 137.02, 130.94, 118.17, 114.91 ppm; ESI-HRMS: m/z [M+H]+ calcd for $C_{11}H_9BrN_5$: 290.0041; found 290.0045; Anal. Calcd for $C_{11}H_8BrN_5$: C 45.54, H 2.78, N 24.14. Found: C 45.44, H 2.77, N 24.16.

1,1'-(4-Bromopyridine-1,6-diyl)bis(3-methylimidazolium) bis(hexafluorophosphate) (P14). A dry solution of 4-bromo-2,6-di(imidazol-1-yl)pyridine (**P9**) (175 mg, 0.603 mmol) in DMF (3 mL) was cooled to -78 °C, and to it was dropwise added MeOTf (0.7 mL, 6 mmol). The resulting mixture was heated to 95 °C, and stirred for 45 h. The resulting reaction solution was allowed to cool to rt and to it was added a solution of NH_4PF_6 (234 mg, 1.44 mmol) in water (10 mL). The resulting precipitate was collected on a glass filter (#4) and wash consecutively with water, petroleum ether and Et_2O, giving the product a white solid (230 mg, 63%). ^{1}H NMR (500 MHz, CD_3CN) δ = 9.45 (d, *J* = 1.8 Hz, 2H, Im-*H*2), 8.18 (s, 2H, Py-*H*3), 8.14 (t, *J* = 2.0 Hz, 2H, Im-*H*5), 7.62 (t, *J* = 1.9 Hz, 2H, Im-*H*4), 4.01 (s, 6H, Im-C*H*$_3$) ppm; ^{13}C NMR (126 MHz, CD_3CN) δ = 146.84 (Py-*C*4), 139.75 (Py-*C*4), 136.56 (Im-*C*2), 126.35 (Im-*C*4), 120.38 (Im-*C*5), 119.29 (Py-*C*3), 37.80 (Im-*C*H$_3$) ppm.

2,6-Di(imidazol-1-yl)-4-((trimethylsilyl)ethynyl)pyridine (P15). To a dry, degassed solution of 4-bromo-2,6-di(imidazol-1-yl)pyridine (**P9**) (99.9 mg, 0.344 mmol), $Pd(PPh_3)_2Cl_2$ (12.5 mg, 0.0178 mmol) and CuI (12.1 mg, 0.0635 mmol) in DIPA (1 mL) and toluene (2.5 mL) was dropwise added trimethylsilylacetylene (0.14 mL, 1.0 mmol). The resulting mixture was heated to 80 °C by MW-irradiation and stirred for 3 h. The resulting reaction mixture was allowed to cool to rt and diluted with water (10 mL). The resulting mixture was extracted with EtOAc (4 x 10 mL). The combined organic phases were washed with brine (40 mL) and evaporated *in vacuo*. The residue was further purified by silica gel chromatography (3 x 15 cm, DCM/MeOH 94:6), giving the product as an off-white solid (87 mg, 82%). ^{1}H NMR (400 MHz, CD_3OD) δ = 8.70 (s, 2H, Im-*H*2), 8.03 (s, 2H, Im-*H*5), 7.76 (s, 2H, Py-*H*3), 7.18 (s, 2H, Im-*H*4), 0.29 (s, 9H, Si-C*H*$_3$) ppm; ^{13}C NMR (126 MHz, CD_3OD) δ = 149.90, 138.82, 133.05, 130.89, 118.23, 113.69, 103.28, 101.91, -0.52 ppm.

Methyl 4-((2,6-di(imidazol-1-yl)pyridin-4-yl)ethynyl)benzoate (P28). To a dry, degassed solution of 2,6-di(imidazol-1-yl)-4-iodopyridine (**P17**) (392 mg, 1.16 mmol), $Pd(PPh_3)_2Cl_2$ (81 mg, 0.12 mmol) and CuI (22 mg, 0.12 mmol) in DIPA (2 mL) and DMF (30 mL) was dropwise added a dry, degassed solution of methyl 4-ethynylbenzoate (217 mg, 1.35 mmol) in DMF (20 mL) over 4 min. The resulting solution was stirred at rt for 17 h. To the resulting reaction mixture was added NH_4Cl (saturated aq., 100 mL), and the resulting suspension was extracted with $CHCl_3$ (3 x 100 mL). The combined organic phases were washed with brine (200 mL), dried over $MgSO_4$, and evaporated *in vacuo*. The residue was further purified by silica gel chromatography (3 x 16 cm, DCM/MeOH 95:5), giving the product as an off-white solid (320 mg, 75%). ^{1}H NMR (500 MHz, $CDCl_3$) δ = 8.40 (s, 2H, Im-*H*2), 8.10 (d, *J* = 8.4 Hz, 2H, Ph-*H*2/Ph-*H*3), 7.71 – 7.64 (m, 4H, Im-*H*5 & Ph-*H*2/Ph-*H*3), 7.38 (s, 2H, Py-*H*3), 7.25 (s, 2H, Im-*H*4), 3.95 (s, 3H, Ph-CO$_2$C*H*$_3$) ppm; ^{13}C NMR (126 MHz, $CDCl_3$) δ = 166.30, 148.80, 137.09, 135.18, 132.17, 131.49, 131.29, 129.91, 125.71, 116.24, 111.63, 95.47, 87.83, 52.59 ppm; ESI-HRMS: m/z $[M+H]^+$ calcd for $C_{21}H_{15}N_5O_2$: 370.1299; found 370.1300.

***tert*-Butyl 4-((2,6-di(imidazol-1-yl)pyridin-4-yl)ethynyl)benzoate (P29).** To a dry, degassed solution of 2,6-di(imidazol-1-yl)-4-iodopyridine (**P17**) (77 mg, 0.23 mmol), $Pd(PPh_3)_2Cl_2$ (17 mg, 0.024 mmol) and CuI (5 mg, 0.03 mmol) in DIPA (0.5 mL) and DMF (5 mL) was dropwise added a dry, degassed solution of *tert*-butyl 4-

ethynylbenzoate (65 mg, 0.32 mmol) in DMF (4.5 mL) over 4 min. The resulting solution was stirred at rt for 14 h. To the resulting reaction mixture was added NH_4Cl (saturated aq., 15 mL), and the resulting suspension was extracted with $CHCl_3$ (3 x 15 mL). The combined organic phases were washed with brine (30 mL), dried over $MgSO_4$, and evaporated *in vacuo*. The residue was further purified by silica gel chromatography (2 x 15 cm, DCM/MeOH 96:4), giving the product as an off-white solid (90 mg, 95%). ^1H NMR (400 MHz, CD_3OD) δ = 7.37 (s, 2H), 6.69 (s, 2H), 6.66 (d, J = 8.6 Hz, 2H), 6.53 (s, 2H), 6.36 (d, J = 8.7 Hz, 2H), 5.84 (s, 2H), 0.25 (s, 9H) ppm.

2,6-Bis(4,5-dimethylimidazol-1-yl)-4-iodopyridine (P32). To a solution of NaH (113 mg, 4.73 mmol) in dry DMF (10 mL), cooled to 0 °C, was added 4,5-dimethylimidazole (390 mg, 4.06 mmol) and the resulting mixture was stirred for 1 h, at 0 °C. To the resulting reaction solution was added 2,6-difluoro-4-iodopyridine (**P16**) (496 mg, 2.06 mmol) and the reaction was heated to 50 °C and stirred for 16 h. The reaction was allowed to cool to rt and diluted with water (50 mL). The resulting suspension was extracted with chloroform (3 x 50 mL) and the combined organic phases were consecutively washed with water (100 mL), dried over $MgSO_4$, and evaporated *in vacuo*, giving the product as an off-white solid (703 mg, 87%). ^1H NMR (400 MHz, $CDCl_3$) δ = 7.86 (s, 2H, Im-*H*2), 7.63 (s, 2H, Py-*H*3), 2.35 (s, 6H, Im5-CH_3), 2.23 (s, 6H, Im4-CH_3) ppm; ^{13}C NMR (101 MHz, $CDCl_3$) δ = 149.65, 136.80, 134.95, 122.84, 122.33, 108.53, 12.84, 10.80 ppm.

4-((4-Bromophenyl)ethynyl)-2,6-bis(4,5-dimethylimidazol-1-yl)pyridine (P33). To a dry, degassed solution of 2,6-bis(4,5-dimethylimidazol-1-yl)-4-iodopyridine (**P32**) (400.2 mg, 1.018 mmol), $Pd(PPh_3)_2Cl_2$ (63.2 mg, 0.0900 mmol) and CuI (24.0 mg, 0.126 mmol) in DIPA (2 mL) and DMF (20 mL) was dropwise added a dry, degassed solution of 1-bromo-4-ethynylbenzene (280.8 mg, 1.551 mmol) in DMF (3 mL). The resulting orange solution was stirred at rt for 20 h. To the resulting reaction mixture was added NH_4Cl (saturated aq., 50 mL), and the resulting suspension was extracted with $CHCl_3$ (3 x 50 mL). The combined organic phases were washed with brine (100 mL), dried over $MgSO_4$, and evaporated *in vacuo*. The residue was further purified by silica gel chromatography (3 x 20 cm, DCM/MeOH 94:6), giving the product as an off-white solid (384 mg, 85%). ^1H NMR (500 MHz, $CDCl_3$) δ = 7.89 (s, 2H, Im-*H*2), 7.57 – 7.53 (m, 2H, Ph-*H*2/Ph-*H*3), 7.47 – 7.43 (m, 2H, Ph-*H*2/Ph-*H*3), 7.32 (s, 2H, Py-*H*3), 2.38 (s, 6H, Im5-CH_3), 2.23 (s, 6H, Im4-CH_3) ppm; ^{13}C NMR (126 MHz, $CDCl_3$) δ = 149.90, 136.51, 134.94, 133.55, 132.15, 128.57, 124.65, 122.37, 120.24, 115.65, 95.30, 86.59, 12.83, 10.83 ppm.

1,1’-(4-((4-Bromophenyl)ethynyl)pyridine-2,6-diyl)bis(3,4,5-trimetylimidazolium) bis(hexafluorophosphate) (P34). A suspension of 4-((4-bromophenyl)ethynyl)-2,6-bis(4,5-dimethylimidazol-1-yl)pyridine (**P33**) (201 mg, 0.450 mmol) in DCM (20 mL), was cooled to 0 °C, and to it was dropwise added MeOTf (0.2 mL, 2 mmol). The resulting mixture was allowed to warm to rt and stirred at that temperature for 21 h. The resulting mixture was evaporated *in vacuo* and the residue was dissolved in MeOH (5 mL). To the resulting solution was added HCl (concd. aq., 0.05 mL), followed by KPF_6 (saturated aq., 5 mL), and the resulting precipitate was collected on a glass filter (#3). The precipitate was washed with water (3 x 5 mL) and dried *in vacuo*, giving the product as an off-white solid (272 mg, 79%). ^{1}H NMR (500 MHz, CD_3CN) δ = 8.80 (s, 2H, Im-*H*2), 7.88 (s, 2H, Py-*H*3), 7.71 – 7.67 (m, 2H, Ph-*H*2/Ph-*H*3), 7.59 – 7.55 (m, 2H, Ph-*H*2/Ph-*H*3), 3.83 (s, 6H, Im3-C*H*$_3$), 2.38 (s, 6H, Im5-C*H*$_3$), 2.32 (s, 6H, Im4-C*H*$_3$) ppm; ^{13}C NMR (126 MHz, CD_3CN) δ = 147.64, 139.28, 135.63, 134.77, 133.22, 130.26, 127.98, 125.64, 123.09, 120.67, 98.42, 86.19, 35.00, 10.04, 8.37 ppm.

Bis(1,1´-(4-((4-bromophenyl)ethynyl)pyridine-2,6-diyl)bis(3,4,5-trimethylimidazolylidene))iron bis(hexafluorophosphate) (25). 1,1´-(4-((4-bromophenyl)ethynyl)pyridine-2,6-diyl)bis(3,4,5-trimethylimidazolium) bis(hexafluorophosphate) (**P34**) (99.8 mg, 0.130 mmol) was heated to 70 °C *in vacuo* for 88 h. The solid was allowed to cool to rt and suspended in dry, degassed THF (7 mL). The resulting suspension was cooled to -40 °C. Separately, to a solution of DIPA (0.04 mL, 0.3 mmol) in dry, degassed THF (5 mL), cooled to -78 °C, was added a solution of *n*-BuLi (2.5 M in hexanes, 0.1 mL, 0.25 mmol) and the resulting solution was stirred for 1 h, at -78 °C. The resulting solution was cannulated slowly to the suspension of 1,1´-(4-((4-Bromophenyl)ethynyl)pyridine-2,6-diyl)bis(3,4,5-trimethylimidazolium) bis(hexafluorophosphate), and the resulting dark red solution was stirred for 30 min, at -40 °C. To the resulting reaction solution was dropwise added a solution of $FeBr_2$ (21 mg, 0.097 mmol) in dry, degassed THF (1.5 mL). The resulting dark mixture was allowed to warm to rt and stirred, at that temperature, for 1 h. The resulting mixture was evaporated *in vacuo* and to the residue was added methanol (40 mL) and hydrochloric acid (concd. aq., 0.6 mL). The resulting mixture was filtered through a glass filter (#3), and to the resulting filtrate was added a solution of ammonium hexafluorophospate (601 mg, 3.69 mmol) in minimal amount of water, followed by slow addition of water (20 mL). The resulting precipitate was collected on a glass filter (#4) and the washed with water (3 x 10 mL). The material was further purified twice by size-exclusion chromatography (3 x 140 cm, MeCN/PhMe 1:1) giving the target complex as a red solid (4 mg, 5%). ^{1}H NMR (500 MHz, CD_3CN) δ = 7.90 (s, 2H, Py-*H*3), 7.71–7.67 (m, *J* = 8.5 Hz, 2H, Ph-*H*2/Ph-*H*3), 7.64–7.60 (m, *J* = 8.5 Hz, 2H, Ph-*H*2/Ph-*H*3), 2.66 (s, 6H, Im5-C*H*$_3$), 2.40 (s, 6H, Im3-C*H*$_3$), 1.97 (s, 6H, Im4-C*H*$_3$) ppm; ^{13}C NMR (126 MHz, CD_3CN) δ = 199.59, 155.93, 134.52, 133.15, 131.35, 130.82, 124.84, 124.60, 121.58, 108.47, 95.63, 88.94, 32.37, 11.59, 8.80 ppm.

8.2 NMR spectra

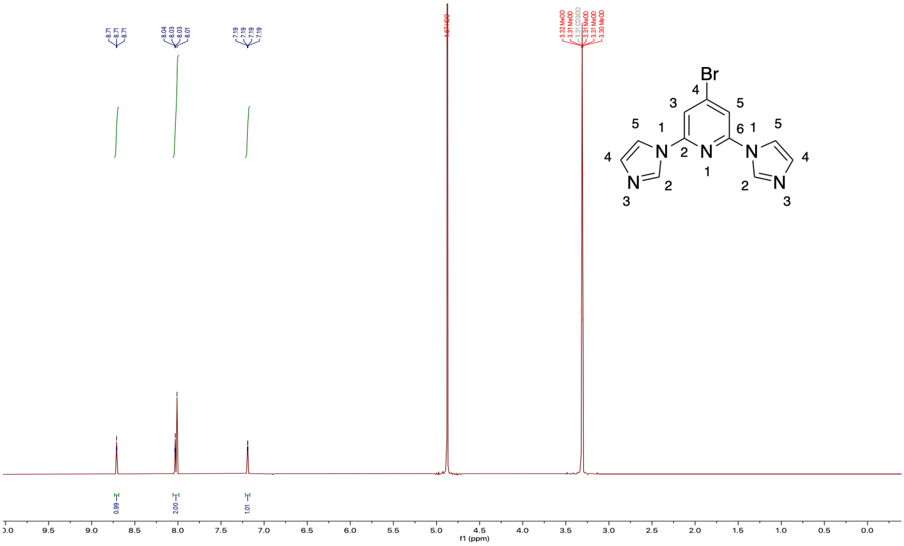

Figure 8.1: ^{1}H NMR of 4-bromo-2,6-di(imidazol-1-yl)pyridine (**P9**).

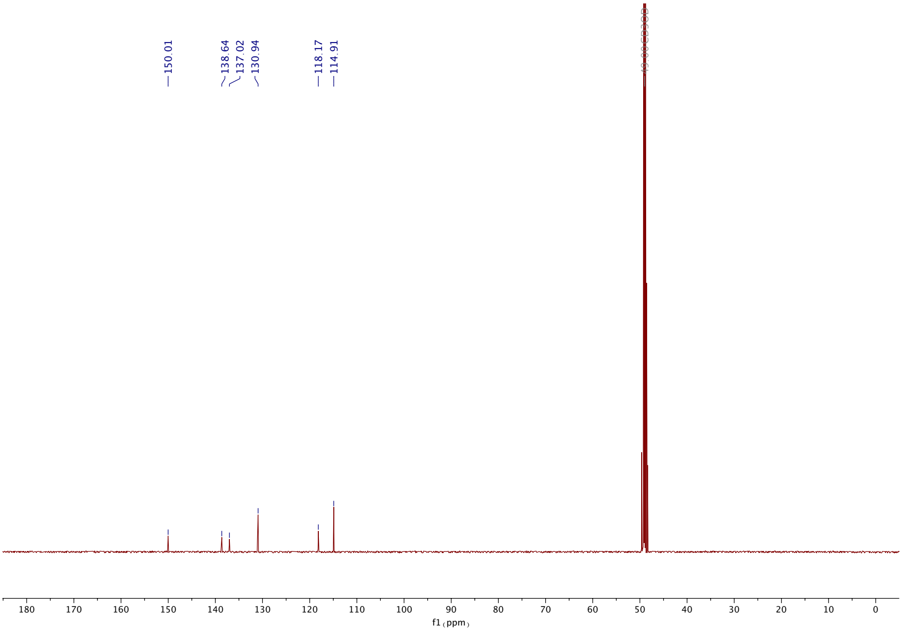

Figure 8.2: ^{13}C NMR of 4-bromo-2,6-di(imidazol-1-yl)pyridine (**P9**).

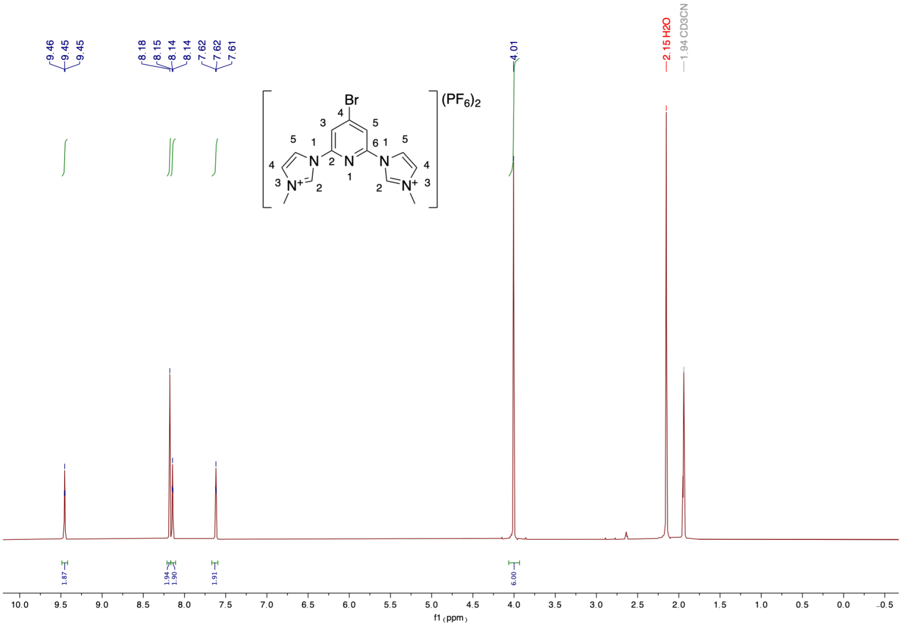

Figure 8.3: ^{1}H NMR of 1,1’-(4-bromopyridine-2,6-diyl)bis(3-methylimidazolium) bis(hexafluorophosphate) (**P14**).

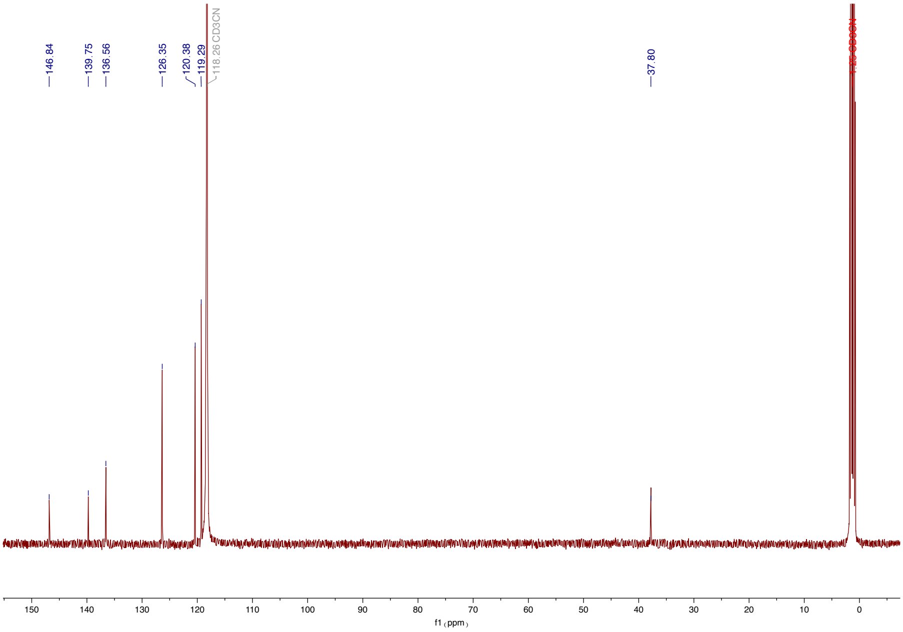

Figure 8.4: ^{13}C NMR of 1,1’-(4-bromopyridine-2,6-diyl)bis(3-methylimidazolium) bis(hexafluorophosphate) (**P14**).

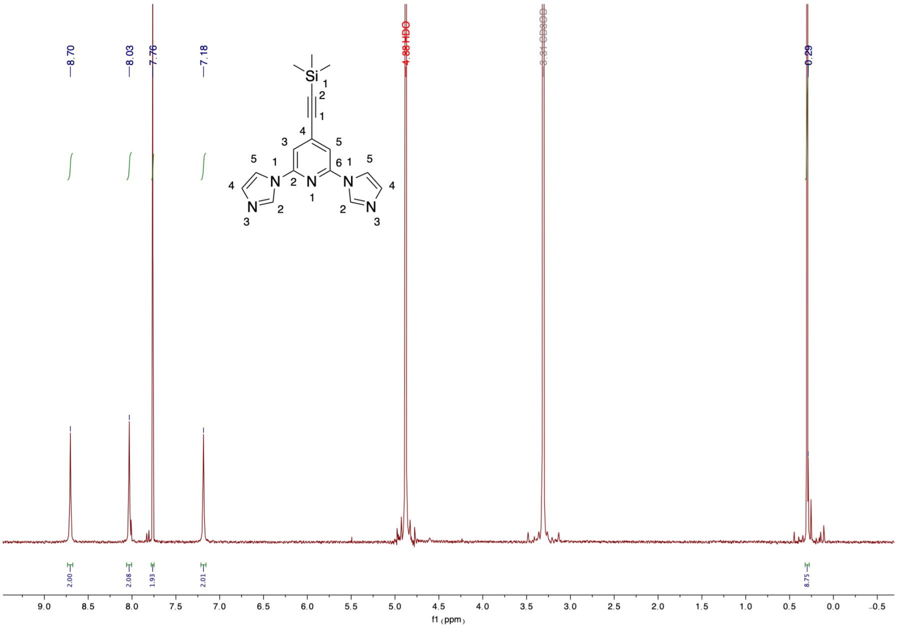

Figure 8.5: ^{1}H NMR of 2,6-di(imidazol-1-yl)-4-((trimethylsilyl)ethynyl)pyridine (**P15**).

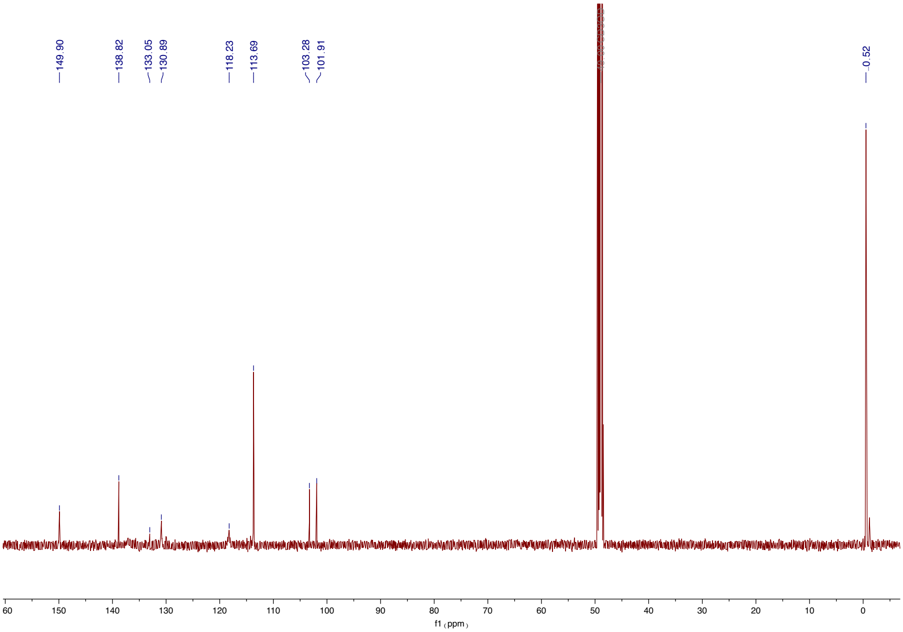

Figure 8.6: ^{13}C NMR of 2,6-di(imidazol-1-yl)-4-((trimethylsilyl)ethynyl)pyridine (**P15**).

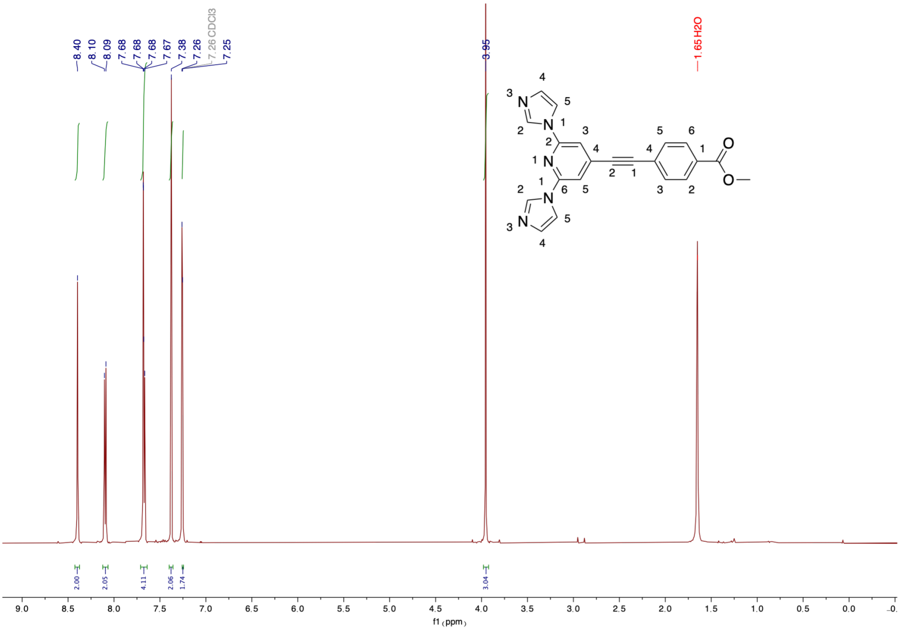

Figure 8.7: ^{1}H NMR of methyl 4-((2,6-di(imidazol-1-yl)pyridin-4-yl)ethynyl)benzoate (**P28**).

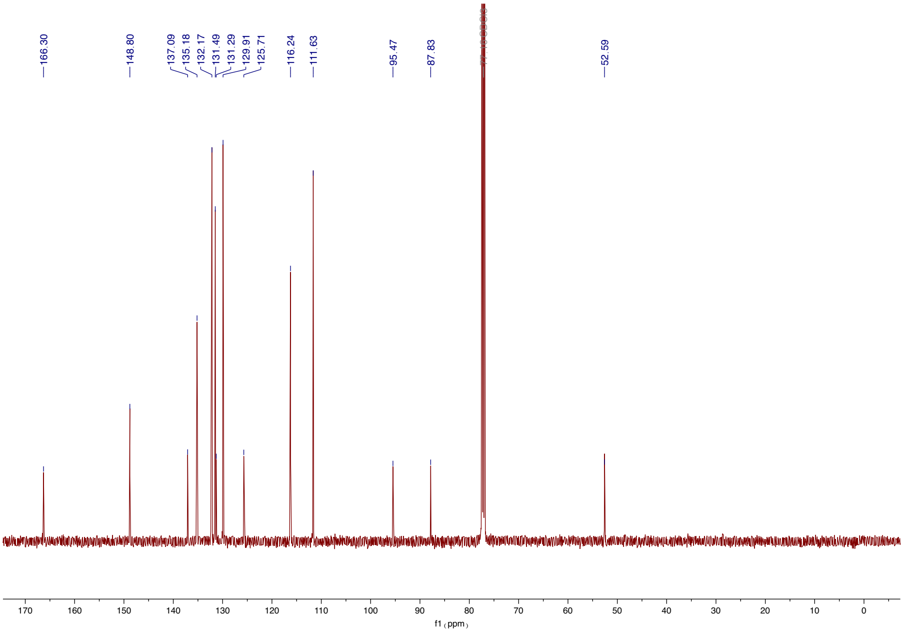

Figure 8.8: ^{1}H NMR of methyl 4-((2,6-di(imidazol-1-yl)pyridin-4-yl)ethynyl)benzoate (**P28**).

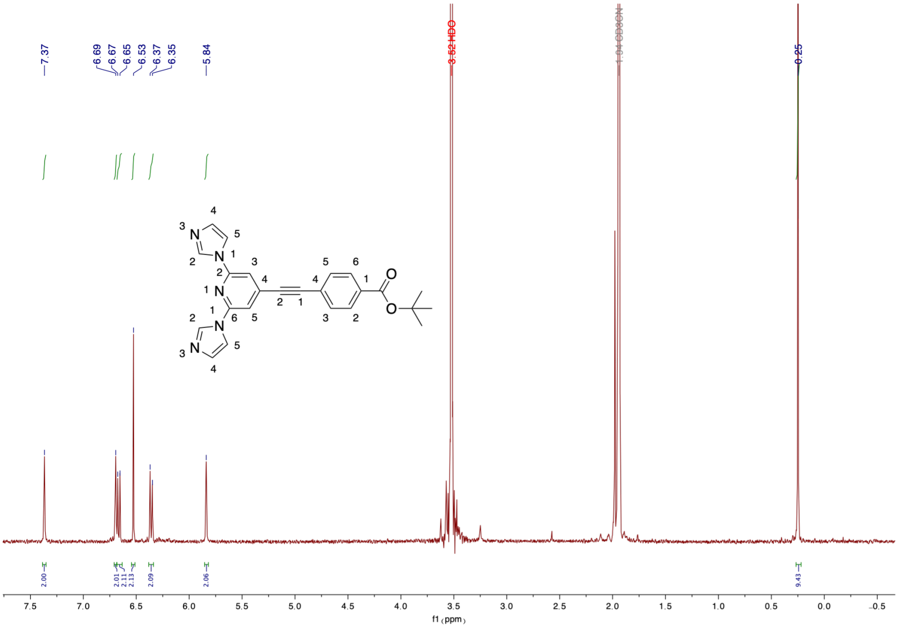

Figure 8.9: ^{1}H NMR of *tert*-butyl 4-((2,6-di(imidazol-1-yl)pyridin-4-yl)ethynyl)benzoate (**P29**).

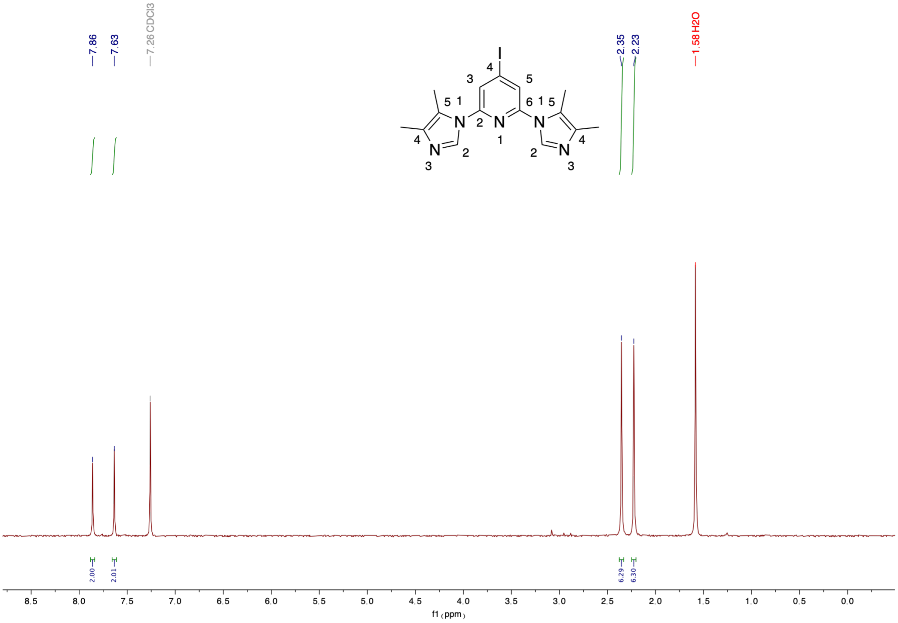

Figure 8.10: ^{1}H NMR of 2,6-bis(4,5-dimethylimidazol-1-yl)-4-iodopyridine (**P32**).

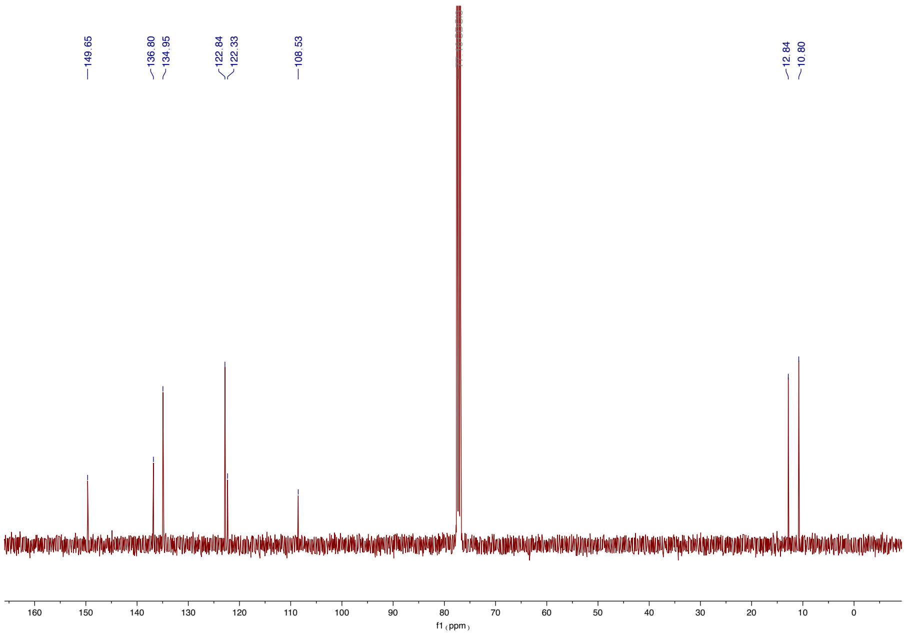

Figure 8.11: ^{13}C NMR of 2,6-bis(4,5-dimethylimidazol-1-yl)-4-iodopyridine (**P32**).

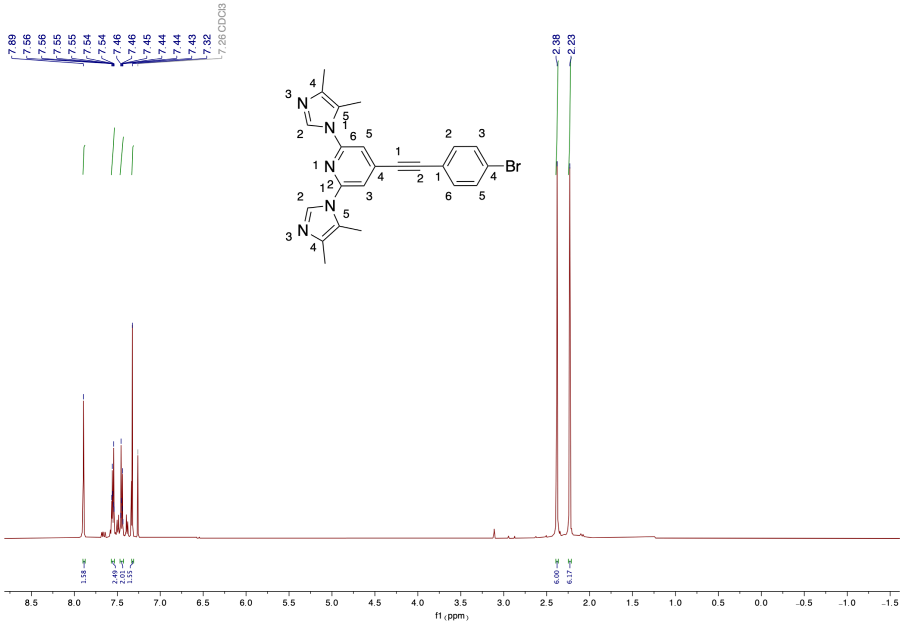

Figure 8.12: ^{1}H NMR of 4-((4-bromophenyl)ethynyl)-2,6-bis(4,5-dimethylimidazol-1-yl)pyridine (**P33**).

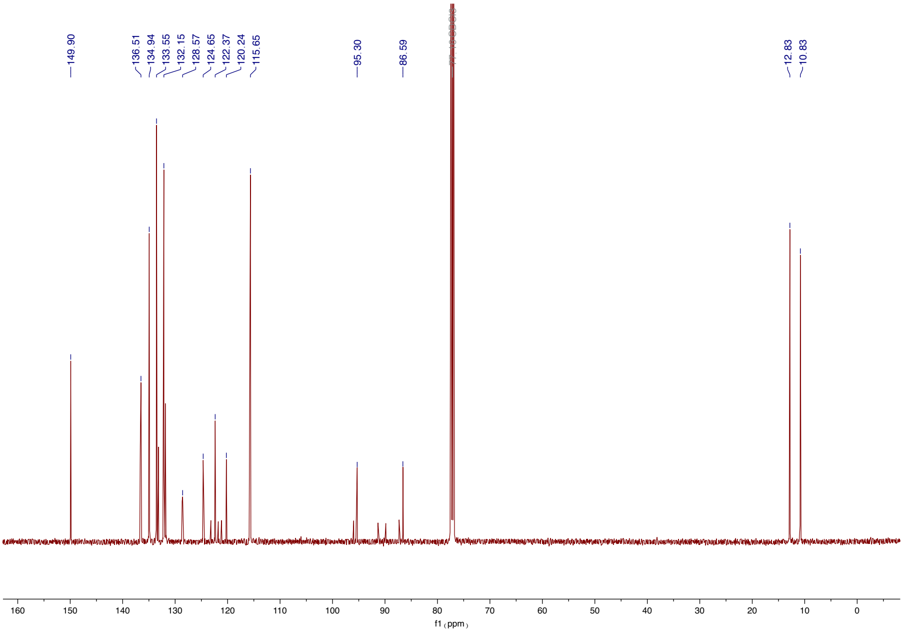

Figure 8.13: ^{13}C NMR of 4-((4-bromophenyl)ethynyl)-2,6-bis(4,5-dimethylimidazol-1-yl)pyridine (**P33**).

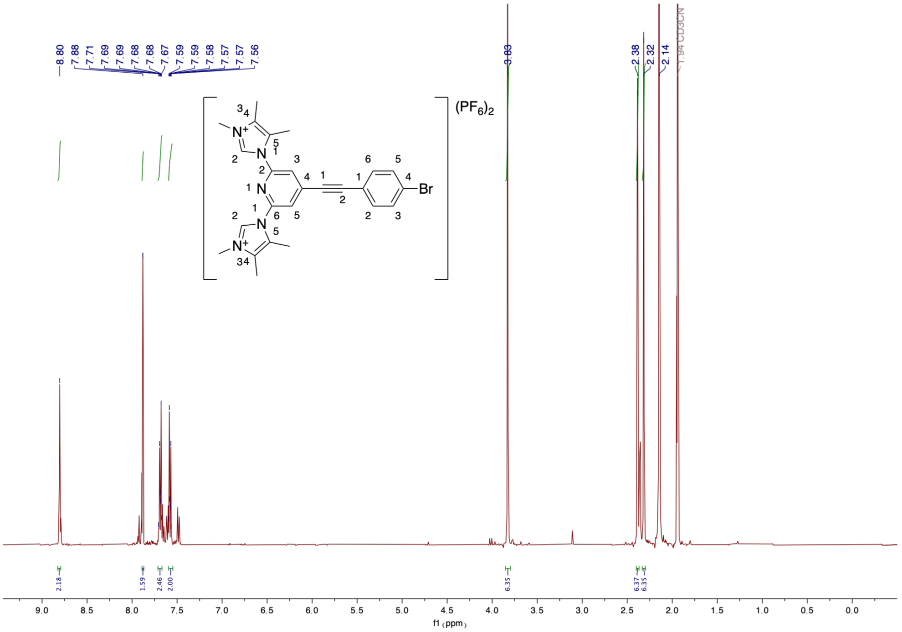

Figure 8.14: ^{1}H NMR of 1,1'-(4-((4-bromophenyl)ethynyl)pyridine-2,6-diyl)bis(3,4,5-trimetylimidazolium) bis(hexafluorophosphate) (**P34**).

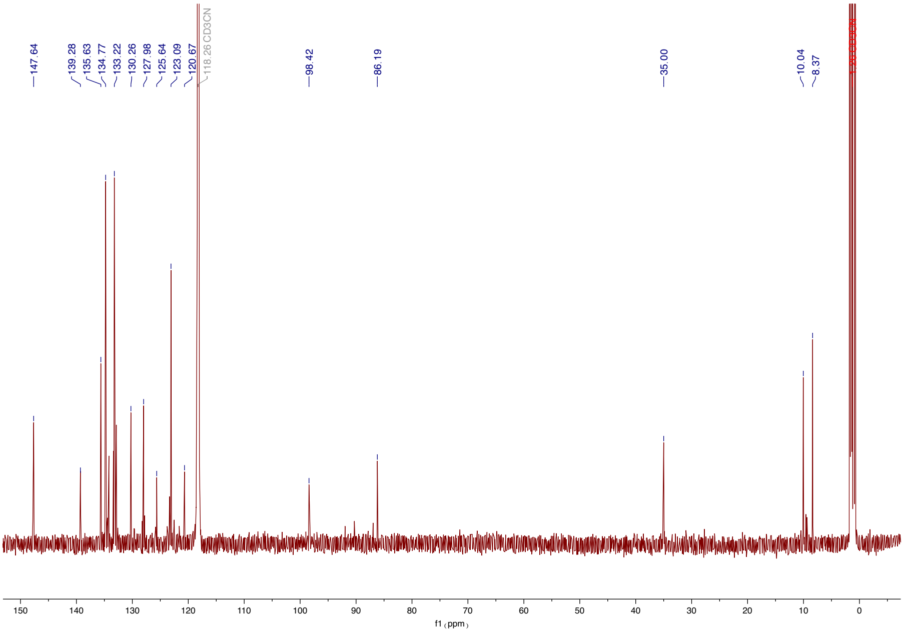

Figure 8.15: ^{13}C NMR of 1,1’-(4-((4-bromophenyl)ethynyl)pyridine-2,6-diyl)bis(3,4,5-trimetylimidazolium) bis(hexafluorophosphate) (**P34**).

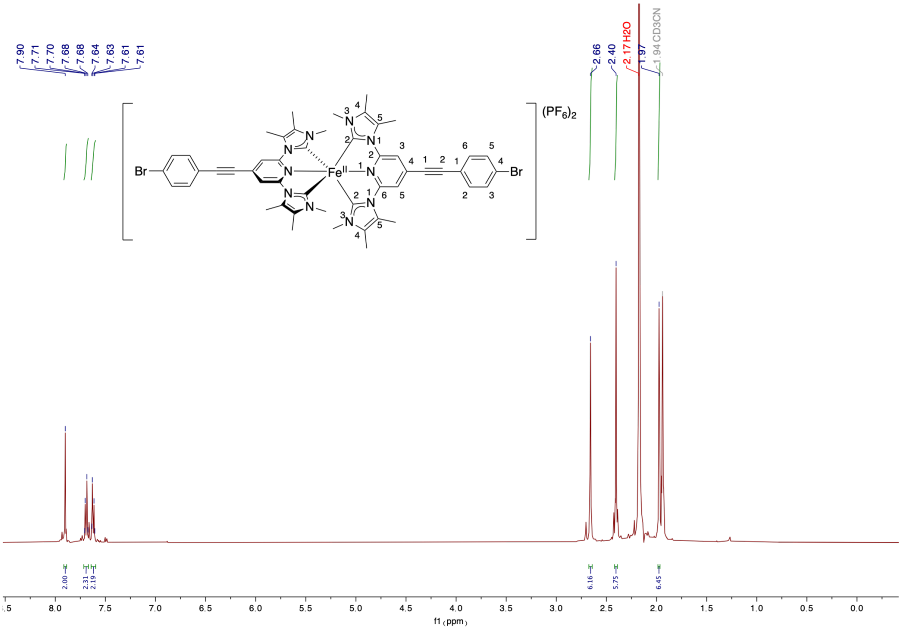

Figure 8.16: ^{1}H NMR of bis(1,1´-(4-((4-bromophenyl)ethynyl)pyridine-2,6-diyl)bis(3,4,5-trimethylimidazolylidene))iron bis(hexafluorophosphate) (**25**).

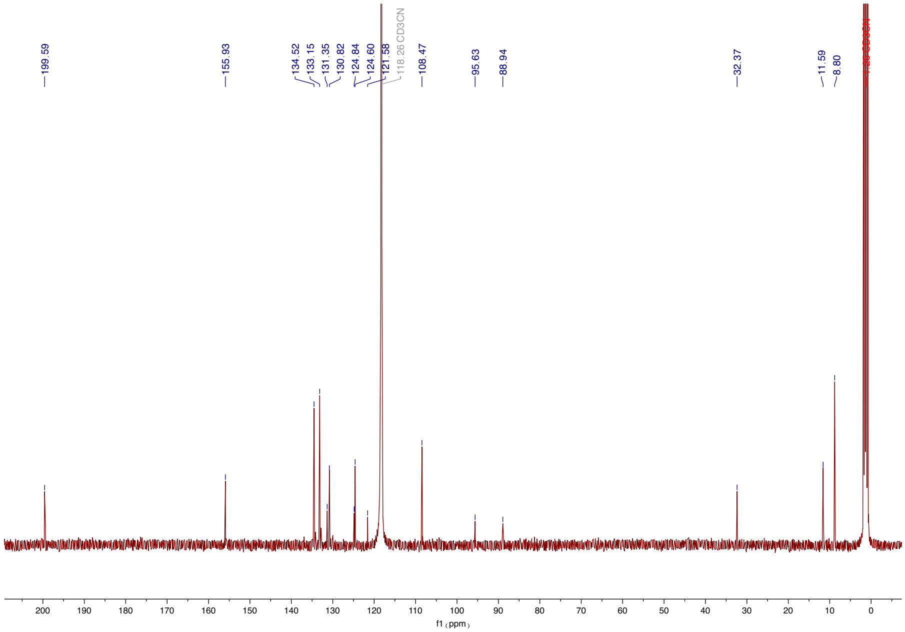

Figure 8.17: ^{1}H NMR of bis(1,1´-(4-((4-bromophenyl)ethynyl)pyridine-2,6-diyl)bis(3,4,5-trimethylimidazolylidene))iron bis(hexafluorophosphate) (**25**).

8.3 Spectrophotometry

Steady-state absorption measurements in the UV-VIS region were performed in an Agilent Technologies Cary 60 UV-Vis Spectrophotometer. Acetonitrile was collected from dry solvent dispenser (Innovative technology, PS-micro) and stored over 3 Å MS. Absorbance was measured after filtration of the analyte solution through a syringe filter (Fisherbrand, PTFE, 0.45 µm porosity, 13 mm diameter), in a standard quartz-glass cuvette of path length 1 cm (HellmaAnalytics – High Precision Quartz Glass). For reference, the same cuvette with pure acetonitrile as used to dissolve the complex, was used.

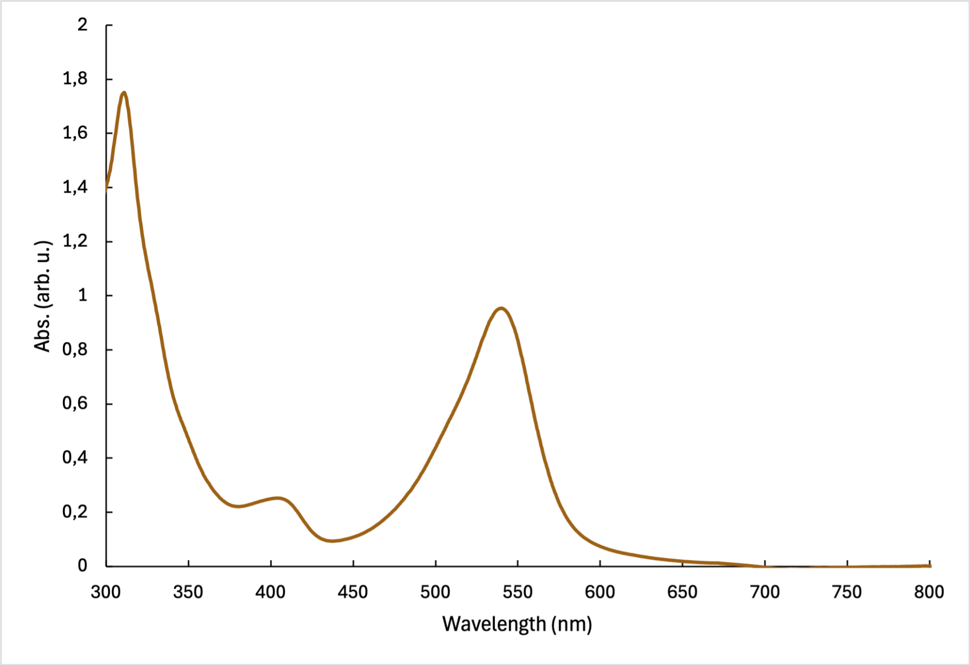

Figure 8.18: Steady state absorption spectrum of bis(1,1´-(4-((4-bromophenyl)ethynyl)pyridine-2,6-diyl)bis(3,4,5-trimethylimidazolylidene))iron bis(hexafluorophosphate) (**25**) in acetontrile.

Acknowledgements

During one’s PhD studies, you have the opportunity to meet many memorable people, enriching one’s experience and development as a researcher. I would here like to take some space to show my gratitude to the most prominent individuals that made this work what it is.

Firstly, to my PhD supervisor KENNETH. Thank you for giving me the opportunity to pursue my PhD within your group. Throughout this entire journey you have assured me of the progress I have made as a scientist, which has made for very important encouragement.

My co-supervisor DANIEL and department representative PATRIC, thank you both for your insightful input to my studies during my time as a PhD student.

To the past and present members of the KW group, my colleagues and friends. Firstly, thanks to my fellow PhD students in the group during my stay: To OLGA for giving me a start with the chemistry involved in this project, back when I was a master’s student working towards my degree. To HAILIANG for welcoming me to share a lab with you. To VICKY for your cheerful mood and friendliness. To VALTÝR, the very first person I spoke to in the group, for being so nice and welcoming from the very start. I am also happy I had another person in the group focused on complex synthesis. To ANNA for keeping the whole group in order and entrusting me to look after your adorable cat. To LISA for being nice company in the office and lab, and for having you as a travel companion to Cancún. To JESPER, after having studied chemistry side by side with you more or less since I got to Lund, saying you were important in me making it here, is needless to say. You have for a long time been someone for me to discuss things with, be they chemistry-related or not. To ALEKSANDRA for being there to bounce project thoughts with and usually around for a nice chat. Thanks also to Aleks and Jesper for your help in proofreading the thesis. To ERIC for joining the group with your obvious efforts in bringing us closer together. To CLARA for sharing the lab with me once everyone else had moved out. Thanks also to all the postdocs that have come and/or gone during my time in the group, SIMON, HAO, OM, ARVIND, ALPESH, KUMKUM, YOGESH, DNYANESHWAR, SURESH and ABHISHEK, I have learned a lot from you that I will carry with me as a chemist in the future. To LUKAS and SALIM, the two undergraduate students I had the luck of supervising during my time at CAS, thank you both for your help in carrying out my research.

I would like to thank my collaborators found in other parts of kemicentrum, who made some of my work a possibility. To PAVEL, NILS, IRIA, YEN, JENS, ARKADY and PETTER, without who's expertise the work would not have been possible. A special thanks to LINNEA for the camaraderie we had working together on our shared publications as well as for the great help you were when learning about the photophysics.

Thanks to MARINA for welcoming me into your lab and to the whole MF group for being inviting and helpful during my stay with you. A special thanks to IACOPO for all your help and instruction with DSC-techniques, and all your efforts on paper I and II. Thanks to HANNES for your work on paper I.

Thanks to RAJ, MINLI and REINER for your work on the investigation of the iron complexes I worked to synthesise and making them matter a bit more.

Thanks also to EYRAM, MAWULI, MARIAM and ELENA for your calculation to bring clarity to the function of the iron complexes.

Thanks to all coworkers at CAS, that make it such a nice and friendly place to work at. A special thanks to MARIA, SARA and KORNELIJE who make everything move along nicely and for helping out with all the other little things so we can focus on our research.

To all the people that have become friends during my time in Lund, for making my time here so enjoyable.

To KLAS, my chemistry teacher from all the way back at gymnasiet. The enjoyment you helped me find in chemistry set me on the journey that has led to this thesis.

Till MAMMA som självklart gjort så mycket för mig. Jag hade inte varit den jag är idag om det inte vore för dig.

And finally, to MARIA mou, I will say that meeting you was the most important thing I did during my time as a PhD student. Wherever life takes me after this, I deeply hope you will be there with me. Σ' αγαπώ γιατί είσαι εσύ.

References

1. Lewis, N. S.; Nocera, D. G., Powering the planet: Chemical challenges in solar energy utilization. *Proc. Natl. Acad. Sci. U.S.A.* **2006,** *103* (43), 15729-15735.
2. Armaroli, N.; Balzani, V., Solar electricity and solar fuels: status and perspectives in the context of the energy transition. *Chem. Eur. J.* **2016,** *22* (1), 32-57.
3. Schiermeier, Q.; Tollefson, J.; Scully, T.; Witze, A.; Morton, O., Energy alternatives: Electricity without carbon. *Nature* **2008,** *454* (7206), 816-823.
4. Lv, J.; Xie, J.; Mohamed, A. G. A.; Zhang, X.; Feng, Y.; Jiao, L.; Zhou, E.; Yuan, D.; Wang, Y., Solar utilization beyond photosynthesis. *Nat. Rev. Chem.* **2023,** *7* (2), 91-105.
5. Höök, M.; Tang, X., Depletion of fossil fuels and anthropogenic climate change—A review. *Energy policy* **2013,** *52*, 797-809.
6. Conti, J.; Holtberg, P.; Diefenderfer, J.; LaRose, A.; Turnure, J. T.; Westfall, L. *International energy outlook 2016 with projections to 2040*; USDOE Energy Information Administration (EIA), Washington, DC (United States …: 2016.
7. Nelson, J. A., *The Physics Of Solar Cells*. World Scientific Publishing Company: 2003.
8. Megía, P. J.; Vizcaíno, A. J.; Calles, J. A.; Carrero, A., Hydrogen production technologies: from fossil fuels toward renewable sources. A mini review. *Energy Fuels* **2021,** *35* (20), 16403-16415.
9. Gust, D.; Moore, T. A.; Moore, A. L., Solar fuels via artificial photosynthesis. *Acc. Chem. Res.* **2009,** *42* (12), 1890-1898.
10. Nguyen, J. D.; D'amato, E. M.; Narayanam, J. M.; Stephenson, C. R., Engaging unactivated alkyl, alkenyl and aryl iodides in visible-light-mediated free radical reactions. *Nat. Chem.* **2012,** *4* (10), 854-859.
11. Crisenza, G. E.; Melchiorre, P., Chemistry glows green with photoredox catalysis. *Nat. Commun.* **2020,** *11* (1), 803.
12. Battaglia, C.; Cuevas, A.; De Wolf, S., High-efficiency crystalline silicon solar cells: status and perspectives. *Energy Environ. Sci.* **2016,** *9* (5), 1552-1576.
13. Kim, J. H.; Hansora, D.; Sharma, P.; Jang, J.-W.; Lee, J. S., Toward practical solar hydrogen production–an artificial photosynthetic leaf-to-farm challenge. *Chem. Soc. Rev.* **2019,** *48* (7), 1908-1971.
14. Prier, C. K.; Rankic, D. A.; MacMillan, D. W., Visible light photoredox catalysis with transition metal complexes: applications in organic synthesis. *Chem. Rev.* **2013,** *113* (7), 5322-5363.

15. Barber, J.; Tran, P. D., From natural to artificial photosynthesis. *J. R. Soc. Interface* **2013,** *10* (81), 20120984.
16. Hagfeldt, A.; Grätzel, M., Molecular Photovoltaics. *Acc. Chem. Res.* **2000,** *33* (5), 269-277.
17. Hagfeldt, A.; Boschloo, G.; Sun, L.; Kloo, L.; Pettersson, H., Dye-sensitized solar cells. *Chem. Rev.* **2010,** *110* (11), 6595-6663.
18. McNaught, A. D.; Wilkinson, A.; International Union of, P.; Applied, C. *Compendium of chemical terminology : IUPAC recommendations*, International Union of Pure and Applied Chemistry: Oxford, 2006.
19. Balzani, V.; Campagna, S., *Photochemistry and Photophysics of Coordination Compounds I*. Springer-Verlag: Berlin, Heidelberg, 2007.
20. Balzani, V.; Campagna, S.; Barbieri, A., *Photochemistry and Photophysics of Coordination Compounds II*. Springer-Verlag: Berlin, Heidelberg, 2007.
21. Wenger, O. S., Is Iron the New Ruthenium? *Chem. – Eur. J.* **2019,** *25* (24), 6043-6052.
22. Marzo, L.; Pagire, S. K.; Reiser, O.; König, B., Visible-light photocatalysis: does it make a difference in organic synthesis? *Angew. Chem. Int. Ed.* **2018,** *57* (32), 10034-10072.
23. Neumann, M.; Füldner, S.; König, B.; Zeitler, K., Metal-free, cooperative asymmetric organophotoredox catalysis with visible light. *Angew. Chem. Int. Ed.* **2011,** *4* (50), 951-954.
24. Romero, N. A.; Nicewicz, D. A., Organic photoredox catalysis. *Chem. Rev.* **2016,** *116* (17), 10075-10166.
25. Kalyanasundaram, K., Photophysics, photochemistry and solar energy conversion with tris (bipyridyl) ruthenium (II) and its analogues. *Coord. Chem. Rev.* **1982,** *46*, 159-244.
26. Turro, N. J.; Ramamurthy, V.; Scaiano, J. C., *Principles of molecular photochemistry : an introduction*. University Science Books: Sausalito, Calif., 2009.
27. Juris, A.; Balzani, V.; Barigelletti, F.; Campagna, S.; Belser, P.; von Zelewsky, A. v., Ru (II) polypyridine complexes: photophysics, photochemistry, eletrochemistry, and chemiluminescence. *Coord. Chem. Rev.* **1988,** *84*, 85-277.
28. Arias-Rotondo, D. M.; McCusker, J. K., The photophysics of photoredox catalysis: a roadmap for catalyst design. *Chem. Soc. Rev.* **2016,** *45* (21), 5803-5820.
29. Balzani, V.; Ceroni, P.; Juris, A., *Photochemistry and photophysics : concepts, research, applications*. Wiley-VCH Verlag GmbH & Co. KGaA: Weinheim, Germany, 2014.
30. Housecroft, C. E.; Sharpe, A. G., *Inorganic chemistry*. 4th ed ed.; Pearson: Harlow, England, 2012.
31. Wardle, B., *Principles and Applications of Photochemistry*. John Wiley & Sons, Incorporated: Newark, 2010.
32. Sutin, N.; Creutz, C., Properties and reactivities of the luminescent excited states of polypyridine complexes of ruthenium (II) and osmium (II). In *Advances in Chemistry, Vol. 168*, ACS Publications: Washington DC, U.S.A., 1978.

33. Juliá, F., Ligand-to-metal charge transfer (LMCT) photochemistry at 3d-metal complexes: an emerging tool for sustainable organic synthesis. *ChemCatChem* **2022,** *14* (19), e202200916.
34. McCusker, J. K., Electronic structure in the transition metal block and its implications for light harvesting. *Science* **2019,** *363* (6426), 484-488.
35. Glaser, F.; Aydogan, A.; Elias, B.; Troian-Gautier, L., The great strides of iron photosensitizers for contemporary organic photoredox catalysis: On our way to the holy grail? *Coord. Chem. Rev.* **2024,** *500*, 215522.
36. Wu, S.; Žurauskas, J.; Domański, M.; Hitzfeld, P. S.; Butera, V.; Scott, D. J.; Rehbein, J.; Kumar, A.; Thyrhaug, E.; Hauer, J., Hole-mediated photoredox catalysis: tris (p-substituted) biarylaminium radical cations as tunable, precomplexing and potent photooxidants. *Org. Chem. Front.* **2021,** *8* (6), 1132-1142.
37. Woodhouse, M. D.; McCusker, J. K., Mechanistic origin of photoredox catalysis involving iron (II) polypyridyl chromophores. *J. Am. Chem. Soc.* **2020,** *142* (38), 16229-16233.
38. Chan, A. Y.; Ghosh, A.; Yarranton, J. T.; Twilton, J.; Jin, J.; Arias-Rotondo, D. M.; Sakai, H. A.; McCusker, J. K.; MacMillan, D. W., Exploiting the Marcus inverted region for first-row transition metal–based photoredox catalysis. *Science* **2023,** *382* (6667), 191-197.
39. Zigmantas, D.; Polívka, T.; Persson, P.; Sundström, V., Ultrafast laser spectroscopy uncovers mechanisms of light energy conversion in photosynthesis and sustainable energy materials. *Chem. Phys. Rev.* **2022,** *3* (4).
40. vandeVen, M.; Ameloot, M.; Valeur, B.; Boens, N., Pitfalls and their remedies in time-resolved fluorescence spectroscopy and microscopy. *J. Fluoresc.* **2005,** *15*, 377-413.
41. Elgrishi, N.; Rountree, K. J.; McCarthy, B. D.; Rountree, E. S.; Eisenhart, T. T.; Dempsey, J. L., A practical beginner's guide to cyclic voltammetry. *J. Chem. Educ.* **2018,** *95* (2), 197-206.
42. Pitre, S. P.; McTiernan, C. D.; Scaiano, J. C., Understanding the kinetics and spectroscopy of photoredox catalysis and transition-metal-free alternatives. *Acc. Chem. Res.* **2016,** *49* (6), 1320-1330.
43. Kaim, W.; Klein, A., *Spectroelectrochemistry*. Royal Society of Chemistry: 2008.
44. Kaim, W.; Fiedler, J., Spectroelectrochemistry: the best of two worlds. *Chem. Soc. Rev.* **2009,** *38* (12), 3373-3382.
45. Brown, A. M.; McCusker, C. E.; McCusker, J. K., Spectroelectrochemical identification of charge-transfer excited states in transition metal-based polypyridyl complexes. *Dalton Trans.* **2014,** *43* (47), 17635-17646.
46. Reinhard, M. E.; Sidhu, B. K.; Lozada, I. B.; Powers-Riggs, N.; Ortiz, R. J.; Lim, H.; Nickel, R.; Lierop, J. v.; Alonso-Mori, R.; Chollet, M., Time-Resolved X-ray Emission Spectroscopy and Synthetic High-Spin Model Complexes Resolve Ambiguities in Excited-State Assignments of Transition-Metal Chromophores: A Case Study of Fe-Amido Complexes. *J. Am. Chem. Soc.* **2024**.
47. Liu, Y.; Persson, P.; Sundström, V.; Wärnmark, K., Fe N-heterocyclic carbene complexes as promising photosensitizers. *Acc. Chem. Res.* **2016,** *49* (8), 1477-1485.

48. Haynes, W. M., *CRC Handbook of Chemistry and Physics, 97th Edition*. CRC Press: 2016.
49. Creutz, C.; Chou, M.; Netzel, T. L.; Okumura, M.; Sutin, N., Lifetimes, spectra, and quenching of the excited states of polypyridine complexes of iron (II), ruthenium (II), and osmium (II). *J. Am. Chem. Soc.* **1980,** *102* (4), 1309-1319.
50. Lindh, L.; Chábera, P.; Rosemann, N. W.; Uhlig, J.; Wärnmark, K.; Yartsev, A.; Sundström, V.; Persson, P., Photophysics and Photochemistry of Iron Carbene Complexes for Solar Energy Conversion and Photocatalysis. *Catalysts* **2020,** *10* (3), 315.
51. Herrmann, W. A., N-heterocyclic carbenes: a new concept in organometallic catalysis. *Angew. Chem. Int. Ed.* **2002,** *41* (8), 1290-1309.
52. Hopkinson, M. N.; Richter, C.; Schedler, M.; Glorius, F., An overview of N-heterocyclic carbenes. *Nature* **2014,** *510* (7506), 485-496.
53. Huynh, H. V.; John, W.; Sons, *The organometallic chemistry of N-heterocyclic carbenes*. Wiley: Chichester, 2017.
54. Liu, Y.; Harlang, T.; Canton, S. E.; Chábera, P.; Suárez-Alcántara, K.; Fleckhaus, A.; Vithanage, D. A.; Göransson, E.; Corani, A.; Lomoth, R.; Sundström, V.; Wärnmark, K., Towards longer-lived metal-to-ligand charge transfer states of iron(ii) complexes: an N-heterocyclic carbene approach. *Chem. Commun.* **2013,** *49* (57), 6412-6414.
55. Harlang, T. C. B.; Liu, Y.; Gordivska, O.; Fredin, L. A.; Ponseca, C. S.; Huang, P.; Chábera, P.; Kjaer, K. S.; Mateos, H.; Uhlig, J.; Lomoth, R.; Wallenberg, R.; Styring, S.; Persson, P.; Sundström, V.; Wärnmark, K., Iron sensitizer converts light to electrons with 92% yield. *Nat. Chem.* **2015,** *7* (11), 883-889.
56. Duchanois, T.; Etienne, T.; Cebrián, C.; Liu, L.; Monari, A.; Beley, M.; Assfeld, X.; Haacke, S.; Gros, P. C., An Iron-Based Photosensitizer with Extended Excited-State Lifetime: Photophysical and Photovoltaic Properties. *Eur. J. Inorg. Chem.* **2015,** *2015* (14), 2469-2477.
57. Liu, L.; Duchanois, T.; Etienne, T.; Monari, A.; Beley, M.; Assfeld, X.; Haacke, S.; Gros, P. C., A new record excited state 3 MLCT lifetime for metalorganic iron (II) complexes. *Phys. Chem. Chem. Phys.* **2016,** *18* (18), 12550-12556.
58. Pastore, M.; Duchanois, T.; Liu, L.; Monari, A.; Assfeld, X.; Haacke, S.; Gros, P. C., Interfacial charge separation and photovoltaic efficiency in Fe (ii)–carbene sensitized solar cells. *Phys. Chem. Chem. Phys.* **2016,** *18* (40), 28069-28081.
59. Darari, M.; Francés-Monerris, A.; Marekha, B.; Doudouh, A.; Wenger, E.; Monari, A.; Haacke, S.; Gros, P. C., Towards Iron (II) Complexes with Octahedral Geometry: Synthesis, Structure and Photophysical Properties. *Molecules* **2020,** *25* (24), 5991.
60. Chábera, P.; Kjaer, K. S.; Prakash, O.; Honarfar, A.; Liu, Y.; Fredin, L. A.; Harlang, T. C.; Lidin, S.; Uhlig, J.; Sundström, V., FeII hexa N-heterocyclic carbene complex with a 528 ps metal-to-ligand charge-transfer excited-state lifetime. *J. Phys. Chem. Lett.* **2018,** *9* (3), 459-463.
61. Ilic, A. Investigation of Iron-N-Heterocyclic Carbene Complexes for Photocatalytic Applications. Ph.D. Thesis, Lund University, Lund, Sweden, 2024.

62. Chábera, P.; Liu, Y.; Prakash, O.; Thyrhaug, E.; Nahhas, A. E.; Honarfar, A.; Essén, S.; Fredin, L. A.; Harlang, T. C.; Kjær, K. S., A low-spin Fe (III) complex with 100-ps ligand-to-metal charge transfer photoluminescence. *Nature* **2017,** *543* (7647), 695-699.

63. Kjær, K. S.; Kaul, N.; Prakash, O.; Chábera, P.; Rosemann, N. W.; Honarfar, A.; Gordivska, O.; Fredin, L. A.; Bergquist, K.-E.; Häggström, L.; Ericsson, T.; Lindh, L.; Yartsev, A.; Styring, S.; Huang, P.; Uhlig, J.; Bendix, J.; Strand, D.; Sundström, V.; Persson, P.; Lomoth, R.; Wärnmark, K., Luminescence and reactivity of a charge-transfer excited iron complex with nanosecond lifetime. *Science* **2019,** *363* (6424), 249-253.

64. Kaufhold, S.; Wärnmark, K., Design and synthesis of photoactive iron n-heterocyclic carbene complexes. *Catalysts* **2020,** *10* (1), 132.

65. Prakash, O.; Chábera, P.; Kaul, N.; Hlynsson, V. F.; Rosemann, N. W.; Losada, I. B.; Hoang Hai, Y. T.; Huang, P.; Bendix, J.; Ericsson, T., How Rigidity and Conjugation of Bidentate Ligands Affect the Geometry and Photophysics of Iron N-Heterocyclic Complexes: A Comparative Study. *Inorg. Chem.* **2024,** *63* (10), 4461-4473.

66. Vukadinovic, Y.; Burkhardt, L.; Päpcke, A.; Miletic, A.; Fritsch, L.; Altenburger, B. r.; Schoch, R.; Neuba, A.; Lochbrunner, S.; Bauer, M., When donors turn into acceptors: Ground and excited state properties of FeII complexes with amine-substituted tridentate bis-imidazole-2-ylidene pyridine ligands. *Inorg. Chem.* **2020,** *59* (13), 8762-8774.

67. Dierks, P.; Päpcke, A.; Bokareva, O. S.; Altenburger, B. r.; Reuter, T.; Heinze, K.; Kühn, O.; Lochbrunner, S.; Bauer, M., Ground-and excited-state properties of iron (II) complexes linked to organic chromophores. *Inorg. Chem.* **2020,** *59* (20), 14746-14761.

68. Lindh, L.; Pascher, T.; Persson, S.; Goriya, Y.; Wärnmark, K.; Uhlig, J.; Chábera, P.; Persson, P.; Yartsev, A., Multifaceted Deactivation Dynamics of Fe (II) N-Heterocyclic Carbene Photosensitizers. *J. Phys. Chem. A* **2023,** *127* (48), 10210-10222.

69. Lindh, L.; Rosemann, N. W.; Losada, I. B.; Persson, S.; Goriya, Y.; Fan, H.; Gordivska, O.; Wärnmark, K.; Uhlig, J.; Chábera, P., Side-group switching between metal-to-ligand charge-transfer and metal-centered excited state properties in iron (II) N-heterocyclic carbene complexes. *Coord. Chem. Rev.* **2024,** *506*, 215709.

70. Kunnus, K.; Vacher, M.; Harlang, T. C. B.; Kjær, K. S.; Haldrup, K.; Biasin, E.; van Driel, T. B.; Pápai, M.; Chabera, P.; Liu, Y.; Tatsuno, H.; Timm, C.; Källman, E.; Delcey, M.; Hartsock, R. W.; Reinhard, M. E.; Koroidov, S.; Laursen, M. G.; Hansen, F. B.; Vester, P.; Christensen, M.; Sandberg, L.; Németh, Z.; Szemes, D. S.; Bajnóczi, É.; Alonso-Mori, R.; Glownia, J. M.; Nelson, S.; Sikorski, M.; Sokaras, D.; Lemke, H. T.; Canton, S. E.; Møller, K. B.; Nielsen, M. M.; Vankó, G.; Wärnmark, K.; Sundström, V.; Persson, P.; Lundberg, M.; Uhlig, J.; Gaffney, K. J., Vibrational wavepacket dynamics in Fe carbene photosensitizer determined with femtosecond X-ray emission and scattering. *Nat. Commun.* **2020,** *11* (1), 634.

71. Leis, W.; Argüello Cordero, M. A.; Lochbrunner, S.; Schubert, H.; Berkefeld, A., A photoreactive iron (II) complex luminophore. *J. Am. Chem. Soc.* **2022,** *144* (3), 1169-1173.

72. Malme, J. T.; Clendening, R. A.; Ash, R.; Curry, T.; Ren, T.; Vura-Weis, J., Nanosecond Metal-to-Ligand Charge-Transfer State in an Fe (II) Chromophore: Lifetime Enhancement via Nested Potentials. *J. Am. Chem. Soc.* **2023,** *145* (11), 6029-6034.

73. Braun, J. D.; Lozada, I. B.; Kolodziej, C.; Burda, C.; Newman, K. M.; van Lierop, J.; Davis, R. L.; Herbert, D. E., Iron (ii) coordination complexes with panchromatic absorption and nanosecond charge-transfer excited state lifetimes. *Nat. Chem.* **2019,** *11* (12), 1144-1150.

74. Muñoz-García, A. B.; Benesperi, I.; Boschloo, G.; Concepcion, J. J.; Delcamp, J. H.; Gibson, E. A.; Meyer, G. J.; Pavone, M.; Pettersson, H.; Hagfeldt, A.; Freitag, M., Dye-sensitized solar cells strike back. *Chem. Soc. Rev.* **2021,** *50* (22), 12450-12550.

75. O'Regan, B.; Grätzel, M., A low-cost, high-efficiency solar cell based on dye-sensitized colloidal TiO2 films. *Nature* **1991,** *353* (6346), 737-740.

76. Grätzel, M., Dye-sensitized solar cells. *J. Photochem. Photobiol., C* **2003,** *4* (2), 145-153.

77. Ferrere, S.; Gregg, B. A., Photosensitization of TiO2 by [FeII (2, 2'-bipyridine-4, 4'-dicarboxylic acid)2(CN)2]: band selective electron injection from ultra-short-lived excited states. *J. Am. Chem. Soc.* **1998,** *120* (4), 843-844.

78. Sen, A.; Putra, M. H.; Biswas, A. K.; Behera, A. K.; Groβ, A., Insight on the choice of sensitizers/dyes for dye sensitized solar cells: A review. *Dyes and Pigments* **2023,** *213*, 111087.

79. He, J.; Lindström, H.; Hagfeldt, A.; Lindquist, S.-E., Dye-Sensitized Nanostructured p-Type Nickel Oxide Film as a Photocathode for a Solar Cell. *J. Phys. Chem. B* **1999,** *103* (42), 8940-8943.

80. Zhang, L.; Yang, X.; Wang, W.; Gurzadyan, G. G.; Li, J.; Li, X.; An, J.; Yu, Z.; Wang, H.; Cai, B., 13.6% efficient organic dye-sensitized solar cells by minimizing energy losses of the excited state. *ACS Energy Lett.* **2019,** *4* (4), 943-951.

81. Mathew, S.; Yella, A.; Gao, P.; Humphry-Baker, R.; Curchod, B. F. E.; Ashari-Astani, N.; Tavernelli, I.; Rothlisberger, U.; Nazeeruddin, M. K.; Grätzel, M., Dye-sensitized solar cells with 13% efficiency achieved through the molecular engineering of porphyrin sensitizers. *Nat. Chem.* **2014,** *6* (3), 242-247.

82. Zeng, K.; Chen, Y.; Zhu, W.-H.; Tian, H.; Xie, Y., Efficient solar cells based on concerted companion dyes containing two complementary components: an alternative approach for cosensitization. *J. Am. Chem. Soc.* **2020,** *142* (11), 5154-5161.

83. Nazeeruddin, M. K.; De Angelis, F.; Fantacci, S.; Selloni, A.; Viscardi, G.; Liska, P.; Ito, S.; Takeru, B.; Grätzel, M., Combined experimental and DFT-TDDFT computational study of photoelectrochemical cell ruthenium sensitizers. *J. Am. Chem. Soc.* **2005,** *127* (48), 16835-16847.

84. Ji, J. M.; Zhou, H.; Eom, Y. K.; Kim, C. H.; Kim, H. K., 14.2% efficiency dye-sensitized solar cells by co-sensitizing novel thieno [3, 2-b] indole-based organic dyes with a promising porphyrin sensitizer. *Adv. Energy Mater.* **2020,** *10* (15), 2000124.

85. Zhang, D.; Stojanovic, M.; Ren, Y.; Cao, Y.; Eickemeyer, F. T.; Socie, E.; Vlachopoulos, N.; Moser, J.-E.; Zakeeruddin, S. M.; Hagfeldt, A., A molecular photosensitizer achieves a Voc of 1.24 V enabling highly efficient and stable dye-sensitized solar cells with copper (II/I)-based electrolyte. *Nat. Commun.* **2021,** *12* (1), 1777.

86. Green, M. A.; Dunlop, E. D.; Yoshita, M.; Kopidakis, N.; Bothe, K.; Siefer, G.; Hinken, D.; Rauer, M.; Hohl-Ebinger, J.; Hao, X., Solar cell efficiency tables (Version 64). *Prog. Photovolt.* **2024**.

87. Kayes, B. M.; Nie, H.; Twist, R.; Spruytte, S. G.; Reinhardt, F.; Kizilyalli, I. C.; Higashi, G. S. In *27.6% Conversion efficiency, a new record for single-junction solar cells under 1 sun illumination*, 2011 37th IEEE Photovoltaic Specialists Conference, 19-24 June 2011; 2011; pp 000004-000008.

88. Michaels, H.; Rinderle, M.; Benesperi, I.; Freitag, R.; Gagliardi, A.; Freitag, M., Emerging indoor photovoltaics for self-powered and self-aware IoT towards sustainable energy management. *Chem. Sci.* **2023,** *14* (20), 5350-5360.

89. Aghazada, S.; Nazeeruddin, M. K., Ruthenium complexes as sensitizers in dye-sensitized solar cells. *Inorganics* **2018,** *6* (2), 52.

90. Housecroft, C. E.; Constable, E. C., Solar energy conversion using first row d-block metal coordination compound sensitizers and redox mediators. *Chem. Sci.* **2022**.

91. Bozic-Weber, B.; Constable, E. C.; Housecroft, C. E., Light harvesting with Earth abundant d-block metals: Development of sensitizers in dye-sensitized solar cells (DSCs). *Coord. Chem. Rev.* **2013,** *257* (21-22), 3089-3106.

92. Marchini, E.; Darari, M.; Lazzarin, L.; Boaretto, R.; Argazzi, R.; Bignozzi, C. A.; Gros, P. C.; Caramori, S., Recombination and regeneration dynamics in FeNHC(ii)-sensitized solar cells. *Chem. Commun.* **2020,** *56* (4), 543-546.

93. Pastore, M.; Caramori, S.; Gros, P. C., Iron-Sensitized Solar Cells (FeSSCs). *Acc. Chem. Res.* **2024,** *57* (4), 439-449.

94. Reddy-Marri, A.; Marchini, E.; Cabanes, V. D.; Argazzi, R.; Pastore, M.; Caramori, S.; Gros, P. C., Panchromatic light harvesting and record power conversion efficiency for carboxylic/cyanoacrylic Fe (ii) NHC co-sensitized FeSSCs. *Chem. Sci.* **2023,** *14* (16), 4288-4301.

95. Marri, A. R.; Marchini, E.; Cabanes, V. D.; Argazzi, R.; Pastore, M.; Caramori, S.; Gros, P. C., Record power conversion efficiencies for Iron (II)-NHC-sensitized DSSCs from rational molecular engineering and electrolyte optimization. *J. Mater. Chem. A* **2021,** *9* (6), 3540-3554.

96. Marri, A. R.; Marchini, E.; Cabanes, V. D.; Argazzi, R.; Pastore, M.; Caramori, S.; Bignozzi, C. A.; Gros, P. C., A series of Iron (II)-NHC Sensitizers with remarkable power conversion efficiency in photoelectrochemical cells. *Chem. Eur. J.* **2021,** *27* (65), 16260-16269.

97. Prakash, O., Unpublished results.

98. Goriya, Y.; Kand, D., Unpublished results.

99. Lutz, V.; Glatthaar, J.; Würtele, C.; Serafin, M.; Hausmann, H.; Schreiner, P. R., Structural Analyses of N-Acetylated 4-(Dimethylamino) pyridine (DMAP) Salts. *Chem. Eur. J.* **2009,** *15* (34), 8548-8557.

100. Lindh, L., Personal communication. 2023.
101. Snaith, H. J.; Abate, A.; Ball, J. M.; Eperon, G. E.; Leijtens, T.; Noel, N. K.; Stranks, S. D.; Wang, J. T.-W.; Wojciechowski, K.; Zhang, W., Anomalous hysteresis in perovskite solar cells. *J. Phys. Chem. Lett.* **2014,** *5* (9), 1511-1515.
102. Sarker, S.; Seo, H. W.; Jin, Y.-K.; Lee, K.-S.; Lee, M.; Kim, D. M., On the hysteresis of current density-voltage curves of dye-sensitized solar cells. *Electrochim. Acta* **2015,** *182*, 493-499.
103. Elbohy, H.; El-Mahalawy, H.; El-Ghamaz, N. A.; Zidan, H., Hysteresis analysis in dye-sensitized solar cell based on different metal alkali cations in the electrolyte. *Electrochim. Acta* **2019,** *319*, 110-117.
104. Becker, M.; Wyss, V.; Housecroft, C. E.; Constable, E. C., The influence of alkyl chains on the performance of DSCs employing iron (II) N-heterocyclic carbene sensitizers. *Dalton Trans.* **2021,** *50* (46), 16961-16969.
105. Goriya, Y.; Kand, D.; Rayavarapu, S., Unpublished results.
106. Nair, S. S.; Bysewski, O. A.; Kupfer, S.; Wächtler, M.; Winter, A.; Schubert, U. S.; Dietzek, B., Excitation Energy-Dependent Branching Dynamics Determines Photostability of Iron (II)–Mesoionic Carbene Complexes. *Inorg. Chem.* **2021,** *60* (12), 9157-9173.
107. Nair, S. S.; Bysewski, O. A.; Klosterhalfen, N.; Sittig, M.; Winter, A.; Schubert, U. S.; Dietzek-Ivanšić, B., Intramolecular Energy Transfer Competing with Light-Driven Intermolecular Proton Transfer in an Iron (II)-NHC Complex? A Query into the Role of Photobasic Ligands and MLCT States. *ACS Omega* **2024,** *9* (11), 13427-13439.
108. Francés-Monerris, A.; Gros, P. C.; Pastore, M.; Assfeld, X.; Monari, A., Photophysical properties of bichromophoric Fe (II) complexes bearing an aromatic electron acceptor. *Theor. Chem. Acc.* **2019,** *138* (7), 86.
109. Jiang, T.; Bai, Y.; Zhang, P.; Han, Q.; Mitzi, D. B.; Therien, M. J., Electronic structure and photophysics of a supermolecular iron complex having a long MLCT-state lifetime and panchromatic absorption. *Proc. Natl. Acad. Sci. U.S.A.* **2020,** *117* (34), 20430-20437.
110. Pomeranc, D.; Heitz, V.; Chambron, J.-C.; Sauvage, J.-P., Octahedral Fe (II) and Ru (II) complexes based on a new bis 1, 10-phenanthroline ligand that imposes a well defined axis. *J. Am. Chem. Soc.* **2001,** *123* (49), 12215-12221.
111. Ren, Y.; Sun, D.; Cao, Y.; Tsao, H. N.; Yuan, Y.; Zakeeruddin, S. M.; Wang, P.; Gratzel, M., A stable blue photosensitizer for color palette of dye-sensitized solar cells reaching 12.6% efficiency. *J. Am. Chem. Soc.* **2018,** *140* (7), 2405-2408.
112. Gordivska, O., Unpublished results.
113. Hlynsson, V. F. Structure-Property Relationships of Iron N-Heterocyclic Carbene Complexes: Synthesis, Characterization and Application. Ph.D. Thesis, Lund University, Lund, Sweden, 2024.
114. Lee, D. G.; Chang, V. S., Oxidation of hydrocarbons. 9. The oxidation of alkynes by potassium permanganate. *J. Org. Chem.* **1979,** *44* (15), 2726-2730.

115. Lee, D. G.; Lee, E. J.; Chandler, W. D., Oxidation of hydrocarbons. 16. Mechanism of the reaction between alkynes and permanganate ion. *J. Org. Chem.* **1985,** *50* (22), 4306-4309.

116. Kocienski, P. J., *Protecting groups*. G. Thieme: Stuttgart, 1994.

117. Heinemann, C.; Müller, T.; Apeloig, Y.; Schwarz, H., On the Question of Stability, Conjugation, and “Aromaticity” in Imidazol-2-ylidenes and Their Silicon Analogs. *J. Am. Chem. Soc.* **1996,** *118* (8), 2023-2038.

118. Yarranton, J. T.; McCusker, J. K., Ligand-field spectroscopy of Co (III) complexes and the development of a spectrochemical series for low-spin d6 charge-transfer chromophores. *J. Am. Chem. Soc.* **2022,** *144* (27), 12488-12500.

119. Bernd, M. A.; Dyckhoff, F.; Hofmann, B. J.; Böth, A. D.; Schlagintweit, J. F.; Oberkofler, J.; Reich, R. M.; Kühn, F. E., Tuning the electronic properties of tetradentate iron-NHC complexes: Towards stable and selective epoxidation catalysts. *J. Catal.* **2020,** *391*, 548-561.

120. Wang, T. C.; Bury, W.; Gómez-Gualdrón, D. A.; Vermeulen, N. A.; Mondloch, J. E.; Deria, P.; Zhang, K.; Moghadam, P. Z.; Sarjeant, A. A.; Snurr, R. Q., Ultrahigh surface area zirconium MOFs and insights into the applicability of the BET theory. *J. Am. Chem. Soc.* **2015,** *137* (10), 3585-3591.

121. Galanti, A.; Santoro, J.; Mannancherry, R.; Duez, Q.; Diez-Cabanes, V.; Valasek, M.; De Winter, J.; Cornil, J.; Gerbaux, P.; Mayor, M., A new class of rigid multi (azobenzene) switches featuring electronic decoupling: Unravelling the isomerization in individual photochromes. *J. Am. Chem. Soc.* **2019,** *141* (23), 9273-9283.

Printed by Media-Tryck, Lund 2024 NORDIC SWAN ECOLABEL 3041 0903

ISBN 978-91-8096-060-1

Centre for Analysis and Synthesis
Department of Chemistry
Faculty of Science
Lund University